University of Southampton

Faculty of Engineering and Applied Sciences
Department of Electronics and Computer Science
Optoelectronics Research Centre

Integrated Optical Surface Plasmon
Resonance for Electrochemically-Addressed Layers

by

Jude C. Abanulo

Thesis submitted for the degree of Doctor of Philosophy
September 2001

UNIVERSITY OF SOUTHAMPTON

ABSTRACT

FACULTY OF ENGINEERING AND APPLIED SCIENCE

DEPARTMENT OF ELECTRONICS AND COMPUTER SCIENCE

Doctor of Philosophy

Integrated Optical Surface Plasmon Resonance for Electrochemically-Addressed Layers

by Jude Chituru Abanulo

This thesis reports on the development of the first integrated optical surface plasmon resonance sensor that combines an optical and electrochemical interrogating technique in sensing electrochemically addressed layers over a gold film. This device brings together the advantages of the analytical technique of surface plasmon resonance and of cyclic voltammetry on a single chip that exhibits portability, miniaturisation capability and compatibility with optical fibre. The integrated optical chip allows the potential introduction of a large number of sensing pads on a single chip thus allowing the acquisition of precise information about a test compound while simultaneously monitoring different test compounds in the same sensing area. The integrated optical surface plasmon resonance (IOSPR) devices fabricated were applied in the study of the oxidation of gold and the removal of the oxide layer in real time. The optical response to the oxidation process was similar to those reported in the literature using ellipsometry and or reflectance spectroscopy. Here the IOSPR device performed better, giving transmittance changes of 60 % in response to the formation of an oxide film. The introduction of a monolayer of copper onto the gold surface of the device via the underpotential deposition process was monitored for the first time using the surface plasmon technique. Here the response and performance of the device was compared with other reported studies in the literature, which combined an optical and electrochemical technique for similar analysis. The IOSPR device performed better with 10 % change in transmittance in comparison to a change of 1 % reported for reflectance measurements. Comparisons were also made with those predicted by a numerical waveguide model. The feasibility of potential applications in biological analysis was demonstrated by applying the device in analysing the adsorption and desorption of thiol and phospholipid layers onto the sensing surface of the device.

Acknowledgement

I would like to thank everyone involved in the ORC Cleanrooms, and everyone in the Electrochemistry Group of the Chemistry department for their help. Particular thanks go to Geoff, Louise, Jonathan and Ping, and to Tracy, Anna and Li Na who gave me the push required in the later stages of my project. I would also like to say thanks to my supervisors James and Phil who were not only great supervisors but also my role models. I would also like to extend my gratitude to Richard who guided me through the initial stages of my PhD project. Finally, I would like to thank my parents, brothers, sisters, and friends, who have always been there for me, and George Attard, who made all this possible.

The heights by great men reached and kept not attained by sudden flight, but they, while their companions slept were toiling upwards in the night

- *Henry W. Longfellow*

A.C. and D.G. Rembley., Leaves of gold. Fort Worth, TX: Brownlow Publishing co., Inc., 1948.

Table of contents

Chapter 1

1.1 Introduction

For a number of years scientists have studied solid-liquid interfaces in great detail in order to understand the basic mechanisms involved in numerous phenomena such as corrosion, oxidation, catalysis and adsorption of biological (lipid) layers. This thesis reports on the application of a novel integrated optical surface plasmon resonance (IOSPR) device, in the study of a variety of electrochemically controlled surface reactions namely oxidation, underpotential deposition of a metal and the adsorption of lipid layers. Corrosion and oxidation are problems prevalent with the use of metal in industrial processes and in our daily life. Metals used in every day work are reactive in ambient conditions thus tend to be covered with a thin oxide layer [1.1]. The first step towards addressing the problem of metal surface corrosion is obviously a full mechanistic understanding of the processes involved in metal oxidation and corrosion. Studies carried out to understand the process of oxidation and corrosion of metals have been done on inert noble metal, over which oxide films are artificially introduced and controlled by the application of an electrode potential [1.1]. The presence of oxides on metals do have positive attributes, for example oxide introduces passivity in metals and ceramics, in addition, an electrode used for electrosynthesis, is required to remain unchanged for long periods even in electrolytes not saturated with the oxide, this can be achieved by the introduction of an of oxide film over the electrode.

The catalytic property of an electrode can be modified or introduced by the deposition of a thin film of a metal (monolayer) possessing the required catalytic property [1.2]. This can be achieved by an electrochemical process known as underpotential deposition. The underpotential deposition of a metal, on a foreign metal substrate, occurs at a potential positive to the reversible potential required for the bulk metal deposition [1.3]. This faradaic adsorption of trace quantities of the metal ions dissolved in the solution of the supporting electrolyte leads to the formation of sub- and monolayer coverage of discharged metal adatoms. The deposited monolayer of metal on the electrode constitutes the first stage in electrocrystallization. The underpotential deposition process has been studied extensively in the last 25 years because of its importance in studying a wide variety of electrochemical phenomena,

such as adsorption, charge transfer, surface diffusion, nucleation and growth, double-layer changes and its fundamental and practical significance in electrocatalysis.

Finally, the functionalisation of electrodes can be carried out using organic monolayer films. Here the common approach for modification of electrode surfaces using organic monolayer films is by self-assembly of the organic films over the electrode surface [1.4-1.6]. Many of these monolayer systems have characteristic structures and properties, for example under the right conditions they exhibit monolayer coverage, highly ordered and tend to be densely packed. These organic monolayers are used in the areas of improving adhesion (see chapter 4.2.4), corrosion [1.7], lubrication, biocompatibility and catalysis [1.4].

An understanding of processes at the solid-liquid interface is the key to the better understanding of many of these technological processes. In order to get a better insight into the solid/liquid interface, analytic techniques such as Auger electron spectroscopy (AES), electron spectroscopy for chemical analysis (ESCA), ion scattering spectrometry (ISS), secondary ion mass spectrometry (SIMS) and low energy electron diffraction (LEED) have been applied in the study of these solid-liquid interfaces, but these techniques do not allow for in situ studies as they require ultrahigh vacuum (UHV) conditions [1.8].

1.2 Electrochemical techniques

Electrochemical studies are particularly attractive for the analysis of the electrode-electrolyte (solid-liquid) interface, as it can be carried out in situ. Here current generated due to the transfer of electrons across the electrode-electrolyte interface, as the electrochemical reaction takes place at the surface of the electrode is monitored [1.9]. The electrochemical technique applied in this project is cyclic voltammetry (CV), which is widely used for the initial characterisation of electrochemically active systems, during which the current-potential behaviour at an electrode surface is measured. During analysis, the potential is varied between two potential limits to cause electroactive chemical species to be reduced or oxidised at the electrode. The resultant current is proportional to the concentration of the chemical species, further analysis of the resultant current reveals the number of different oxidation states and

their relative free energies. Cyclic voltammetry can also be used for mechanistic studies of systems where, the electron transfer reactions are coupled to chemical reactions. The cyclic voltammogram obtained will depend on the mechanisms of the chemical reaction taking place. The introduction of films such as gold oxide, a monolayer of metal and lipid layers may signal their presence in a variety of ways. The electrode may exhibit electrocatalytic properties as in the case of underpotential deposition of a metal or exhibit a marked change in interfacial properties such as capacitance for the oxidation of the gold film. In cases such as those involving lipid layers and thiol layers there may be a complete cessation of all electrochemical activity [1.10].

1.3 Optical techniques

Optical techniques such as ellipsometry [1.8, 1.11-1.13], reflectance [1.14] and surface plasmon resonance [1.15-1.18] permit a more detailed chemical and structural analysis of the solid-liquid interface in real time allowing the determination of the optical constants and thickness of a layer system. These optical techniques are well established for the characterisation of thin films and surfaces. The widely used ellipsometer works by using the fact that the state of polarisation of an incident beam changes upon reflection at a film covered surface. These changes in the state of polarisation can be described by two measurable quantities, ψ (relative amplitude change) and Δ (relative phase change), which in turn are related to the optical properties of the film. If the sample undergoes a change, for example, a thin film on the surface changes its thickness, then its reflection properties will also change. Measuring these changes in ψ and Δ, allows one to deduce the actual change in the film's thickness.

Within the last few years, the possibility of implementing the surface plasmon resonance (SPR) sensing principle into optical waveguide structures has attracted much attention. SPR sensors based on optical waveguides offer various advantageous features for sensing, they are small in size, exhibit ruggedness, there is the prospect of fabrication of multiple and/or multichannel sensors on a single optical chip and they may, in conjunction with optical fibers, be used for remote sensing applications. A surface plasmon can be regarded as a bound electromagnetic wave propagating at the

metal-dielectric interface and is an analytical technique that uses evanescent waves to probe thin films. This technique works by responding to changes in the refractive index of the dielectric (see fig 3.9), as well as changes in the thickness and refractive indices of thin films introduced over the metal surface. The principle of this analytical technique is discussed in further detail in chapter 3. Surface plasmon resonance has been applied for the analysis of gases (e.g. aesthetic gases [1.19]), liquids (e.g. binary mixture analysis of methanol [1.20] and ethanol [1.21] in water) and solids (e.g. inorganic solids [1.22-1.24], organic Langmuir-Blodgett films [1.25]). However, to date most of the research and commercial interest in SPR sensors has been in the field of biosensors [1.26-1.27]. SPR has been used to analyse many biomolecular systems, such as, antigen-antibody, enzyme-substrate, hormone-receptor, drug-receptor and DNA-DNA interactions [1.28-1.29]. Surface plasmon resonance offers a number of important practical advantages over current biological analytical techniques such as ELISA. The time from sample application to reported result varies with the specific chemistry but can be as short as 5 minutes. In most cases, there is no need to pretreat the sample before its presentation to the sensor. An attractive feature of this approach is the ability to determine concentration and binding kinetic data that is the equilibrium constant, association and dissociation constants, for specific biological analytes [1.30] Unlike other biological techniques such as ELISA, the measurement does not require molecule labelling.

An important limitation of the SPR technique, is the fact that SPR although sensitive to changes in refractive index in the vicinity to the sensor surface, cannot distinguish between bulk refractive index changes of sample solution (caused for example by temperature variations), specific binding of analyte and non-specific adsorption of other non-target molecules. This limitation can be overcome by increasing the SPR signal in response to the analyte of interest. One way is to label the protein, or some secondary reagent (e.g. a secondary antibody), with a substance possessing a high refractive index. The drawback of this technique is that SPR is transformed from a non-labelling technique to a labelling technique, which involves the risk of the label influencing the kinetics or the equilibrium of the biomolecular binding event. Another way is to enhance the sensitive layer to increase the specific binding response. Such an improvement can be attained with sensitive layer comprising of three-dimensional matrix of receptors and top screening layer, [1.31]. Introduction of multichannel

sensors opens ways to reference many background effects, which interfere with the SPR measurement and thus improve the SPR measurement reliability. Research in multichannel sensing is also crucial for design of high throughput sensor systems, substantial for successful competing of SPR technology with standard ELISA-like methods.

Nowadays commercial SPR biosensors are used in analytical research laboratories, but breakthrough into the food industry or medicine has still not been attained. In order to reach out of specialised laboratories and gain appreciable share of the biochemical market, parameters including sensor specificity, stability and sensitivity needs to be improved. Especially the specificity enhancement is very crucial because sensed samples in these areas are very complex (blood plasma, urine, saliva and food). The combination of electrochemical and optical techniques brings together the advantages of both techniques resulting in one device that has enhanced specificity, sensitivity, real time measurement, portability, stability, cheap, recyclable device to state a few of the potential properties of an electrochemical-IOSPR device. The purpose of this project is to demonstrate how the combination of surface plasmon resonance and cyclic voltammetry can be used to obtain information concerning adsorption phenomena, by studying the three areas of oxide formation, underpotential deposition of metals and the adsorption of thiol and lipid layers on a gold electrode surface. Some of the potential areas of application of the IOSPR device include medical diagnostics, environmental monitoring, agriculture pesticide and antibiotic monitoring, food additive testing, military and civilian airborne biological and chemical agent testing and real time chemical and biological production process monitoring.

1.4 Outline of thesis structure.

Chapter 2 gives a review of optical and electrochemical interrogation of the oxidation of a gold film, underpotential deposition of copper onto gold and the adsorption of thiol and phospholipid layers over a gold film. Chapter 3 deals with the principle behind the optical (SPR) and electrochemical (cyclic voltammetry) technique applied using the IOSPR device. Chapter 4 describes the fabrication of the integrated optical device and optical experiments carried out to validate the sensor device. In addition a

brief report on the work done to improve the adhesion of the gold films on the Pyrex glass substrate is also discussed. Chapter 5 covers the experimental work carried out, using the integrated optical surface plasmon resonance device to monitor simultaneously the optical and electrochemical interrogation of electrochemically formed gold oxide layers and its removal. Chapter 6 describes the application of the IOSPR device for the first time to monitor the underpotential deposition of copper onto a gold film. Chapter 7 deals with the experimental results obtained during the functionalisation of the gold film using biological layers, that is thiol and phospholipid layers. Overall conclusions and discussion of potential future work and modification that can be carried out is discussed in chapter 8.

1.5 Reference:

1.1 H. Angerstien-Kozlowska, B.E. Conway, A. Hamelin and L. Stoicoviciu, J. Electroanal. Chem. 228 (1987) 429.

1.2 S. Swathirajan and S. Bruckenstein, Electrochimica Acta 28 (1983) 865.

1.3 R. Adzic, E. Yeager and B.D. Cahan, J. Electrochem. Soc. 121 (1974) 474.

1.4 Frank Auer, Borje Sellergren, Aleksander Swietlow and Andreas Offenhauser, Langmuir 16 (2000) 5936.

1.5 Christian D. Hodneland and Milan Mrksich, Langmuir, 13 (1997) 6001.

1.6 Valeria Molinero, Ernesto J. Calvo, Journal of Electroanalytical Chemistry 445 (1998) 17.

1.7 Gregory E. Poirier, Chem. Rev 97 (1997) 1117.

1.8 Y-T. Kim, R.W. Collins and K. Vedam, Surface Science 233 (1990) 341.

1.9 R. Greef, R. Peat, L.M. Peter, D. Pletcher, J. Robinson, Instrumental methods in Electrochemistry Southampton Electrochemistry group 179.

1.10 Vladimir M. Mirsky, M. Mass, C. Krause and O. S. Wolfbeis, Anal Chem. 70 (1998) 3674.

1.11 R.S Sirohi and M.A. Genshaw, J. Electrochem. Soc. 116 (1969) 910.

1.12 J. Horkans, B.D. Cahan and E. Yeager, Surface Science 46 (1974) 1.

1.13 A. Hamnett J. Chem. Soc. Faraday Trans, 89 (1993) 1593.

1.14 T. Takamura, K. Takamura, W. Nippe and E. Yeager, J. Electrochem. Soc. 117 (1970) 626.

1.15 C.B. Brennan, L. Sun and S.G. Weber, Sensor and Actuators B 72 (2001) 1.

1.16 L.S. Jung, C.T. Campbell, T.M. Chinowsky, M.N. Ar and S.S. Yee, Langmuir 14 (1998) 5636.

1.17 I. Pockrand, J.D. Swalen, J.G. Gordon II and M.R.. Philpott, Surface Science 74 (1977) 237.

1.18 K.A. Peterlinz and R. Georgiadis, Langmuir 12 (1996) 4731.

1.19 C. Nylander. B. Liedberg, T. Lind, Sensors and Actuators 3 (1982/83) 79.

1.20 K. Matsubara. S. Kawata, S. Minami, Appl. Spectrosc. 42 (1988) 1375.

1.21 K. Matsubara. S. Kawata, S. Minami, Appl. Opt. 27 (1988) 1160.

1.22 J.J. Cowan. E.T. Arakawa, Phys. Stat. Sol. 1 (1970) 695.

1.23 A. Otto. Spectroscopy of surface polaritons by attenuated total reflection. In: B.O. Seraphin (Ed.), Optical property of solids, new developments, North-Holland, Amsterdam, 1976. Chapter 13.

1.24 H. Raether, Excitation of plasmons and interband transitions by electrons. In: Springer tracts in moderns physics, 88, Springer, Berlin, 1980.

1.25 C.R. Lawrence. A.S. Martin, J.R. Sambles, Thin Solid Films 208 (1992) 269.

1.26 B. Liedberg. C. Nylander, I. Lundström, Sensors and Actuators 4 (1983) 299.

1.27 M.T. Flanagan. R.H. Pantell, Electron. Lett. 20 (1984) 968.

1.28 I. Davies. I. Faulkner, Surface plasmon resonance-theory and experimental considerations, in: J. Davies (Ed.), Surface analytical techniques for probing biomaterial processes, CRC Press, Boca Raton, 1996, Chapter 3.

1.29 www.biocore.com.

1.30 B. Liedberg, I. Lunström, E. Stenberg, Sensor and Actuators B, 11 (1993) 63-72.

1.31 E. Brynda and M. Houska, Biosensors with Surface Immobilized Protein Networks, Proceeding of 8th Wienna Opt(r)ode Worshop, Prague, October 7-8, 1998.

Chapter 2

Review of the interrogation of selected thin film processes on gold films.

2.1 Introduction

The nature of an electrode surface strongly influences the electrochemical reactions occurring on it. An understanding of these reactions can be achieved by carrying out detailed analysis of the electrode-electrolyte interface and the structural attributes of the metal. Optical techniques such as ellipsometry and reflectance allow for the study of chemical reaction such as the oxidation of a gold film *in situ,* which cannot be achieved using ultrahigh vacuum techniques. This chapter reviews work previously carried out in the study of the oxidation of a gold film, underpotential deposition of Cu and the interrogation of lipid layers on gold using optical techniques such as ellipsometry, reflectance and electrochemical voltammetric methods.

2.2 Oxidation

The breadth of application of metals in industrial processes and commercial usage is limitless, but their application is often restricted by reactions such as corrosion and surface oxidation. Extensive studies of the oxidation process have been carried out with the aim of finding solutions to these problems. Examples include studies carried out on noble metals, such as gold, where the application of potential introduces controlled accelerated oxidation of the gold. Such studies on gold date back over 40 years [2.1]. For gold the generally agreed mechanism for the formation of the oxide is that given by Conway *et al.* [2.2-2.5]. A brief overview of the accepted mechanism for the electrochemical oxidation of gold is outlined below. Fig 2.1 gives a schematic view on the mechanism of oxide formation on a gold metal. The application of potential in the anodic direction, positive of the potential of zero charge, gives rise to a reversible electrostatic adsorption of hydrated anions on the metal. Further application of potential gives rise to the chemisorption of the anions on the Au surface, that is the anions undergo partial or full charge transfer (for partial discharge: $anion^- \rightarrow anion^{(1-\delta)-}$). These chemisorbed anions depends on the conductive electrolyte, e.g. sulphuric acid would have HSO_4^- and SO_4^{2-} while perchloric acid will produce ClO_4^- anions. The chemisorbed anions cover the surface of the metal forming an overlayer lattice or lattices of anions H-bonded to H_2O molecules. As the

coverage of chemisorbed anions on the metal surface increases with increasing anodic potential, the number of water molecules bond to each anion decreases. Partial discharge of H_2O ($yH_2O \rightarrow (y-1)H_2O.OH^{(1-\gamma)} + H^+$), hydrogen bonded to the oxygen atoms of the anions occurs at the onset of the oxidation of the metal. A further increase in the anodic potential leads to the complete discharge of the OH^- species. This complete discharge also involves the incorporation of the OH onto the metal surface with the loss of the previously chemisorbed anions (see equation 1), followed by replacement turnover giving rise to an anion free surface that can be further oxidised.

$$M + H_2O \rightarrow MOH + H^+ + e^- \qquad (1)$$

This replacement turnover process is driven by the repulsive interaction between the MOH oriented parallel dipoles on the surface at the initial adsorption. This change in the orientation of the MOH state at the surface causes hysteresis between the processes of oxidation and reduction of the oxide observed on all noble metals and in particular gold. The replacement turnover introduces irreversibility to the system as the surface of the electrode before turnover cannot be reformed. The adsorbed anions determine the potential at which the oxidation of the surface occurs, because they compete with the electrosorption of OH species on the metal surface [2.4]. The passage of the second electron produces the surface gold oxide (AuO).

$$MOH \rightarrow MO + H^+ + e^- \qquad (2)$$

At potentials anodic of 2.0 V films of thickness greater than that of a monolayer of oxide are formed over the gold surface, these have been shown to be Au_2O_3 or hydrated Au_2O_3 [2.6].

The refractive index of the oxide film is complex due to the absorbing property of the oxide film [2.7-2.8].

$$\boldsymbol{n} = n - ik \qquad (3)$$

Where n and k are the real and imaginary part, k is related to the absorption coefficient, α by;

$$\alpha = (4\pi k) / \lambda \qquad (4)$$

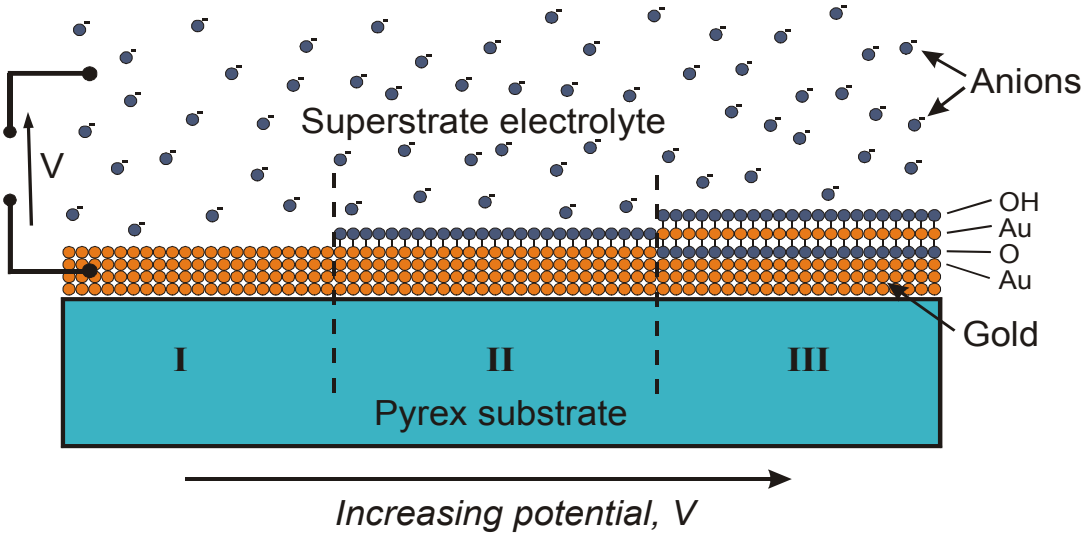

Fig 2.1 Schematic view on the mechanism of oxide formation on gold metals. Region I shows the state of the gold surface when no potential is applied, region II is that showing the adsorption of the OH ion onto the gold surface while region III shows the surface of the gold film having undergone replacement turn over and further oxidation of the gold surface.

This chapter, reviews reported studies on the combination of electrochemical and optical techniques such as ellipsometry and reflectance in the analysis of the electrochemical oxidation of gold. This allows comparison to be made with the experimental result obtained in this project combining cyclic voltammetry and surface plasmon resonance analytical technique for the study of oxidation of gold. At the electrode-electrolyte interface charging the electrode creates an electric field localised near the surface of the electrode. Optical techniques such as ellipsometry and reflectance analyse changes in this narrow interfacial zone as the potential between the working and reference electrode is changed.

Ellipsometry is an optical technique applied in the analysis / study of surfaces and thin films where measurements of changes in the polarisation state of light reflected from a surface of a substrate are analysed (see fig 2.2). The ellipticity and polarisation of the reflected light depends on the angle of the incident light, the direction of the polarisation of the incident light and the reflective properties of the surface. Changes in the optical properties of the surface due to processes such as the oxidation of the metal surface, are relayed by changes in the reflective properties of the surface, observed as changes in the relative phase change, Δ and the relative amplitude change,Ψ of the reflected light.

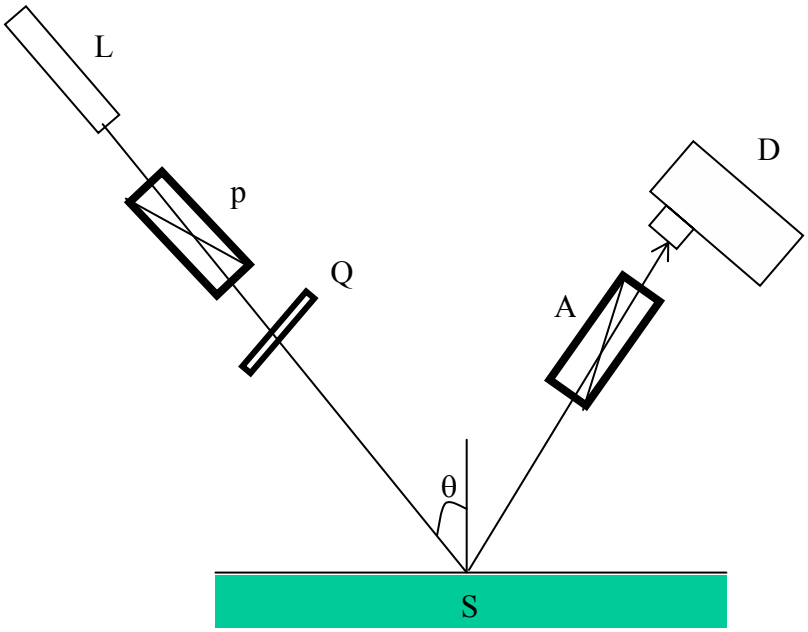

Fig 2.2 A schematic diagram of an ellipsometer. L - light source, P - polarising prism, Q - quarter-wave plate compensator, S-sample surface, A - analyser prism and D - light detector.

Experimentally the ratio of the intensity of the p – polarised wave to the s – polarised wave, r_p / r_s is measured and this ratio of the sample's Fresnel reflection coefficient, r_p/r_s, define the ellipticity, σ (a complex number). The two ellipsometric angles, ψ and Δ are related to the ratio of the sample's Fresnel reflection coefficient by the following equation

$$\sigma = \tan \psi \exp(i\Delta) = r_p / r_s \qquad (5)$$

In reflectance, changes in the optical properties of the surface due to reactions taking place on the metal surface (e.g. the formation of oxide layer), are relayed by changes in the intensity of reflected light from the surface. See reference 2.9 for detailed description of the experimental set up for the reflectance measurement.

Cyclic voltammetry (see chapter 3) has provided much information on the kinetic and thermodynamic properties of the oxidation of gold film. This is achieved by monitoring of current generated as a potential is applied between the working electrode and the reference electrode. The current measured allows the charge involved in the oxidation of the metal to be obtained, this gives a measurement of the

coverage of the substrate by the oxide layer. This is achieved by integrating the area under the peak current representing the stripping of the oxide layer from the substrate surface.

Sirohi *et al.* [2.7] combined optical (ellipsometry) and electrochemical (staircase voltammetry) measurements in their study of oxide formation on gold, allowing measurements of changes in relative phase change Δ and relative amplitude change Ψ in the reflected light from the gold surface to be made as a function of the potential. Here they obtained two regions, region 1 exhibited a slow change in the optical output (the pre-oxidation region), the potential was applied between 0 V and 1.1 V in 1 N H_2SO_4 acid. In region 1 the measured apparent capacity was 20 $\mu F / cm^2$ which was suggested to be characteristic of the double layer capacity of the bare surface. Sirohi *et al.* obtained a value of 0.236 - 3.504i for the refractive index of gold at 632.8 nm using this system. In region 1, the slow change in the optical output was attributed to a slow chemisoption of a species now known to be anions of the electrolyte which induces changes in the optical constants of the metal producing the observed changes in the ellipsometric parameters Δ and ψ. The potential region between 1.1 V and 1.5 V was classified as region 2, which revealed a rapid change in the optical output (oxidation region). The percentage change in optical response to the formation of the oxide was approximately 1.3 % for relative phase change Δ and 0.3 % for relative amplitude change.

In a subsequent study Horkans *et al.* using scanning ellipsometry, investigated the oxidation of gold at wavelengths in the visible region [2.10] with the main emphasis on determining the optical constants and thickness of the oxide formed on gold as a function of the electrode potential and wavelength. The characterisation of an optically absorbing surface film such as an oxide film (that is the complex refractive index $\boldsymbol{n} = n - ik$ and the film thickness) requires 3 optical measurements to be made simultaneously and independently of each other [2.10]. Horkans *et al.* measuring changes in light intensity in the ellipsometric experiment determined the changes in Δ, ψ and in addition, reflectivity measurements of the surfaces were carried out. The oxidation of the gold electrode was carried out in 1 M $HClO_4$ at a scan rate of 50 mV/s. Using the values obtained from Δ, ψ and reflectivity they were able to

determine the optical constants and thickness of the oxide film on the gold surface. The optical constants obtained were found to be independent of the wavelength used in the range 602 nm to 715 nm. The refractive index of the oxide in this region was n = 3.3 - 1.3i with an estimated precision of 10 % while the thickness of the oxide film was estimated to be 5.4 ± 0.6 Å. The percentage of the relative reflectivity change, dR/R, in response to oxide formation was approximately 1 %. In 1990 Kim *et al.* [2.11], using what was described as a rapid - scan spectroscopic ellipsometry-optical multichannel analyser detector, suggested that more detailed chemical and structural analysis of solid / liquid interface could be obtained. Using this technique they showed that the oxide film on gold is absorbing and determined that the monolayer of gold oxide was approximately 4 Å thick. This is close to previously reported values; for example, Chao [2.12] concluded that a monolayer of gold oxide assumed to be Au_2O_3 is 3.7 Å thick.

Reflectance techniques have been exploited in the study of electrochemical systems in the wavelength region 300 nm - 900 nm. This method has its drawbacks as the probe beam will interrogate not only the surface, but also the near - electrode region. The reflectivity of a surface with a film present will be affected by the solvent, the substrate and the film itself and not just by the thickness of the film. To over come this drawback, slight modifications were made to this technique. In 1970, Takamura *et al*. [2.9] demonstrated, using a simple multiple specular reflection technique, that interesting information concerning adsorption phenomena, oxide formation and the electronic properties of metal electrode surface could be obtained by combining optical (multiple specular reflection) and electrochemical (cyclic voltammetry) techniques. By carrying out cyclic voltammetry in 0.2 M perchloric acid and measuring reflectance at 540 nm they obtained 1 % response change optically to formation of a monolayer of oxide. The sensitivity of the reflectance method reported here is similar to that obtained by Sirohi [2.7] for the relative phase change in response to oxide formation on a gold surface. By measuring the change in reflectivity at a wavelength of 675 nm and the charge passed as a function of time following a potential step from 0.96 V (no oxidation) to 1.20 V (oxidation) in 0.1 M H_2SO_4, they observed a change in the slope of a plot of reflectivity against charge at 500 $\mu C/cm^2$, which was suggested to represent the point of complete oxide monolayer formation. The charge is slightly higher than that expected for a monolayer of oxide

film formed on a polycrystalline gold surface (400 μC/cm^2 - see chapter 5). These reported results allow comparisons to be made with the results obtained here using the IOSPR device in the following chapters.

2.3 Underpotential deposition

This subsection discusses reported studies using electrochemical and optical techniques for the analysis of underpotential deposition of a monolayer of a metal onto the surface of the working electrode. The voltage reading without the application of a potential between the working electrode and the reference electrode is the resting potential. The application of a potential significantly negative of the resting potential in a solution containing metal ions such as copper will lend to the copper ions depositing out of the solution onto the working electrode. This will tend to millions of monolayers of copper depositing onto the surface of the working electrode. However, at potentials closer to the resting potential but positive of the Nernst potential, a monolayer or (submonolayer) of copper are deposited onto the working electrode and this phenomenon is known as the underpotential deposition [2.13]. At these potentials, copper prefers to deposit onto the working electrode rather than onto copper. Fig 2.3 illustrates the potential regions involved in this process and that leading to the bulk deposition of the metal from solution. Catalytic activity can be introduced to the surface of an electrode by the underpotential deposition (UPD) of metals onto the electrode. In addition, UPD provides a means of controlling the microscopic surface structure through the electrolyte composition and the applied potential. Reactions of interest using gold electrodes are hydrogen evolution, oxygen reduction and the oxidation of organic molecules [2.14]. There is a technological need to understand the physical and chemical processes involved in the deposition of the metals deposited onto the working electrode. In response to this demand there has been a growing interest in the application of surface techniques such as scanning tunnelling microscopy (STM) [2.15-2.16] and atomic force microscopy (AFM) [2.17-2.19] in the study of underpotential deposition of metal. As in the oxidation, process cyclic voltammetry has provided many information on the kinetic and thermodynamic properties of the underpotential deposition process. The position, shapes and number of peaks (that is in the case of single-crystal) in the voltammogram depend on the substrate and the crystal plane on which the deposition occurs as well as the

electrolyte used [2.20]. The number of the surface sites of the substrate occupied by the adsorbate is related to the total number of substrate sites available by the fractional coverage (θ).

$$\theta = N_s/N \qquad (6)$$

where (N_s) is the number of surface sites occupied by the adsorbate and (N) is the total number of substrate adsorption sites.

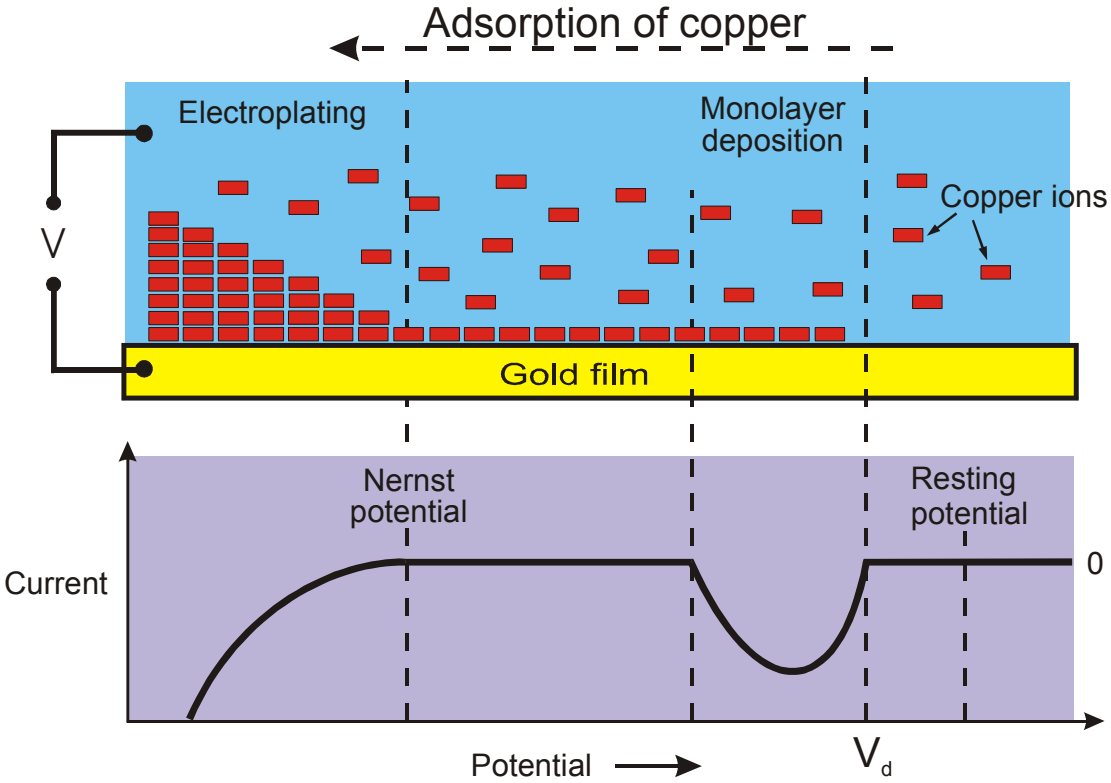

Fig 2.3 Diagram showing the bulk and monolayer deposition regions. The monolayer deposition of the metal occurs at specific potential that depend on the concentration and the metal been studied.

The current measured allows for the charge involved in the deposition of the metal to be obtained, in addition the peak current associated with deposition of the metal is proportional to the concentration of the metal deposited onto the metal surface. A quantitative measurement of the coverage of the substrate by the deposited metal can be determined by integrating the area under the peak current representing the deposition of the metal onto the substrate surface (see appendix 2). Charges reported in the literature for monolayer underpotential deposition of Cu on gold vary from 0.35mC/cm^2 [2.21] to 0.46 mC/cm^2 depending on the gold surface [2.16]. Table 2.1 shows the effect of gold surface on the measured charge as reported by Schultze *et al.* [2.20].

Gold surface	Charge μC / cm^2
(111)	395 ± 20
(100)	370 ± 20
(110)	240 ± 30

Table 2.1 showing the effect of gold surface to measured charge [2.20].

The charge required for the oxidation of a gold film forming a complete monolayer is suggested to be approximately equal to that required to deposit a monolayer of Cu onto a polycrystalline gold surface that is 390μC / cm^2 as both cases involves 2-electron reaction. The deposition of every Cu^{2+} ion will be accompanied by the transfer of two electrons to the electrode thus by monitoring the amount of charge flowing through the electrode one can monitor the degree of coverage of the electrode by the metal. Similarity in the atomic radius of Cu and Au (Au = 1.46 Å [2.22] and Cu = 1.28 Å [2.23]) suggests negligible misfit and epitaxial deposition is expected [2.24]. The deposition of Cu on gold during the UPD process has been shown to involve the co-adsorption of anions such as HSO^-_4 and SO^{2-}_4 where the anion adsorbs on the copper layer [2.25-2.26]. This has been shown by X-ray absorption fine structure spectroscopy study and further confirmed by Watanabe *et al* [2.27] using the electrochemical quartz crystal microbalance.

More studies have been carried out on single crystal gold surfaces than on polycrystalline ones as the single crystal faces displays sharp current peaks. However polycrystalline gold finds application in every day fundamental electrochemistry and electrocatalysis. The cyclic voltammetry for the different gold surfaces is relatively similar, the main difference lying in the number of current peaks associated with either the deposition or removal of the deposited metal from the gold surface. Taking Au (111) as an example, the cyclic voltammetry of copper UPD on Au (111) in sulphuric acid solutions is characterised by a double deposition and stripping peak structure. The deposition and striping current peaks closer to the Nernst potential for Au (111), varying with changes in the scan rate. The shift in the deposition and stripping peaks due to changes in the scan rate during the UPD of Cu^{2+} onto Au (111) in sulphuric acid, occurs with the stripping peak moving towards the positive potential, while the deposition peak moves towards the negative potential.

M. Cappadonia *et al.* [2.28] carried out a detailed analysis of the effect of the anion in the electrolyte on the UPD of copper on Au (100), using perchloric acid (weakly adsorbing ClO_4^- anions) and sulphuric acid (strongly adsorbing SO_4^{2-} anions). M. Cappadonia *et al.* [2.29] using a solution containing 0.1 mol/dm^3 $HClO_4$ + 5 mmol/dm^3 ($Cu(ClO_4)_2$) and sulphuric acid of concentration ranging from 1μmol/dm^3 to 5 mmol/dm^3, obtained a broad deposition peak and a sharp stripping peak. This paper showed that the stripping peak potentials are affected by the sweep rate as the stripping peak shifts towards more positive potential as the sweep rate increases. Analysing the change in cyclic voltammetry behaviour as a function of sweep rate, v, Hachiya *et al.* [2.16] found that the peak current was proportional to v up to 5 mV/s and then above 5 mV/s, approx. proportional to $v^{1/2}$ this observation deviates from the norm. The peak current for surface reactions are usually proportional to the scan rate, here the deviation to the norm was attributed to the face of the working electrode. M. Cappadonia *et al.* [2.28] observed that the second deposition peak, that is the peak closer to the Nernst potential for copper in sulphuric acid at low concentrations shifted towards the first deposition peak as the concentration was increased until they became superimposed at concentration > 1mmol /dm^3. In this paper the influence of the anion is suggested to be important, as different anions lead to different deposition properties for copper, it should be added that the variation in concentration of sulphuric acid also contributed to this difference. Shi *et al.* [2.29] carried out further studies on the interaction between anions and the metal, they kept the concentration of Cu^{2+} fixed while the concentration of sulphuric acid was reduced. This resulted in a reduction in the peak height of the deposition peak and merging of the two deposition peaks for copper ions on the gold (111) electrode.

2.4 Thiol layers

Studies in the literature have shown that electron transfer between the electrolyte and the electrode surface can be retarded by the introduction of self assembled monolayer (SAM) of thiol onto the electrode surface. This introduction of the thiol layer reduces the active area of the electrode and retards the exchange of redox species between the electrolyte and the electrode surface [2.30]. The analysis of thiol layers deposited over a gold electrode surface has been carried out using cyclic voltammetry. This technique has been applied as, (i) a qualitative tool to evaluate the film density or compactness of the thiol layer (ii) to probe the nature of the film-substrate interaction and (iii) to control the deposition of thiol layers onto a gold electrode surface through an applied voltage [2.31]. Electrodes modified with thiol layers give a decrease in peak current (CV) in response to reactions occurring at the electrode surface such as the oxidation of a redox probe. In addition, an increase in the difference between the potentials for oxidation and reduction peak potential of the redox probe and a tendency of voltammetry to adopt a sigmoidal line shape was observed [2.32]. These are all due to the blocking nature of the thiol layer on the gold electrode, in addition the passivity of the thiol layer will depend on the nature of the interrogating probe. The latter was shown by Krysiński et al [2.32] using cyclic voltammetry and different redox probes molecules; ruthenium hexamine chloride ($Ru(NH_3)Cl_3$), potassium ferrocyanide ($K_4Fe(CN)_6$) and benzoquinone to investigate the passive behaviour of a self assembled octadecanethiol monolayer on a polycrystalline gold electrode and observed differences in their heterogeneous electron transfer rate constants. The electrochemical behaviour of ruthenium hexamine chloride ($Ru(NH_3)Cl_3$) and potassium ferrocyanide ($K_4Fe(CN)_6$) were found to correspond to a reversible, diffusion – controlled electrode process, suggesting that the electron transfer might be occurring at pinhole sites [2.33]. The supporting electrolyte does have an effect on the analytical data as shown by Anna and Porter [2.34 & 2.35], who observed that capacitance measurements for a hexanethiol monolayer were sensitive to the choice of supporting electrolyte. They obtained, comparing the capacitance of a thiol layer in the presence of KCl and NaF, a larger capacitance in KCl than in NaF. Here they suggested that this difference was due to the larger, hydrated F^- ion been less likely to penetrate defect sites that the smaller Cl^- ion. The nature of the substrate surface has been suggested to affect the electrochemical behaviour of the monolayer film since the coverage of the film is affected by the smoothness of the substrate [2.36].

Structurally the alkanethiol monolayer formed on gold surfaces have been shown to exhibit a chain tilt of 20 - 30° form IR measurements [2.35].

In order to better understanding the interaction between the thiol layer and the working electrode, the stability of Au-SAMs have been investigated. Here electrochemical reductive, desorption studies have been carried out to probe the strength of the Au-S interaction and the intermolecular forces which stabilize the organic monolayer [2.37-2.38]. These investigations show that the film desorbs in alkaline solution through a one-electron reductive pathway as shown in equation 7.

$$AuS\,(CH_2)_n\,X + e^- \rightarrow Au(0) + S^-(CH_2)_nX \qquad (7)$$

Where X = CH_3, COOH, OH. Widrig *et al*. [2.39], in their study of the adsorption of monolayer of n-alkanethiols on Au and Ag surfaces, showed that upon adsorption of a thiol at the Au surface the hydrogen of the thiol group is lost and the sulphur atom undergoes a one electron oxidation.

2.5 Phospholipid layer studies

The desire to study the biological membrane in the laboratory has led to the reconstruction of the bilayer lipid membrane in vitro [2.40]. These lipid layers have also found other applications as tools for electrode functionalisation, in electrocatalysis, microelectronics and biosensors [2.41, 2.34 & 2.42]. Lipid layers can be doped with membrane constituents such as peptides, ion carriers, receptors, chromophores, redox-active species, oligonucleotides, proteins and whole cells allowing the study of electrical, optical and transport process occurring across the lipid bilayer [2.43].

Lipids are molecules composed predominately of hydrogen and carbon atoms, linked together by covalent bonds and they make up forty percent of the human body's organic matter. Triacylglycerols (fatty acid), phospholipids and steroids are examples of lipids present in the human body. Phospholipids are the lipids of interest for this project and are structurally similar to triacylglycerols, but for the presence of a phosphate group in place of a molecule of fatty acid (see fig 2.4). Phospholipids are

amphiphilic molecules that possess both hydrophilic headgroups (phosphate group) and hydrophobic tails (hydrocarbons chains) thus dissolution in the aqueous solution is not easy. However depending on the concentration and the ratio of the sizes of the headgroups and tails, they can spontaneously form different structures such as bilayer sheets (lipids with two hydrocarbon tails attached to each head group), micelles (lipids with a single hydrocarbon chain to each head group) and liposomes in the aqueous media. In these structures, the hydrophobic tails are concealed from the water while the hydrophilic groups remain in the water.

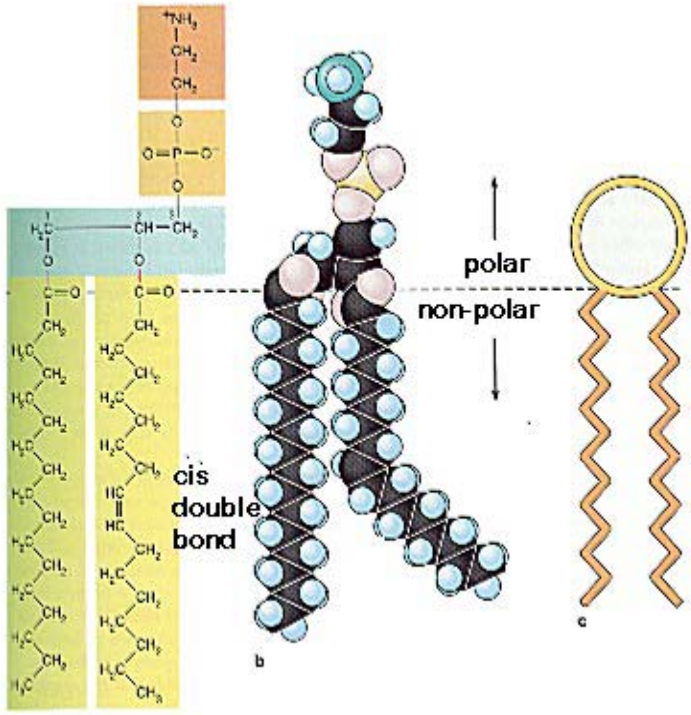

Fig 2.4 Diagram showing chemical structure of phosphotidylethanolamine. b; molecular structure and c; stick diagram of phosphotidylethanolamine. [2.44].

Interest in planar phospholipid layer membranes has been further supported by the relative ease and reproducibility of preparation involved and their long-term stability following its adsorption on a solid support. Long term stability is achieved by the immobilisation of the lipid layer onto a solid surface. Phospholipid membranes attached to solid surfaces are referred to as supported membranes. They can take a

variety of forms these include, integrated bilayer with a monolayer attached to the substrate surface either covalently or via ion bridges, or attachment to the surface could be achieved using thiol layers or thin polymer film such as dextran [2.45]. In this project the attachment of the phospholipid layer to the gold surface was carried out using thiol layer. The sulphur groups of thiol molecules form covalent bonds with gold films this combined with the hydrophobic interaction between the carbon chains of the thiol layer and lipids improve the bonding strength of the lipid layers to the gold films. Since the report that showed that dialkyl disulfides form oriented monolayers on gold [2.46] there has been a growing interest in this area. J. Sagiv [2.47] applied the silanization method for the attachment of lipids to solid supports. This method was extended by using alkoxysilanes in place of alkylchlorosilanes to covalenty attach molecular surface layers which contain exposed terminal –OH, -SH, -COOH or –NH groups. These terminal groups can be used to introduce either hydrophilic or hydrophobic reactive surfaces onto the thiol layer. [2.48-2.51]. Following on from this was the covalent attachment of sulphur bearing compounds on noble metals e.g. Au, Ag, Pt and Cu. These sulphur bearing compounds are applied mainly in their low oxidation states as thiols, thioethers and disulphides [2.35, 2.42, 2.46-2.51].

The processes involved in the interrogation of the lipid layer by electrical and optical techniques differ. The electrochemical method requires the exchange of ions between the working electrode and the bulk electrolyte (excluding capacitance studies), while optical techniques such as surface plasmon resonance technique directly probes the interface between the gold and lipid layer in contact with the gold surface for changes in the refractive index. A variety of other surface interrogative spectroscopic techniques have been applied in the study of lipid layers, such as surface enhanced Raman scattering [2.53] and electroreflectance [2.54]. Surface plasmon polaritons are coupled photon-plasmon surface electromagnetic waves that propagate parallel to a metal-dielectric interface within optical field that decays exponentially away from the metal surface. This optical field is sensitive to changes in refractive index occurring within this decay length of 200 nm. Surface plasmon resonance technique employs its sensitivity to this region in the analysis thin films, in order to determine index of refraction and thickness of the thin film. Surface plasmon resonance using the Kretschmann configuration has been applied in the study of biological molecules

adsorption where analysis is carried out by monitoring the shifts in the surface plasmon resonance minimum (see chapter 3). This shift are related to the thickness or refractive index change of the adsorped film that is by comparing the bare or modified electrode angle at surface plasmon resonance minimum to that when the adsorped film is introduced.

The modified electrode usually involves the immobilisation of a substance that is selective for the test analyte, e.g. adsorption of protein onto silane and alkanethiol self assembled monolayer [2.55-2.56], DNA hybridisation [2.57-2.58] and biotin-streptavidin (or avidin) binding studies [2.59]. Interest in the application of surface plasmon resonance technique in the study of adsorption of materials has grown over the years and this is reflected in is commercial application e.g. Biocore surface plasmon resonance adsorption instrument (by Pharmacia). Here the gold film is coated with carboxymethylated dextran (prevents non specific adsorption) where changes in the refractive index of the dextran due to the adsorption of the test analyte are monitored by the instrument. Surface plasmon resonance based on the Kretschmann configuration has been used to monitor, in situ, the electrochemically controlled film deposition and stripping processes [2.60-2.62]. Pockrand *et al*. [2.63], measured quantitatively the changes in SPR response to the deposition of closely packed self assembled monolayer of thickness 26.8Å. Applying a range of wavelengths between 4416Å and 6328Å they observed a shift in the resonance position to greater angles of incidence and a corresponding increase in the width of the resonance as the number of layers increased. These effects were more pronounced at the shorter wavelengths.

The electrochemical interrogation is widely applied in biosensing where most of the sensing reactions carried out using lipid layers, involves molecular recognition (ligand-receptor interactions) [2.64]. These biological layers introduce specificity to the analytical reaction carried out on the surface of the sensing device. The type of reaction observed is described as ligand-receptor reaction, which involve interactions such as substrate-enzyme reactions, hormone-gated channels, antibody-antigen reactions, redox-species induced or ion-channel specificity reactions. The principal function of the lipid layer is to modulate the transfer of ions across the analyte solution and the electrode surface. These processes can be monitored

electrochemically using methods such as cyclic voltammetry and ac impedance from which structural information of the lipid layer can be obtained. The lipid layer limits the transfer of ions through it due to its hydrophobic properties. Thus, the transfer of ions through the lipid layer is achieved in sensing devices based on electrochemical techniques by doping the membrane with ion channels or carriers. Lipid layers may also be doped with enzymes such as oxidases or dehydrogenases, in order to stimulate the conversion of the test analyte to an electroactive species, in addition the lipid layer can be modified with electron mediators such as TCNQ (tetracyanoquinodimethane), TTF (tetrathiofulvalene) or bipyridine, [2.65-2.68]. Compounds such as Fullerenes (C_{60}), which are highly hydrophobic in nature, have also being added to the lipid layer where they act as electron mediators [2.69] or photosensitizers [2.70].

The analytical potential of combining optical and electrochemical techniques for biological analysis has been previously demonstrated, where the combination of surface plasmon resonance and impedance spectroscopy gave sensitivities similar to those achievable using techniques such as enzyme-linked immunosorbent assays (ELISA). Here detection of changes of 0.5 Å or 50 pg / mm^2 [2.71-2.72] was reported.

2.6 Reference

2.1 H. A. Laitinen and M.S. Chao, J Electrochem. Soc. 108 (1961) 726.

2.2 H. Angerstein-Kozlowska, B.E. Conway, A. Hamelin and L. Stoicoviciu, Electrochimica Acta. 31 (1986) 1051.

2.3 H. Angerstein-Kozlowska, B.E. Conway, A. Hamelin and L. Stoicoviciu, J. Electroanal. Chem. 228 (1987) 429.

2.4 H. Angerstein-Kozlowska, B.E. Conway, K. Tellefsen and B. Barnett, Electrochim Acta. 34 (1989) 1045.

2.5 B.E. Conway, Prog. Surf. Sci. 49 (1995) 331.

2.6 G.M. Schmid and N. Hackerman, J. Electrochem. Soc. 109 (1962) 243.

2.7 R.S. Sirohi and M.A. Genshaw, J. Electrochem. Soc. 116 (1969) 910.

2.8 R.C. Plumb, J Phys. 25 (1964) 69.

2.9 T. Takamura, K. Takamura, W. Nippe and E. Yeager, J. Electrochem. Soc. 117 (1970) 626.

2.10 J. Horkans, B.D. Cahan and E. Yeager, Surface Science. 46 (1974) 1.

2.11 Y-T Kim, R.W. Collins and K. Vedam, Surface Science. 233 (1990) 341.

2.12 F. Chao, M. Costa, A. Tadjeddine, F. Abeles, T. Lopez-Rios and M-L. Theye, J. Electroanal. Chem. 83 (1977) 65.

2.13 D.M. Kolb in: H. Gerischer, W. Tobias (Eds), Advances in Electrochemistry Engineering, vol. 1, p 125, Wiley, New York, 1978.

2.14 J.Zhang, Y-E Sung, P.A. Rikvold, A. Wieckowski, J. Chem. Phys. 104 (1996) 5699.

2.15 J. Hotlos, O.M. Magnussen, R.I. Behm, Surf. Sci 335 (1995) 129.

2.16 T. Hachiya, H. Honbo, K. Itaya, J. Electroanal. Chem. 315 (1991) 275.

2.17 T. Nishizawa, T. Nakada, Y. Kinoshita, S. Miyashita, G. Sazaki, Hara, Sazaki, H. Komatsu, Surf. Sci. 367 (1996) L73.

2.18 N. Ikemiya, S. Miyaoka, S. Hara, Surf. Sci. 311 (1994) L641.

2.19 S. Manne, P.K. Hansma, J. Massie, V.B. Elings, A.A. Gewirth, Science. 251 (1991) 183.

2.20 J.W. Schultze and D. Dickertmann, Surf. Sci. 54 (1976) 489.

2.21 Z. Shi, J. Lipkowski, S. Mirwald, B. Pettinger, J. Electroanal. Chem. 396 (1995) 115.

2.22 T. M. Riedhammer, L.S. Melnicki and S. Bruckenstein, Phys. Chem. NF 11 (1978) 177.

2.23 N. Furuya and S. Motoo, J. Electroanal. Chem. 98 (1979) 189.

2.24 M.C. Santos, L.H. Mascaro and S.A.S Machado, Electrochimica Acta 43 (1998) 2263-2272.

2.25 O. R. Melroy, M. G. Samant, G. L. Borges, J. G. Gordon II, L. Blum J. H. White, M. J. Albarelli, M. McMillan and H. D. Abruna, Langmuir 4 (1988) 728.

2.26 M. Legault, L. Blum and D. A. Huckaby, J. Electroanal. Chem. 406 (1996) 79.

2.27 M. Watanabe, H. Uchida and N. Ikeda, J. Electroanal. Chem. 308 (1995) 255.

2.28 M. Cappadonia, U. Linke, K.M. Robinson, J. Schmidberger, U. Stimming, J. Electroanal. Chem. 405 (1996) 227.

2.29 Z. Shi and J. Lipkowski, J. Electroanal. Chem. 364 (1994) 289.

2.30 C.E.D. Chidsey, Science 251 (1991) 919.

2.31 O. Pierrat, N. Lechat, C. Bourdilion and J-M Laval, Langmuir 13 (1997) 4112.

2.32 P. Krysiński, M. Brzostowska-Smolska, J. Electroanal Chem. 424 (1997) 61.

2.33 H.O. Finklea, D.A. Snider, J. Fedyk, Langmuir 9 (1993) 3660.

2.34 Anna L. Plant, Langmuir 9 (1993) 2764.

2.35 M.D. Porter, T.B. Bright, D.L. Allura, C.E.D. Chidsey, J. Am. Chem. Soc 109 (1987) 3559.

2.36 R.P. Janek and W.R. Fawcett, Langmuir 14 (1998) 3011.

2.37 S. Arnold, Z.Q. Feng, T. Kakiuchi, W. Knoll, K. Niki, J. Electroanal. Chem. 438 (1997) 199.

2.38 T.W. Scneider, D.A. Buttry, J. Am. Chem. Soc 115 (1993) 12391.

2.39 C.A. Widrig, C. Chung and M.D. Porter, J. Electroanal. Chem. 310 (1991) 335.

2.40 D. Mueller, O. Rubin, H.T. Tien and W.C. Wescott, J. Phys. Chem. 67 (1963) 534.

2.41 P.E. Laibinis and G.M. Whitesides, J. Am. Chem. Soc. 114 (1992) 9022.

2.42 J.O. Swalen, D.L. Allara, J.B. Andrade, E.A. Chandross, S. Garoff, J. Isrealachivilli, T.J. McCarty, R. Murray, R.F. Pease, J.F. Rabolt, K.J. Wynne and H. Yu, Langmuir 3 (1987) 932.

2.43 A. Badia, S. Arnold, V. Scheumann, M. Zizlsperger, J. Mack, G. Jung, W. Knoll, Sensors and Actuators B 54 (1999) 145.

2.44 S.L. Wolfe, Molecular and Cellular Biology, Wadsworth Publishing company, 1993 p 155.

2.45 www.biocore.com.

2.46 R.G Nuzzo, F.A. Fusco and D.L. Allara, J. Am. Chem. Soc. 109 (1987) 2358.

2.47 J. Sagiv, J. Am. Chem. Soc. 102 (1980) 92.

2.48 J.D. Miller, H. Ishada Langmuir 2 (1986) 127.

2.49 I. Haller, J. Am. Chem. Soc. 100 (1987) 8050.

2.50 J.K. Yee, D.B. Parry. K.D. Caldwell. J.M. Harris, Langmuir 7 (1991) 307.

2.51 C.R. Kessel and S. Granick, Langmuir 7 (1991) 532.

2.52 S.D. Evans, E. Urankar, A Ulman, N. Ferris, J. Am. Chem. Soc. 113 (1991) 4121.

2.53 J. Pemberton, Electrochemical interfaces: Modern Techniques for in-situ interface characterization (H.D. Abruna, ed.), VCH, New York, 1991, ch. 5.

2.54 D. M. Kolb, Spectroelectrochemistry: Theory and Practice (R. J. Gale, ed.), Plenum Press, New York, 1988, chapter 4.

2.55 M. Mrkisch, G.B Sigal and G.M. Whitesides, Langmuir 11 (1995) 4383.

2.56 G. B. Sigal, C. Bamdad, A. Barberis, J. Strominger, G. M. Whitesides, Anal. Chem. 68 (1996) 490.

2.57 K. A Peterlinz, R. Georgiadis, T.M. Herne and M.J. Tarlov, J. Am. Chem. Soc. 119 (1997) 3401.

2.58 A.A. Kruchinin and Y.G. Vlasov, Sensors Actuators B 30 (1996) 77.

2.59 I. Haussling, H. Ringsdorf, F-J. Schmitt and W. Knoll, Langmuir 7 (1991) 1837.

2.60 E.F. Aust, S. Ito, M. Sawodny, W. Knoll, Trends polym. Sci 2 (1994) 313.

2.61 S. Heyse, H. Vogel, M. Saenger, H. Sigrist, Protein Sci 4 (1995) 2532.

2.62 E.F. Aust, M. Sawodny, S. Ito, W. Knoll, Scanning 16 (1994) 353.

2.63 I. Pockrand, J.D. Swalen, J.G. Gordon II, M.R. Philpott, Surface Science 74 (1977) 237.

2.64 J.R. Bourne, Biomed. Eng, 18 no 5 (1991) 323.

2.65 I.B. Ivanov, Thin Liquid Films: fundamentals and applications. Dekker, New York (1988) 927.

2.66 H.T. Tien, J. Phys. Chem. 88 (1984) 3172.

2.67 H.T. Tien, J. Electroanal. Chem. 174 (1984) 299.

2.68 H.T. Tien, J. Electroanal. Chem. 211 (1986) 19.

2.69 L.-G. Wang, X. Wang, A.L. Ottova and H.T. Tien, Electroanalysis 8 (1996) 1020.

2.70 L.-G. Wang, X. Wang and A.L. Ottova, Bioelectrochem. Bioenerg. 42 (1997) 161.

2.71 B. Rothenhäusler and W. Knoll, Nature 332 (1988) 615.

2.72 M.M.S. Löfas, I Ronneberg, E. Senberg, Bliedberg, I. Lundström, Sensors and Actuators B 5 (1991) 79.

Chapter 3

Principle of operation and design of the integrated optical surface plasmon resonance (IOSPR) sensor

3.1 Introduction

The development of integrated optical surface plasmon resonance device has been rapid since the recognition of the potential of surface plasmon resonance as a sensing technique [3.1-3.6]. This chapter gives a review on the principle of the interrogatory techniques applied using the integrated optical surface plasmon resonance device (IOSPR) for this project that is surface plasmon resonance and cyclic voltammetry. In addition a brief discussion of the design for the IOSPR device is given. Surface plasmon resonance is an optical technique that allows probing of refractive index changes occurring within the vicinity of a sensor surface where any phenomenon at the surface, which alters the refractive index, will elicit a change of the resonance. This change in the resonance is a direct result of changes in coupling conditions between the surface plasmon and exciting the optical wave due to alterations in the refractive index or thickness of the sensitive layer. The electrochemical technique applied here, that is cyclic voltammetry monitors the current in response to the chemical reaction occurring on the working electrode following the application of a potential between the working and reference electrode.

3.2 Surface plasmon resonance

A surface plasmon (SP) is an oscillation of free electrons that propagates along the surface of a metal such as gold. Excitation of these electrons can be achieved when both incident and created particle have the same frequency and momentum (fig 3.1). Surface plasmon (SP) is a TM-polarized wave, its vector of magnetic intensity is parallel to the metal-dielectrics interface and its field exponentially decays from the interface into both metal and dielectrics. This mode exists when Re (ε_m) < 0 and $|\mathrm{Re}(\varepsilon_m)| < \varepsilon_s$, where ε_m is the relative permittivity of the metal and (ε_s) is the relative permittivity of the dielectric. However, figure 3.2 indicates that the dispersion relation of the surface plasmon at a metal-dielectric interface lies always on lower ω for given β from the dispersion relation of the photon propagating in the dielectrics. This implies that at a particular frequency the photon's propagation constant in the dielectric is always lower than that of the surface plasmon.

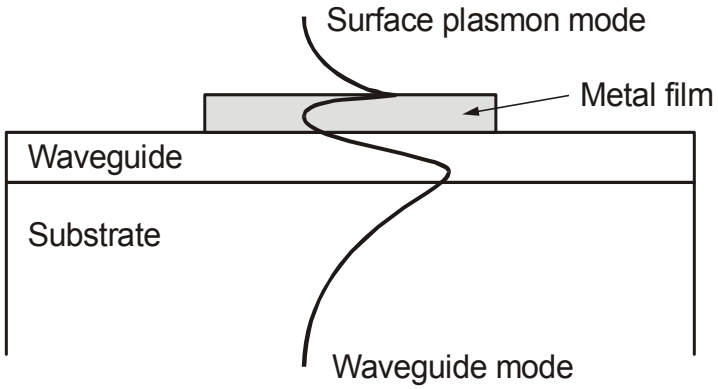

Fig 3.1 Excitation of surface plasmon

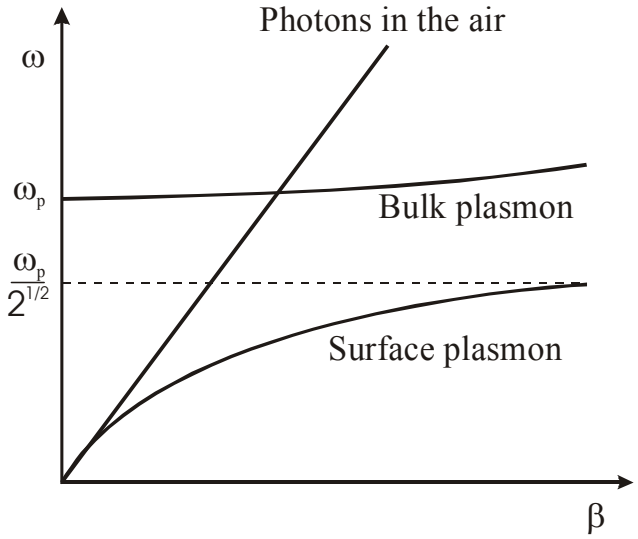

Fig. 3.2 Dispersion relation of bulk plasmon and surface plasmon at metal – air interface. Where, ω *is the angular frequency and* ω_p *is the plasma frequency.*

The propagation constant (β) of the SPR wave propagating at the interface between the dielectric and metal is given by the expression below:

$$\beta = \kappa_o \sqrt{(E_m n_a^2 / E_m + n_a^2)} \qquad (3.1)$$

Where $\kappa_o = 2\pi / \lambda$ is the free space wave number, λ is the free space wavelength, E_m is the dielectric constant of the metal ($E_m = E_{mr} + iE_{mi}$ that is the real and imaginary parts of the dielectric respectively) and n_a^2 is the square of the refractive index of the dielectric (analyte). Efficient coupling of light energy into the surface plasmon requires a device to slow the light, as surface plasmons can not be excited directly, thus a photon-surface plasmon coupler needs to be introduced. The latter allows the photon momentum to be increased, in order to match that of the surface plasmon. This can be achieved by using a prism (see fig 3.3), grating coupler (see fig 3.4-3.5) or an integrated SPR planar waveguide (see fig 3.6).

3.2.1 Prism methods

The prism coupler employs the ATR method (Attenuated Total Reflection), where an incident photon (p-polarised light) propagates through a prism, totally reflects at the prism base and its evanescent field reaches the metal-dielectric interface at which the surface plasmon may be excited. Excitation occurs when the component of the wavevector of the incident light parallel to the interface is equal to the surface plasmon wavevector.

$$K = (2\pi /\lambda)n \sin\theta = K_{sp} \qquad 3.2$$

Where K_{sp} is the surface plasmon wavevector.

$$K_{sp} = 2\pi/\lambda \, (E_m E_s / E_m + E_s)^{1/2} \qquad 3.3$$

E_m= dielectric of metal

E_s= dielectric of the dielectric over the gold surface

This reveals itself as a drop in the intensity of light reflected out of the prism. Enlargement of the incident photon propagation constant is attained when the prism refractive index is higher then refractive index of the dielectric at whose interface the surface plasmon is excited. This excitation of the surface plasmon is achieved by varying θ until a minimum is observed in the intensity of the reflected light.

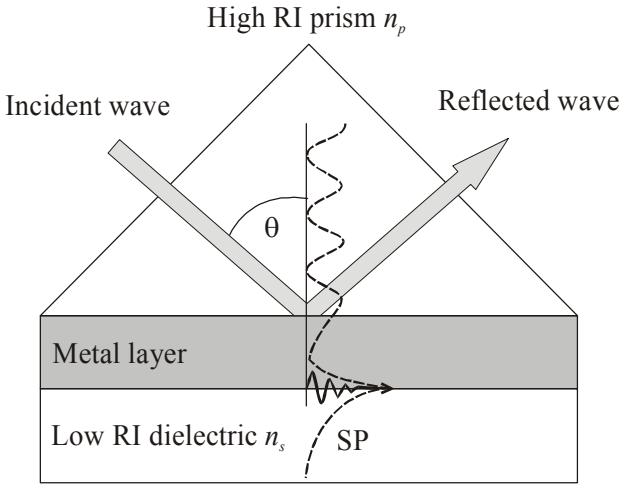

Fig. 3.3 Kretschmann configuration of the ATR prism coupler.

The exponential field at the boundary between the metal and the dielectric, extends into both regions, that is the metal and the dielectric. These exponential fields decrease exponentially with distance from the interface with a penetration depth [3.8] of:

$$t_d = 1/k_o\varepsilon_d \,|\mathrm{Im}\,\{\sqrt{(\varepsilon_m + \varepsilon_d)}\,\}|, \text{ into the dielectric} \qquad (3.5)$$

$$t_d = 1/k_o \,|\mathrm{Im}\,\{\sqrt{(\varepsilon_m + \varepsilon_d / \varepsilon_m)}\,\}|, \text{ into the metal.} \qquad (3.6)$$

Where ε_m and ε_d are relative permittivities of the metal and dielectric respectively. This configuration has been applied for surface analysis and biological sensing. Here changes in the dielectric of the dielectric due to the introduction of a layer onto the surface, changes in the refractive index of bulk analyte or test molecules entering the evanescent field will affect the coupling conditions required for the excitation of the surface plasmon. In order to compensate for this change in the coupling conditions, the angle θ has to be varied until maximum attenuation is obtained from the reflected light. When the Kretschmann configuration is applied for surface analysis, the change in θ or shift in the position of resonance minimum is related to the observed change at the surface of the metal. Improvement in the analytical potential of the Kretschmann configuration has seen modifications to the architecture of the device with the introduction of multichannel sensing capabilities and dual channel sensor with wavelength interrogation [3.11 & 3.12], sixteen channel sensor with intensity

measurement involving CCD camera have been reported. In addition, there are commercially available four - channel sensors with angular interrogation marketed by BIAcore [3.13].

3.2.2 Grating coupler methods

In the case of the grating coupler, the photon propagation constant is increased via diffraction on a metal grating. At diffraction, momentum of diffracted photons is altered as given in the equation below, allowing the excitation of the SP on the metal grating surface.

$$\beta_{diff} = k_o n_s \sin(\theta) + m(2\pi/\Lambda) \qquad (3.4)$$

Where Λ is the grating period, n_s is the dielectric refractive index (RI), $m = 0, \pm 1\ldots$ is the diffraction order, θ is the output coupling angle and k_o is the light wave propagation constant in the vacuum.

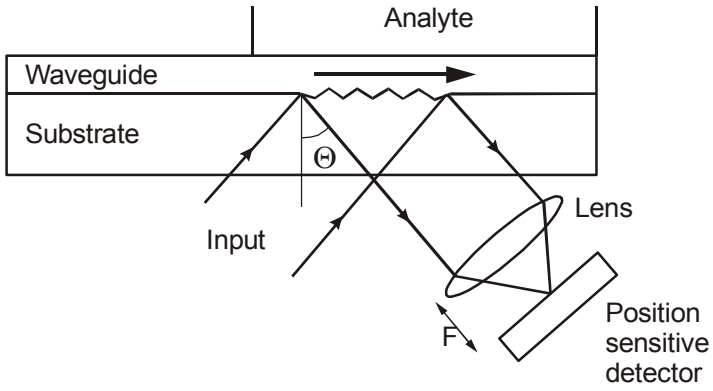

Fig. 3.4 Scheme of an input grating photon-SP coupler.

The grating coupler, as with the Krestschmann configuration, can be applied to sensing changes in the refractive index of the dielectric above the metal surface. There are two forms of the grating couplers, namely the input and the output grating couplers. With the input grating coupler, the light is coupled directly onto the grating and the information required is then obtained by either coupling light reflected from the grating as shown in fig 3.4 or coupling light transmitted through the waveguide, following its interaction with the grating.

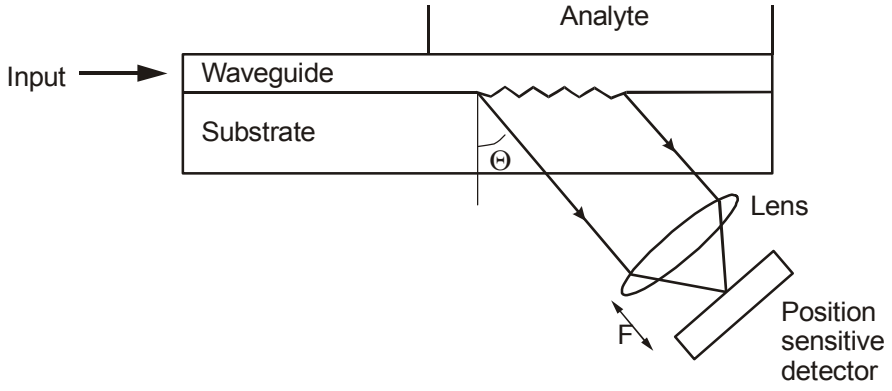

Fig. 3.5 Scheme of output grating photon-SP coupler.

Output grating coupler works by coupling light into the waveguide and this is transmitted along the waveguide onto the grating. The light reflected from the grating as shown in fig 3.5 is then coupled out of the structure, onto a detector and analysed. Equation 3.4 shows that the angle made by the reflected beam from the grating is related to the photon propagation constant. Thus, changes in the propagation constant in response to changes in the refractive index at the grating will cause a change in the output coupling angle θ. The observed shift in the output coupling angle θ is related to the changes occurring at the grating surface.

3.2.3 Integrated optical surface plasmon resonance (IOSPR).

In the case of the integrated optical surface plasmon resonance device, the incident wave that propagates along the waveguide is transverse magnetic polarized. This transverse magnetic wave has its principal component of the magnetic field parallel to the substrate and waveguide surface and normal to the direction of propagation while the principal component of the electric field is normal to the substrate surface [3.7]. The coupling of light into the metal surface results in the creation of a plasmon, which in turn generates an electromagnetic field that extends about 100-200 nanometers above and below the metal surface (see fig 3.6).

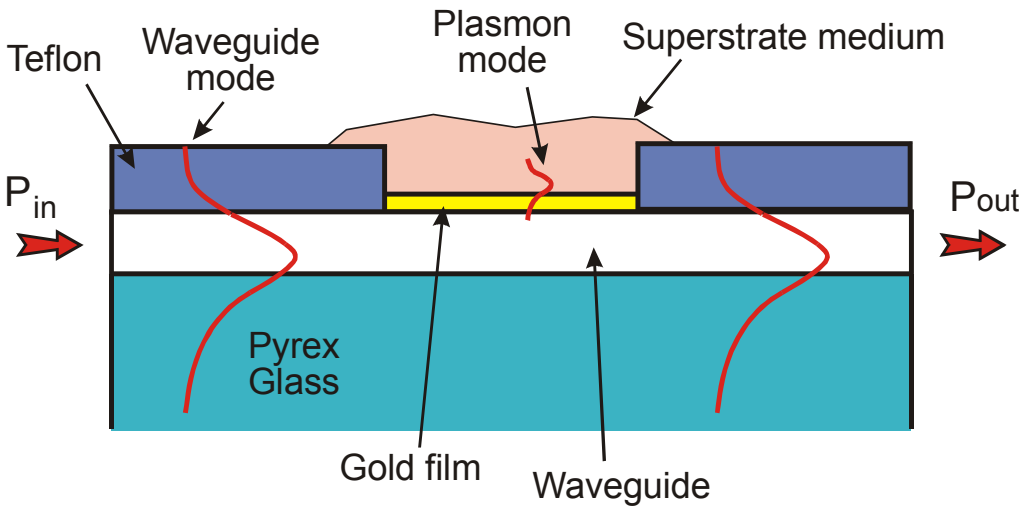

Fig 3.6 Side view of the integrated optical device

Excitation is shown by a drop in the intensity of the light coupled out of the waveguide substrate when compared to that initially launched into the waveguide. This drop is a direct result of the lossy nature of the surface plasmon. The refractive indices of these materials on both sides of the metal (substrate and superstrate region) affect the amount of coupling and the intensity of the plasmon. Small variations in the refractive index of the sensed medium (superstrate region) produce large changes in the attenuation of the waveguide mode, that is a change in the observed transmittance. This allows for reactions that modify the refractive index at the superstrate region to be followed. Gold is the preferred metal for application, although a variety of other metals can sustain surface plasmon resonance, where the metal must have conduction band electrons capable of resonating with light of the appropriate wavelength. These other metals are not as practical as some are violently reactive (Na), too broad in their SPR response (Cu, Al), or too susceptible to oxidation (Ag).

The use of the waveguide obviates the need for bulk-optical components and accurate angle measurement that are required for the Kretschmann configuration. In addition, batch production and multichannel sensors are easily achievable using waveguide optical systems. This multichannel sensing architectural ability improves the analytical potential of the device in terms of referencing out background noise, in addition to the obvious advantage of possible simultaneous analysis of different test compounds. The integrated optics technologies are better suited for these applications

as a much higher number of parallel channels can be integrated on a single chip [3.4-3.5 & 3.9]. The resonance interrogatory technique applied in this thesis using the integrated optical device is based on analysis of intensity change.

3.3 Cyclic voltammetry

Cyclic voltammetry is invaluable in the preliminary investigation of any electrochemical system. The cyclic voltammogram obtained gives an insight into what reactions are taking place, such as adsorption reactions, coupled homogeneous reactions (electron transfer reactions that are coupled to homogeneous reactions), e.g.

Electron transfer: $Y\ (aq) + e\ (m) \rightarrow X\ (aq)$ (3.7)

Homogeneous chemical reaction: $X\ (aq) \rightarrow$ products (3.8)

Reference [3.14] gives a detailed analysis of diagnostic tests that can be carried out to determine the reaction taking place at the working electrode.

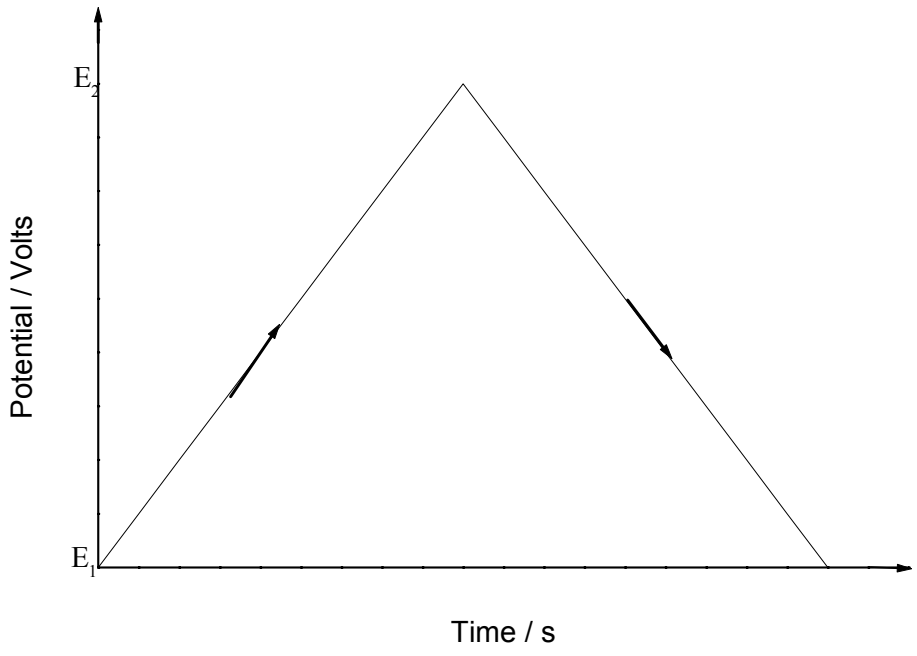

Fig 3.7 Potential time profiles for cyclic voltammetry

Cyclic voltammetry is carried out by scanning the electrode potential between two limits E_1 and E_2 and then scanning back to E_1. This may be repeated several times at

a given sweep rate (see fig 3.7). The sweep rate in the anodic scan in most cases is similar to that of the cathodic (negative) scan [3.15].

Generally, as the potential is swept from E_1 to the more positive potential E_2, no current is observed initially due to the applied potential not sufficient to cause the transfer of electrons to the electrode from the species in solution. A gradual increase in current is observed as the potential is increased to potentials that are capable of causing the oxidation of X (see equation 3.7). A peak current is obtained after which further application of potential leads to a decrease in current in an unstirred solution. This decrease is due to the rate of diffusion of new X to the electrode becoming a limiting factor assuming no migration or random convection current is present. Diffusion is the only means of mass transport to the electrode when the reaction is in an unstirred solution. The initial store of X at the immediate vicinity of the electrode would have been used up thus X would have to travel further to get to the electrode. At the potential E_2 the direction of scan is reversed and the opposite effect observed in the forward direction is seen, that is in terms of the current generated and the product formed (the reduction of Y to X). The three-electrode system is used here in place of a two-electrode system. The two-electrode system involves the auxiliary electrode (reference) passing current in the circuit and at the same time controlling the potential of the set up. This sometimes generates problems in terms of potential stability of the reference electrode. This stability problem can be attributed to the alteration of the species activities at the vicinity of the reference electrode when current is passed though the circuit. This leads to a variation of the reference electrode potential, in which case the measured current can not be assigned solely to the working electrode. When a potential is applied between the working and reference electrodes any measurements made would be a combination of the reaction at the electrode of interest and that of the reference electrode. Thus, making it impossible to separate the effects of the two electrodes.

$$E = (\phi_m - \phi_s) + iR + (\phi_s - \phi_{REF}) \qquad (3.9)$$

Where E, is the potential, ϕ_m is the metal potential, ϕ_s is the solution potential, iR is the iR drop (voltage drop) R is the electrical resistance of the solution and ϕ_{REF} is the

reference potential. Ideally, (ϕ_m -ϕ_s) would vary while (ϕ_s - ϕ_{REF}) should remain constant. This is not the case with a two-electrode system when a large current is applied, thus a third electrode is introduced known as the counter electrode.

With the three-electrode system, the potential is applied between the working electrode and the reference electrode while the current flows between the working and the counter electrode. This allows the potential at the reference electrode to remain constant. The system is controlled by a potentiostat, which also has built into it a triangular wave generator that allows the potential to be swept in the anodic direction and back in the cathodic directions during the cyclic voltammetry runs.

3.3 Design of the integrated optical device

The initial steps carried out in the design of the integrated optical surface plasmon device required the application of a numerical waveguide design model written by R.D. Harris [3.16], which allows one to identify a practical sensor design, when considering the large number of variable parameters that need to be addressed. These variable parameters are the choice of glass, metal and laser source. With the question of what metal, gold was the obvious choice due to its inert property when exposed to an aqueous environment. Gold is also a good electrical conductor for electrochemical application and can be bound firmly to the glass following surface treatment to the glass using either thiol or chromium (see chapter 4).

The solutions of the reactions carried in this project have refractive indices close to 1.35, thus a surface plasmon formed between gold and a dielectric of index 1.35 at a wavelength of 633 nm, has an effective index of 1.47 [3.16]. To create phase matching between the surface plasmon formed at the gold-dielectric interface and a TM waveguide mode in a glass, this TM guided mode should have an effective index close to 1.47. Pyrex glass has a refractive index of 1.47 at 633nm and the exchange of the mobile sodium ions in this glass for potassium ion gives rise to a surface index of approximately 1.478. The guided TM modes transmitted through the waveguide formed by K^+ ion exchange will then have an effective index of 1.47-1.48, which falls within the range required for phase matching between the surface plasmon and waveguide mode.

The device used in this project was a K^+ - Na^+ ion exchanged Y-junction waveguide formed in a Pyrex glass. The exchange of the Na^+ ion in the Pyrex glass for K^+ gives rise to one of the smallest change in the refractive index of the surface of the Pyrex achievable using any of the ion exchanges available. This is required, in order to keep the refractive index of the waveguide as close as possible to that of the Pyrex glass. In addition, the process of ion exchange carried out in a molten bath, is a cheap and practical way of introducing single moded waveguide onto the Pyrex glass.

The numerical model in addition, to its application in the design of the device was used in predicting the performance of the device following modification of the gold-dielectric interface. This changes in the gold-dielectric interface causes shifts in the surface plasmon curve as shown in figs 3.9-3.10 following the introduction of a thiol and phospholipid layer over the gold film.

Application of a Y-junction waveguide shown in fig 3.8 allowed for the excitation and referencing to be carried out using a single polarisation (the TM polarisation). Here one of the arms of the Y-junction waveguide acts as the reference arm and is physically isolated from the superstrate medium by the presence of the Teflon layer. The other arm is coated with a gold film of 35 ± 5 nm and is exposed to the superstrate medium. The data obtained is a ratio of the intensity of both reference and sensing arms of the waveguide. Teflon of 700 nm was deposited over the whole substrate surface, leaving windows over the gold pads to allow for interaction with the analyte. The deposited Teflon insulates the reference arm from the analyte, protects the gold contacts allowing for reuse (clamping of the cell over the substrate will damage the gold contacts). In addition, this reduced the potential of the clamped cell adsorbing light transmitted across the transducer (see fig 3.8). A cylindrical glass cell of diameter 1.5 cm and both ends open was placed over this substrate in most of the reactions carried out involving the electrochemical electrodes. The gold pads serve as the working electrode, with a platinum wire (counter electrode) and saturated calomel electrode (reference electrode) were placed in the cell (see fig 5.2 chapter 5).

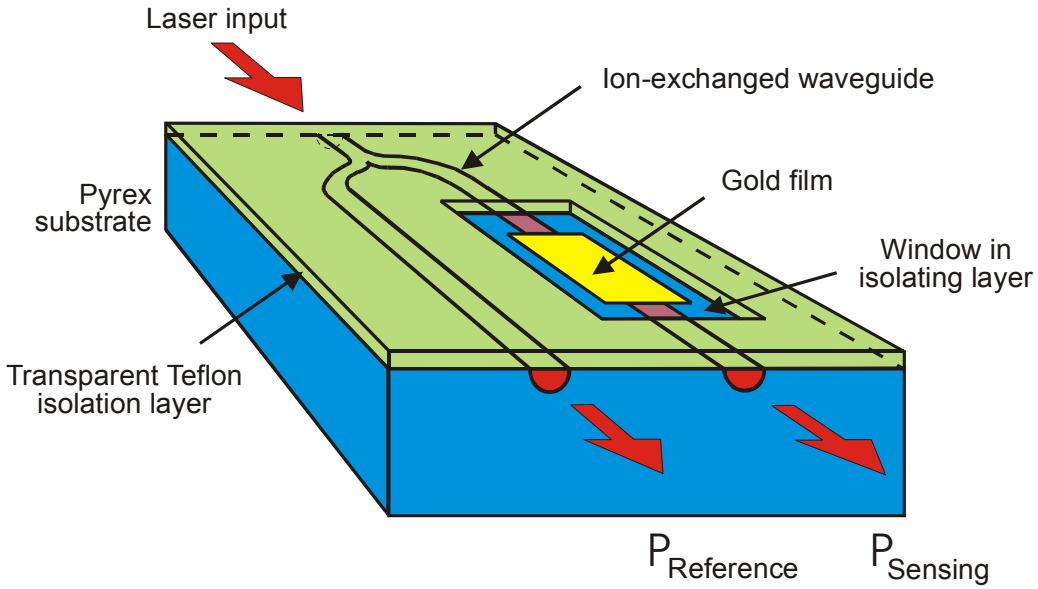

Fig 3.8 Diagram of the IOSPR sensor Y-junction waveguide

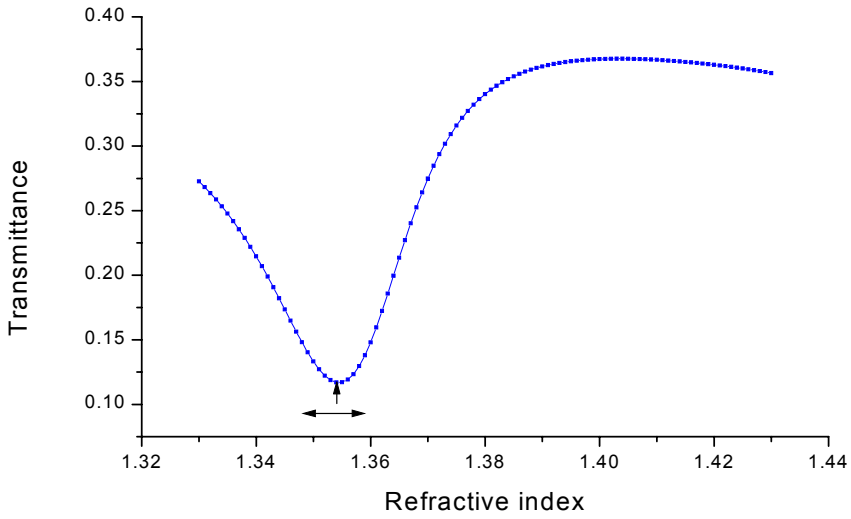

Fig 3.9 numerical surface plasmon resonance curve

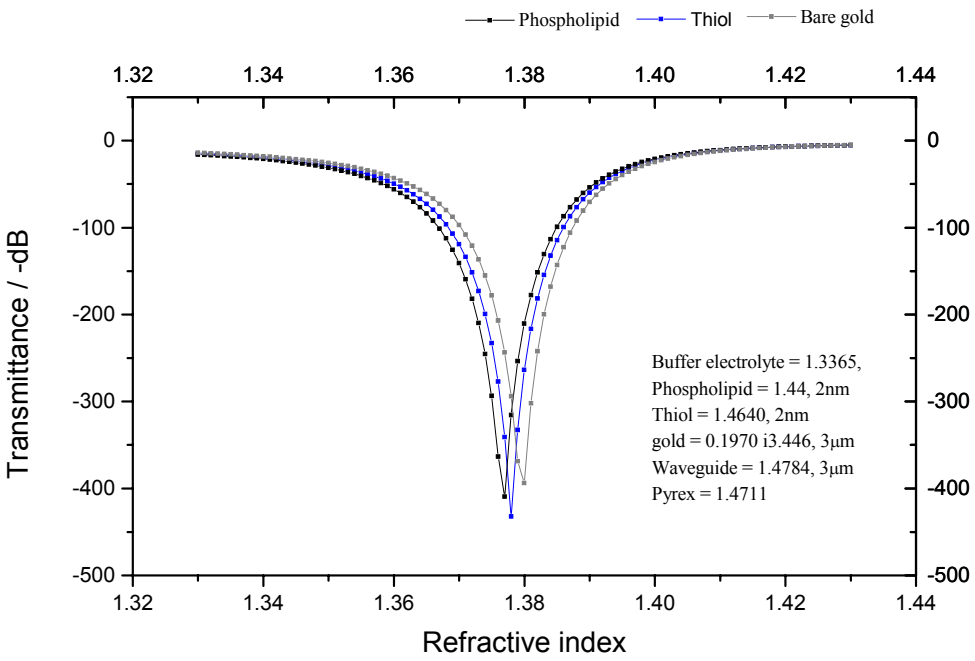

Fig 3.10 plot showing the log of the transmittance value against refractive index of a numerical curve in response to the introduction of thiol and phospholipid layers over the gold film.

3.4 References:

3.1 C. Nylander, B. Liedberg, T. Lind, Sensors and Actuators 3 (1982) 79.

3.2 B. Liedberg, C. Nylander, I Lundstrom, Sensors Actuators 4 (1983) 299.

3.3 B. Liedberg, C. Nylander, I Lundstrom, Biosensors Bioelectron. 10 (1995) i-ix).

3.4 C.R. Lavers, J.S. Wilkinson., Sensors and Actuators B 22 (1994) 75.

3.5 R.D. Harris, J.S. Wilkinson Sensors and Actuators B 29 (1995) 261.

3.6 C. Mouvet, R.D. Harris, C. Maciag, *et al*. Anal. Chim. Acta 338 (1997) 109.

3.7 D. Marcuse, Theory of Dielectric Optical Waveguides, Academic press, London (1991) 2nd edition.

3.8 H. Raether, Surface Plasmons Springer, Berlin 1988.

3.9 J. Homola, R. Slavík, J. Ctyroký, Optics Letters 22 (1997).

3.10 J. Ètyroký, J. Homola, P.V. Lambeck, S. Musa, H.J.W.M. Hoekstra, R.D. Harris, J.S.Wilkinson, B. Usievich, N.M. Lyndin, Sensors and Actuators B, 54 (1999) 66.

3.11 J. Homola, H. B. Lu and S. S. Yee, Electronics Letters 35 (1999) 1105.

3.12 G.C. Nenninger, J.B. Clendenning, C.E. Furlong, S.S. Yee, Sensors and Actuators B, 51 (1998) 38.

3.13 www.biacore.com

3.14 R. Greef, R. Peat, L.M. Peter, D. Pletcher, J. Robinson, Instrumental methods in electrochemistry Southampton electrochemistry group 179.

3.15 C.M. Ferro, A.J. Calandra and A. J. Arvia, J. Electroanal. Chem., 65 (1975) 963.

3.16 Thesis by R. D. Harris, Waveguide Surface Plasmon Resonance Biosensors (1996) University of Southampton.

Chapter 4

Fabrication and Verification of IOSPR Device

4.1 Introduction

This chapter deals with the fabrication and characterisation of the integrated optical surface plasmon resonance (IOSPR) device. Following the fabrication of the IOSPR device, a number of experiments were carried out to test the optical properties of the device. The experimental optical analysis of the device involved measuring the optical response of the device to changes in refractive index and the effect of varying the length of the gold film on the transmittance. The surface plasmon resonance (SPR) plot obtained from varying the refractive index revealed the sensitivity of the device to detecting changes in the refractive index of the test compound. This SPR plot also gave the detection limit of the device. The underlying theories for the operation of this device has been studied and discussed previously [4.1] and the fabricated device used for the project is based on that reported.

4.2 Fabrication of optical waveguides

4.2.1 Cleaning process

Pyrex glass (substrate 5 x 5 mm) was cleaned using a Q – tip soaked in Ecoclear ™, in order to remove wax from the Pyrex glass. This substrate was then rinsed in de-ionised water, wiped with acetone to remove inorganic molecules and finally rinsed in propanol to remove acetone. The Pyrex glass was then sonicated in Ecoclear ™ for 20 min, then in acetone for 20 mins and finally in propan-2-ol for 20 min. The substrate was later placed in a beaker containing H_2O_2 and H_2SO_4, in the volume ratio 1:2 (piranha solution) for 15 minutes at room temperature. Following the treatment of the substrate with piranha solution this substrate was rinsed thoroughly with de – ionised water and dried using nitrogen gas.

4.2.2 Ion exchange

Next 200 nm of aluminium was deposited on the substrate by thermal evaporation. Two sets of five Y-Junction waveguide channels of widths 2 μm and 3 μm were opened in the aluminium film by conventional photolithography giving rise to a diffusion mask. The substrate was then immersed in the ion source that is pure

KNO_3 for 7.5 hours [4.1] at 389 °C then rinsed using de – ionised water. The required diffusion depth of the K^+ ions is controlled by the temperature and the period of immersion.

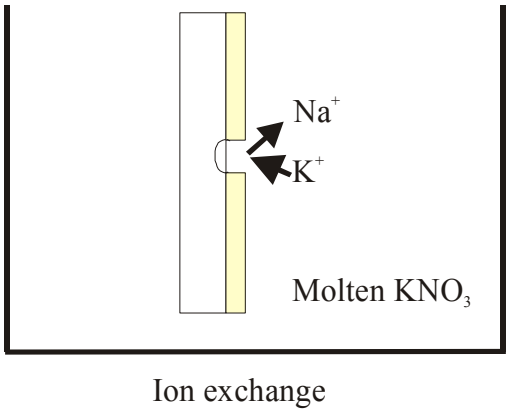

Fig 4.1 The exchange of Na^+ ion for K^+ Ion in the glass via the diffusion mask.

Pyrex glass has a higher concentration of mobile Na^+ ion than in the KNO_3 melt, while the melt has a higher concentration of K^+ ion than in the substrate. These two species, Na^+ and K^+ counter diffuse, so that material is exchanged between the substrate and the melt (see fig 4.1). The diffusion mask acts as an effective barrier to the ions allowing only transfer of the mobile ions to occur at the opening. This results in the K^+ ions from the melt occupying the place left by the Na^+ ions. The structure of the Pyrex glass remains the same but the optical properties of the glass are changed at the point of exchange. Changes in optical properties are due to the different electrical polarizabilities of the ions, their different sizes (ionic radii) and the formation of mechanical strain [4.2].

Table 4.1

	Na^+	**K^+**
Ionic radius	0.95×10^{-10} m	1.33×10^{-10}m
Electrical polarizability	0.43×10^{-30} m^3	1.33×10^{-30} m^3

These different properties introduce an increase in refractive index at the region of ion exchange, thus giving rise to a guiding region. Alignment marks were then etched into the glass using an ion beam etcher, applying an exposure time of 10 min, finally

the Al mask was etched off using an Al etch at 50 °C then rinsed in de – ionised water and dried in a nitrogen gas stream.

4.2.3 Polishing of the waveguide:

The edges of the ion-exchanged substrate were polished to allow for efficient end – fire coupling of the incident light into and out of the waveguide. The edge of the waveguide has to be smooth that is free of defects such as scratches and pits at the edge and below the edge surface. Presence of cracks often occurs under the edge surface of the substrate after polishing. These cracks will cause an increase in waveguide loss if the cracks are formed at the site at which the waveguide is formed. The presence of these cracks will lead to scattering of the light coupled into the waveguide. The problem of cracks also applies to the surface of the substrate on which the gold film is deposited. The evanescent wave associated with the light in the waveguide travelling in the damaged area will give rise to a very lossy waveguide. Pure mechanical polishing tends to leave scratches just below the mirror finished surface, but optical interrogation technique requires a scratch – free surface. This is achieved by combining chemical polishing to the mechanical polishing. Chemical polishing gives rise to a surface that is free of damage but is not smooth, mechanical polishing solves the lack of smoothness. Syton is used in the polishing of the end face of the Pyrex glass, as it is chemo–mechanical in its polishing property. Syton when applied during the polishing process of glass produces one with a surface that is defect free and smooth.

4.2.4 Deposition of the gold film

The cleaning process described above was then repeated again before gold could be deposited onto the glass. In order to improve the adhesion of gold to the substrate, the substrate was treated with the organic compound (3-mercaptopropyl) trimethoxysilane (MPS). MPS, water and propan-2-ol (IPA) in the ratio 1 : 1 : 46 (mass) were placed in a reflux evaporator with the substrate in the solution. The solution was brought to reflux then left under reflux for 15 min after which the substrate was rinsed with IPA, blow dried with a jet of nitrogen gas, then placed in an oven at 100 °C for 8 min. This step with the MPS treatment was repeated one more time before the deposition of gold.

Gold was then deposited on the glass slide using the Edwards thermal evaporator at 1 nm/s deposition rate and a pressure of $1x\ 10^{-6}$ torr. Using the second

photolithographic mask the electrode pattern was defined by photolithography (see fig 4.2). The thickness of gold deposited was measured using an alpha – step 200 stylus profilometer.

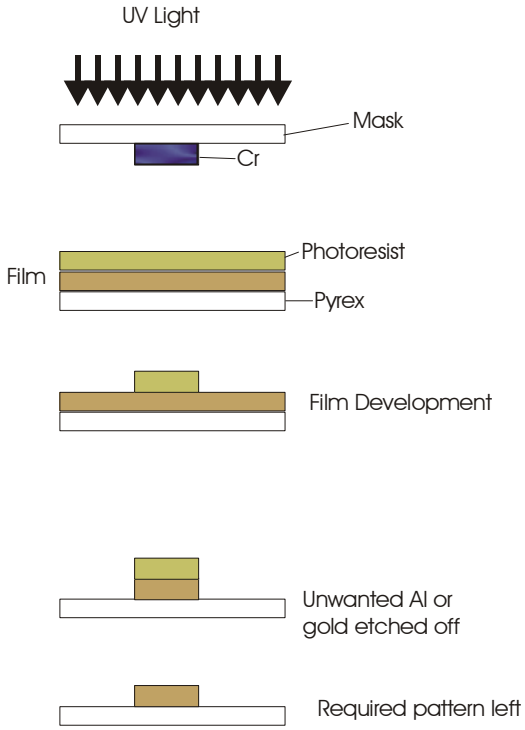

Fig 4.2 Photolithography

One principal problem with metal coating is the poor adhesion of the film (e.g. gold) to the substrate (e.g. Pyrex glass). Metals that can be used for SPR include Al, Cu, Ag and Au. Both Au and Ag are more generally used but do not form chemical bonds with glass, thus the adhesion of these films is low [4.3]. Chromium has been used to improve the adhesion of gold onto glass [4.4]. However this method has its drawbacks, as gold films of the thickness applied in this project (35 ± 5 nm) are appreciably porous thus allowing for the diffusion of chromium through the gold film. Literature report on cyclic voltammetry of gold in perchloric acid with chromium underlayer indicate that the cyclic voltammogram obtained exhibited peaks characteristic of a chromium in perchloric acid plus that of gold in perchloric acid [4.5]. Optically the presence of chromium will broaden the SPR curve thus limiting its analytical application [4.6]. Titanium has also been used to improve the adhesion of gold film on glass [4.7].

An alternative to this method is application of (3-mercaptopropyl) trimethoxysilane (MPS) to the surface of the glass before the deposition of the gold film.

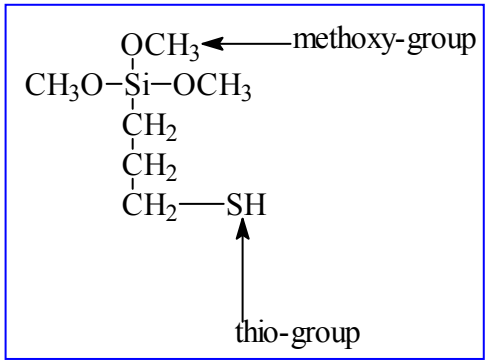

Fig 4.3 Chemical structure of (3-mercaptopropyl) trimethoxysilane.

The chemical structure of the compound MPS is shown in fig 4.3. The chemical bond involved in its adhesive property is achieved by a combination of chemical reactions [4.8]. The methoxy group reacts with water in the solution containing water + MPS + propan-2 ol to form silanol (Si-OH) groups which in turn reacts with the hydroxyl groups present on the surface of the Pyrex glass to form interfacial covalent bonds. Subsequent adsorption results in the silanol groups condensing with each other to form a polysiloxane (Si-O-Si) network. The sulphur group reacts with the gold film to form silane-gold covalent bonds [4.9].

The application of MPS to the Pyrex glass in this project initially followed the process laid out by Goss *et al.* [4.5], but work carried out in this project showed that about 50 % of the gold strip was lost after carrying out cyclic voltammetry in sulphuric acid. Few modifications were applied to Goss *et al.* stated method of leaving the glass after reflux in the solution for 10 min, initially this time period was increased to 20 minutes but no improvement was observed. Below is a picture of a typical gold strip with the joint between the "sensor strip" and the connection to the electrical contact strip lost (fig 4.4). In some cases such as that shown below, the stripping of the sensor strip was also observed.

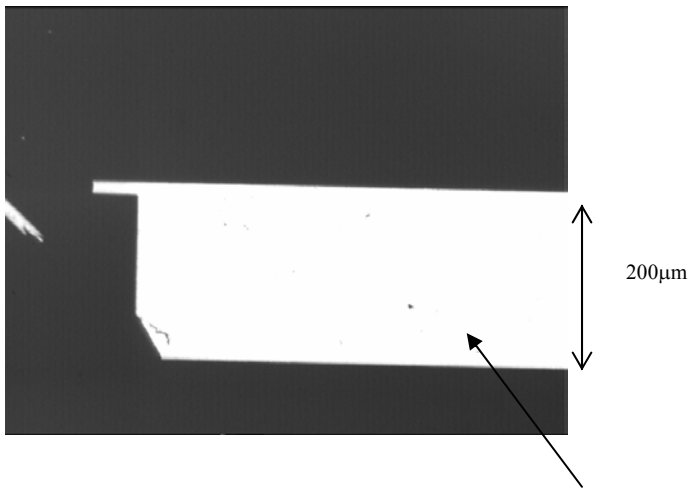

Fig 4.4. A picture of a gold film strip taken from the integrated optical device, showing a broken connection between the sensing surface and connection track following the oxidation of the gold film in a solution of 0.2 M sulphuric acid.

In order to circumvent this problem, the number of cycles of coating and the curing at the MPS treatment phase was repeated three times, which solved the problem. This increase in MPS treatment created a problem of its own when the substrate was later subjected to repeated gold etching and gold re-deposition that is recycling of the device. The time required for the etching of the gold to occur (usually 8 s) varied from sample to sample. The information derived from this observation was that repetitive coating and stripping of gold from the Pyrex glass produced successive gold film of better adhesion. Thus in place of leave the Pyrex glass in a hot solution of the MPS mixture for 10 min as suggested by Gross *et al*. [4.5] the Pyrex glass was left under reflux for 15 min with the cycle repeated twice. This solved the adhesive problem. The thin film electrode fabricated using a thermal evaporator that was used solely for gold deposition had better adhesive property when compared with the thin film fabricated using an evaporator used for other metal deposition. The evaporator used solely for gold deposition gave 100 % gold strip retention after electrolysis in comparison to 60 % obtained using the thermal evaporator used for other metal deposition. It should be stated that pre-coating of the latter using a dummy sample gave 100 % gold strip retention.

4.2.5 Deposition of the Teflon layer

The next fabrication process was carried out to insulate the reference arm from the analyte and protect the gold contacts from mechanical damage, as clamping of the cell over the substrate will damage the gold contacts. The presence of Teflon also reduced the potential of the clamped cell's o-ring to adsorb light transmitted across the substrate. The substrate which now had a gold film deposited over one of the Y-junction waveguide arm was gently cleaned using acetone, IPA and then rinsed in de–ionised water. Primer and photoresist were then applied onto the substrate by spin coating and softbaked at approximately 75°C for 30 min. The mask used for the photolithography was designed so that on lift off, the entire surface of substrate is covered with Teflon with exception of the gold film pads (see fig 4.5) and the two gold contacts at the edges [4.1]. After the alignment of the substrate in the mask aligner, the substrate was then exposed to UV light for eight seconds. Following the exposure, the substrate was placed in a beaker containing chlorobenzene for five minutes, before being developed. Teflon AF 1600 of 700 nm thickness was then thermally deposited on top of the photoresist covered substrate. The openings at the gold film pads and contacts at the edges were created by soaking the sample in acetone, then rinsed off using IPA and finally deionised water.

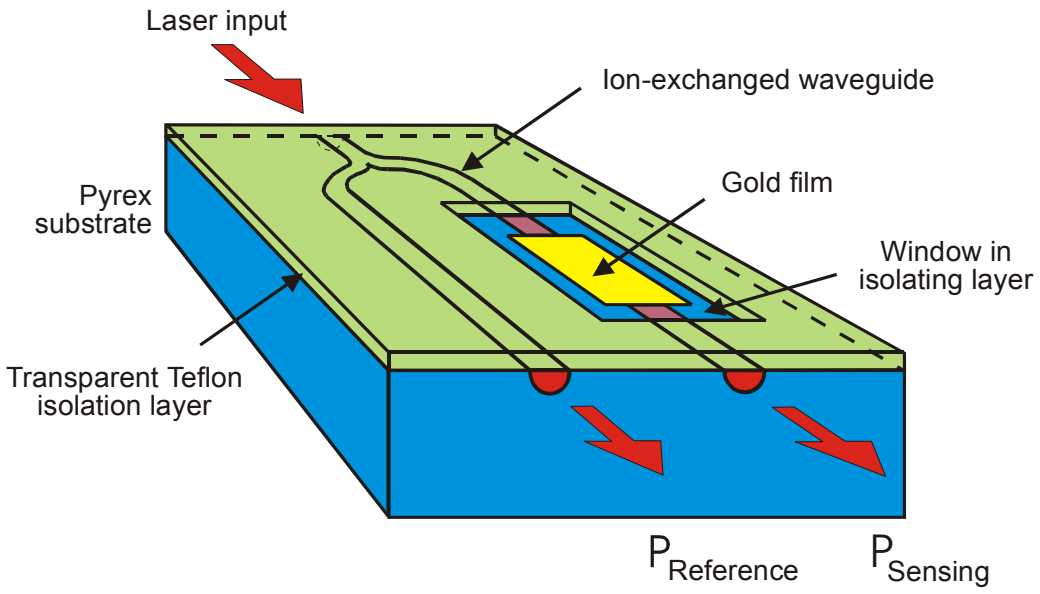

Fig 4.5. Diagram of the IOSPR sensor Y-junction waveguide [4.1]

4.2.6 Electrochemical cleaning of electrode.

The transfer of electrons between the electrode surface and molecules in the interfacial region is a fundamental process in electrochemical reactions. The microstructure, roughness of the electrode surface and presence of adsorbed materials that block the active sites of the electrode surface affects the kinetics of electrochemical reactions carried out on the electrode surface. In addition, the reproducibility of electrochemical analytical technique such as cyclic voltammetry is affected by the state of the electrode surface. Steps were carried out in this project to reduce variation in analytical data due to the electrode surface finish. Mechanical polishing can be applied to solve the problem of unwanted adsorbed materials. Mechanical polishing alters the microstructure, roughness and functional groups of the electrode surface in addition to removing adsorbed species. This is not an option when using IOSPR device due to the thin film of gold involved. Electrochemical cleaning of the electrode is carried out which consists of applying conditioning potentials to the electrode surface before each experimental run, that is. the application of potential into the oxidation region and back through the reduction region several times until a stable response is achieved (≈ 6-8 cycles are required) see chapters 5-6 of this thesis for more details.

4.3 Optical waveguide response to varying superstrate index

4.3.1 Procedure

The measurement of the transmittance against the changes in the refractive index was carried out using the set-up in fig 4.6. This involved using a flow injection analyser connected to a flow cell. The flow injection analyser allowed selection between the background solution, which for this particular analysis was de-ionised water and sample solution that is different concentrations of sucrose. The flow cell has a central input port and two output ports located at the edges of the cylindrical cell. This flow cell was clamped over the substrate.

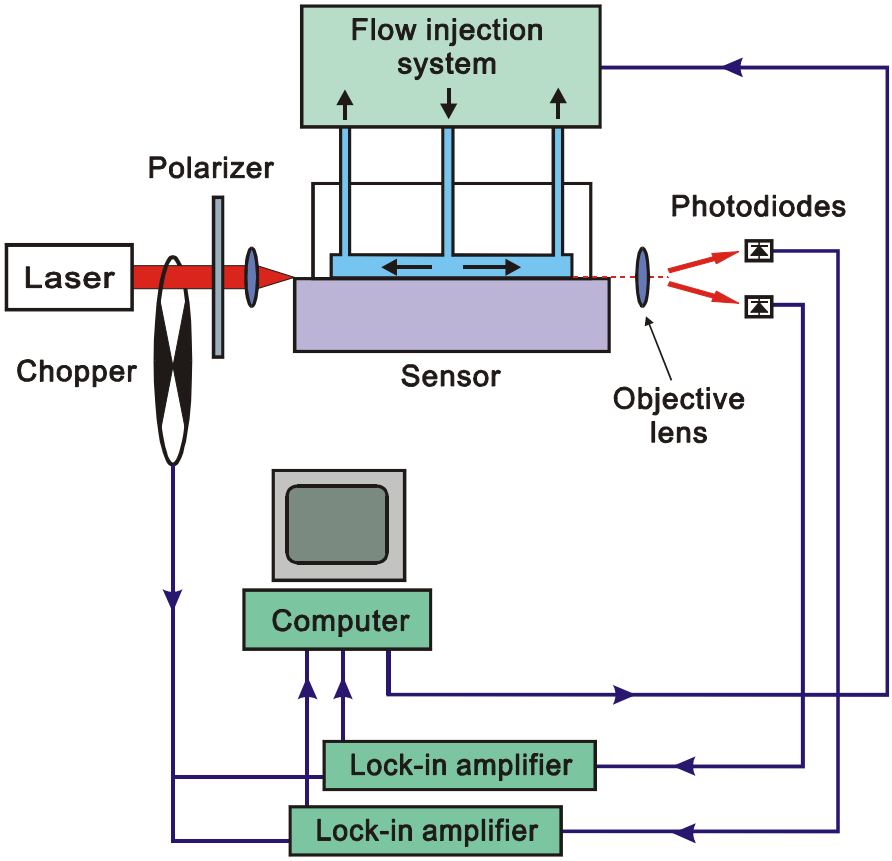

Fig 4.6 Experimental setup

Using a mechanical chopper connected to the lock–in amplifiers the light from the 10 mW linearly polarised, He–Ne laser, at 632.8 nm was chopped then passed though a half–wave plate and a polariser, allowing for the selection of the transverse magnetic mode. This light was then coupled into the waveguide using a X10 microscope objective lens via a filter to reduce the light intensity. The two spots resulting from the sensing and reference arm were coupled out of the waveguide using a X25 microscope objective lens onto a pair of silicon photodiodes. At the start of the experiment before the injection of sucrose, de–ionised water was pumped through the flow cell creating a baseline. This was carried out under argon pressure (0.5 bar) to help remove any gas bubbles that might have got into the system via the sample loop. In addition to this the sample loop was pumped though with 3 times the sample loop volume of test sample so any air bubbles present would be lost to the sample waste container. Different concentrations of sucrose solution were made by adding varying amount of sucrose to de–ionised water then stirred using a magnetic stirrer. The

refractive index of these solutions was determined using the Abbé refractometer. These sucrose solutions of different concentrations were rapidly injected into the flow cell using the flow injection analyser via the sample loop. The rate of flow of 0.58 ml/min was maintained for approximately 2 min, after which the rate of flow though the flow cell was reduced to 0.14 ml/min to achieve a stable state. The sucrose solution in the cell was then flushed out of the flow cell by injecting de–ionised water rapidly into the flow cell. This cycle was repeated several times, applying higher concentration of sucrose with each step (see fig 4.7).

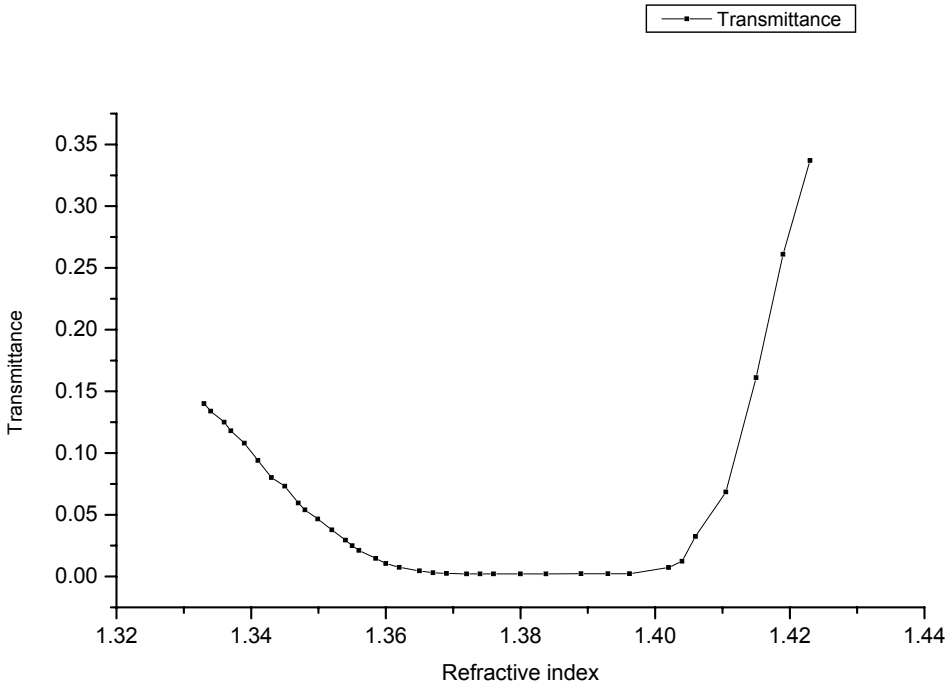

FIG. 4.7 Surface plasmon resonance plot for gold film of 30nm thickness, 3 mm in length and 200 nm width. The transmisson minimum occurred at refractive index of 1.376.

4.3.2 Results

Fig 4.7 shows the surface plasmon resonance (SPR) curve obtained using 30 nm thick gold film of 3 mm length. The characteristic U-shaped plot for an SPR response to refractive index variation was obtained. Here a drop in transmittance in response to increase in refractive index from a value of 1.334 is observed, these trend stops at an index of 1.366 following which further increase in refractive index gave rise to a plateau.

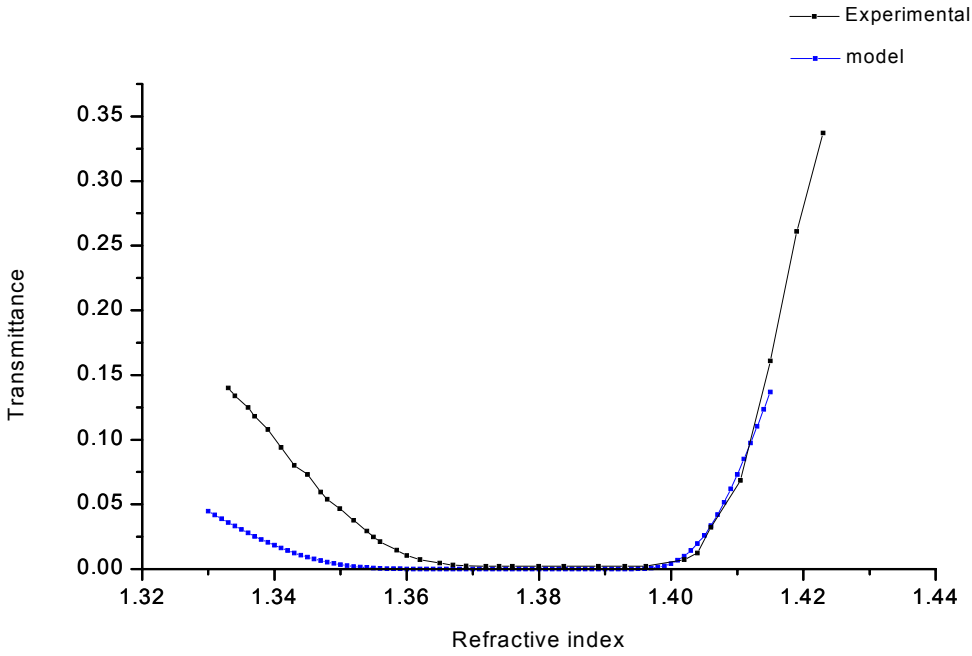

Fig 4.8 Comparison of experimental and theoretical model result

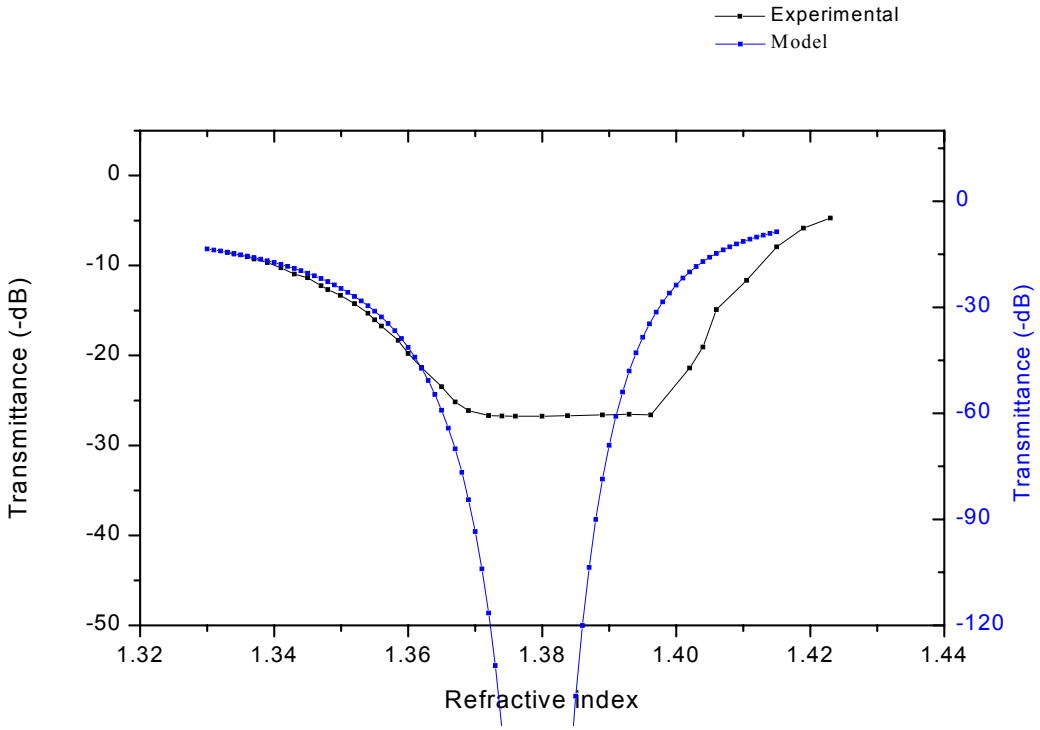

Fig 4.9 Comparison of experimental and theoretical model result

The broadness of the bottom of the curve is due to the presence of substrate light and the fact that the gold film is relatively thin in thickness (see fig 4.9). Fig 4.9 compares the log of the transmittance of both experimental and model results, here the experimental result gives a broad bottom while the model does not as the latter does not take the substrate radiation into account. Further increase in refractive index from 1.395 resulted in an increase in the transmittance. This observation compares well with that predicted by the model (see fig 4.8) used in the development of the device [4.1] but for the deviation at refractive indices below 1.37.

4.4 Optical waveguide response to varying length of gold film in air and water

4.4.1 Procedure

Light was coupled into the waveguide and the ratio of the output power on both arms of the bare Y –junction waveguide was determined. This allows for likely result bias occurring due to the presence of damaged waveguides on further analysis following the deposition of gold to be determined. The gold film was then deposited using the method described previously. This gold film had a thickness of 45 ± 5 nm and film length varying from 0.5 to 5 mm with increase steps of 0.5 mm. The waveguide loss due to the presence of gold, as a function of the different gold film length was studied. During this analysis, light from the 10 mW, linearly polarised, He–Ne laser operating at 632.8 nm was passed though a half–wave plate and a polariser allowing the TM mode to be selected. This light was then coupled into the waveguide using a x 10 microscope objective lens and out coupled using a x 25 microscope objective lens then focused into a photodetector. An iris was placed in front of the detector to cut out most of the substrate light. The ratio of the output power for the reference arm (arm with no gold) and then sensing arm (arm with the gold) was then obtained for each gold film length and the logarithmic value of the ratio of these arms were plotted against the length of the gold films. The analysis of waveguide loss due to the presence of gold, as a function of the different gold film length was carried out in air and then repeated in water.

4.4.2 Results

In both cases, that is, in air and water, a decrease in the output power as the length of gold film is increased is observed. This is expected, due to the total area of gold

interacting with the waveguide increasing with the increase in the length of the gold film, thus the amount of light coupled out of the waveguide increases as well.

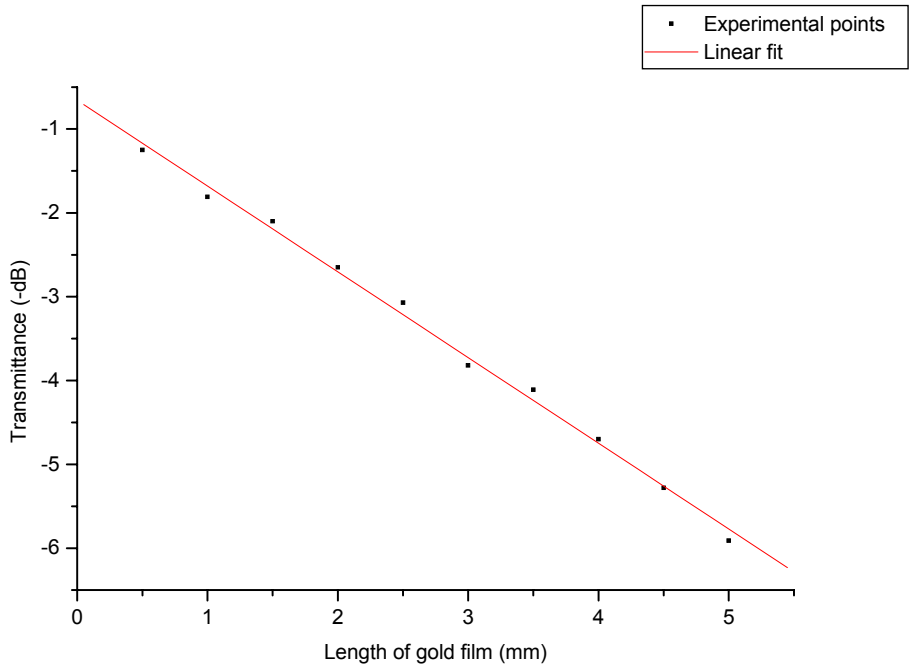

Fig 4.10 Transmittance of the IOSPR device vs length of the gold film, in air.

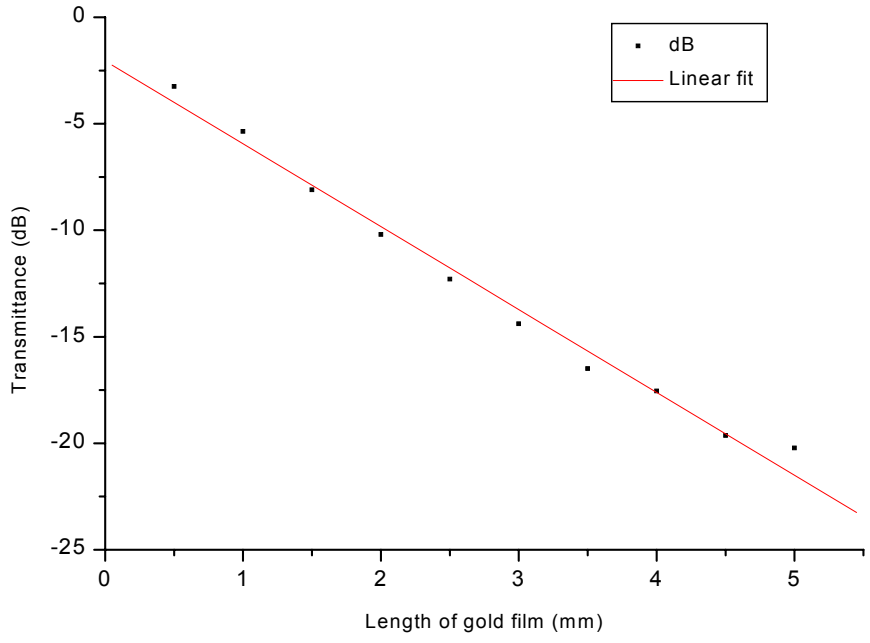

Fig 4.11 Transmittance of the IOSPR device vs interaction length of the gold film, in water.

4.5 Discussion

Analysis carried out on the waveguide was to determine if the expected optical properties could be reproduced before both analytical systems that is the optical / electrochemical are used for further analysis. The test carried out was in two phases, first the ratio of the output power (transmittance) from both arms of the Y – junction waveguide as a function of superstrate index was measured. Next, the ratio of the output power (transmittance) coupled out of the Y – junction waveguide arms, was measured as a function of the length of gold film in air and then in water. A linear plot was obtained for the measured output power ratio of both sensing and reference arm of the device, in relation to the varying length of the gold film, (fig 4.10 and 4.11) with the power output decreasing with increasing gold film length. The results obtained for IOSPR device response to the variation of refractive index compared well to that previously reported [4.1].

The problem of poor adhesion of the gold film on Pyrex glass was initially solved as previously stated by increasing the number of times the MPS treatment was performed on the glass. This later created another problem, that is the formation of strongly bonded gold films after repeated etching and re-deposition of gold. This led to a situation where the fabrication procedure changed, as the developing and etching time varied with every fabricated IOSPR device. This problem was resolved by leaving the substrate, under reflux for 15 minutes, then heating in an oven at approximately 100°C, with a total of two cycles.

4.6 Conclusion

The results reported in this chapter shows that the optical properties of the fabricated IOSPR device did exhibit similar trends to that predicted by the numerical model.

4.7 Reference:

4.1 R.D. Harris, 'Waveguide Surface Plasmon Resonance Biosensors' PhD thesis, University of Southampton (1996).

4.2 A. Opilski, R. Rogozinski, M. Blahut, P. Karasinski, K. Gut, Z. Opilski. Optical Engineering, 36 (1997) 1625.

4.3 R. Sym and J. Cozens. Optical Guided Waves and Devices, Mc Graw – Hill Book Company, page 393.

4.4 V.I. Chegel, Yu. M. Shirshou, E.V. Piletskaya, S.A. Piletsky. Sensors and Actuators B 48 (1998) 456.

4.5 C.A. Gross, D.H. Charych, M. Majda. Anal Chem, 63 (1991) 85.

4.6 M.I. Newton, G. Mc Hale, P.D. Hooper, M.R. Willis, S.D. Burt. Vacuum 46 (1995) 315.

4.7 Y. Iwasaki, T. Horiachi, M. Morita, O. Niwa. Sensors and Actuators B 50 (1998) 145.

4.8 W.R. Thompson, M. Cai, M. Ho, J.E. Pemberton. Langmuir, 13, (1997) 2291.

4.9 N.G. Cave and A.J. Kinloch. Polymer, 33 (1992) 1162.

Chapter 5
Optical – Electrochemical interrogation of electrochemically formed gold oxide layers.

5.1 Introduction

This chapter discusses studies carried out on electrochemically grown oxide layers on a thin film gold electrode (integrated optical surface plasmon resonance device) in 0.2 M sulphuric acid and 0.1 M perchloric acid. Optical and electrochemical studies of the oxide formation and removal on gold in sulphuric and perchloric acid were carried out to test the analytical potential of combining both techniques in the interrogation electrochemically modified surfaces. The oxidation of the gold surface allows one to determine the useful working potential range for both optical and electrochemical interrogation. Qualitative and quantitative analysis of the optical and electrochemical response to the oxidation of the gold film is reported in this chapter. In addition, the effect of different anions, that is ClO_4^- and HSO_4^-, on the optical response to the oxidation of the gold film was also studied. Extensive work has been carried out in the study of oxide layers using techniques such as ellipsometry and reflectance measurements [5.1-5.4], more recently STM [5.5] and AFM have been applied in the study of oxide films on gold. Ellipsometry has the disadvantages that the optical path passes though the bulk solution, the sensitivity is low, the potential for multisensor integration is poor and the interpretation of the data is complex. Traditionally, chronoamperometry [5.6] and chronopotentiometry [5.7] were mainly used in the study of oxidation of gold. SPR has also been employed, in the standard Kretschmann configuration, for studies of gold oxidation [5.8] but this approach is ill suited for dense multisensor integration. In the analysis of the data obtained during our investigations, comparisons will be drawn between results reported using the ellipsometry and reflectance techniques and the data obtained here using surface plasmon resonance technique.

5.2 Oxidation of gold film in sulphuric acid

5.2.1 Experimental procedure

Fig 4.6 of chapter 4 shows the configuration of the IOSPR sensor chip. Polished Pyrex glass wafers 50mm square were coated with a 200 nm thick aluminium film and channels of 2 μm and 3μm wide were opened in this film, in the form of a Y-junction, giving rise to a diffusion mask. The coated wafer was then immersed in molten KNO_3 at 390^{o}C for 7.4 hours, to form potassium ion-exchanged waveguides and the aluminium mask was removed. The surface of the glass was treated to promote gold adhesion by refluxing in a solution of (3-mercaptopropyl) trimethoxysilane (MPS) in water and propan-2-ol in the ratio 1:1:46 (by mass) for 15 minutes. The wafer was patterned with gold pads 35 nm ± 5 nm thick and with lengths varying in steps of 0.5 mm from 0.5 mm to 5 mm on one arm of the waveguide Y-junction. The gold film serves both to guide the surface plasma wave (SPW) and as a working electrode in electrochemical studies. The second waveguide is used to provide a reference output allowing compensation for the effects of input power fluctuations, so that the device transmittivity, T is defined as:

$$T = P_{sensing}/P_{reference} \qquad (5.1)$$

Where $P_{sensing}$ is the optical output from the sensing arm and $P_{reference}$ is the optical output from the reference arm. The electrodes were connected by a track to pads at the edges of the substrate. Finally, a 700 nm thick layer of Teflon AF 1600 (n = 1.31) was deposited on the surface of the substrate and patterned to form windows exposing only the gold electrodes on each Y-junction device.

Using a mechanical chopper connected to the lock–in amplifiers the light from the 10 mW linearly polarised, He–Ne laser, at 632.8 nm was chopped then passed though a half–wave plate and a polariser, which were used to select the transverse magnetic mode (TM). This light was then coupled into the waveguide using a X10 microscope objective lens, via a variable attenuator to reduce the light intensity thus preventing over loading of lock-ins (see fig 5.1). The two spots resulting from the sensing and reference arm were coupled out of the waveguide using a X25 microscope objective

lens onto a pair of silicon photodiodes. A cylindrical cell with both ends open was clamped over the substrate.

Cyclic voltammetric measurements were carried out using a standard three electrode configuration consisting of a thin film gold electrode, a high area platinum mesh as the counter electrode and an in-house built standard calomel electrode used as the reference electrode connected to a computer controlled potentiostat. The control commands and data were relayed via a data acquisition board (National Instrument) to and from the computer (Gateway 2000). The working electrode, (gold film) the counter electrode, (platinum wire) and the reference electrode, (saturated calomel electrode) were placed in the cell containing either 2 ml of 0.2 M sulphuric acid or 2 ml of 0.1 M perchloric acid. The glass frit of reference electrode which separates the content of the reference electrode from that of the reaction solution was doubled to prevent the leakage of Cl^- ions from the reference electrode into the reaction solution. The leakage of Cl^- ions from the reference electrode will contaminate the reaction solution. The reference electrode maintains a fixed potential, thus any change in the applied potential to the cell appears directly across the working electrode - solution interface. The oxidation of the gold film was carried out using sulphuric and perchloric acid in turn, to determine if the optical response for comparatively weakly adsorbed anions (ClO_4^-) [5.9-5.10] would differ from that for strongly adsorbed anions (HSO_4^- and SO_4^{2-}) [5.11]. The experimental data were obtained by applying a potential between the working electrode and the reference electrode from a potential positive of 0.5 V and scanned positively to study the oxidation of the gold film. The direction of scan was then reversed to investigate the reduction of the oxide layer previously formed. In all cases unless otherwise stated the scan rate of the cyclic voltammetry was 20 mV/s. The optical and electrochemical results that is the change in output ratio (transmittance) and current generated were obtained simultaneously and stored in the computer.

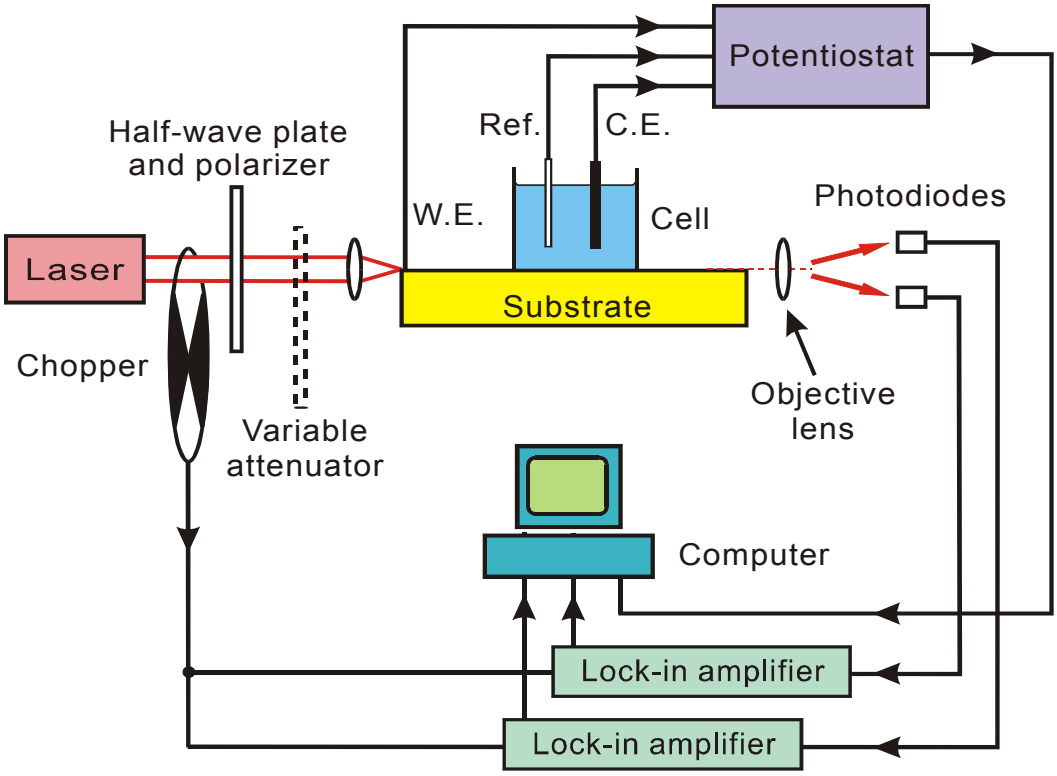

Fig 5.1 Diagram of the experimental set up.

5.2.2 Results and Discussion

Fig 5.2 shows a plot of a typical optical and electrochemical [5.12-5.15] response to the formation of an oxide layer and its removal electrochemically recorded simultaneously. The transmittance-potential curve obtained here resembles the relative change in reflectivity-potential plot (wavelength of 540 nm) obtained by Takamura *et al.* [5.16] and Laitinen *et al.* [5.6]. It is also similar to that reported by R.S. Sirohi [5.1] and others [5.2-5.3], using ellipsometry at a wavelength of 632.8 nm. The conductive electrolyte used for most of these reported oxide formation study was perchloric acid except for Sirohi where using ellipsometry a 1.3 % relative phase change in response to the oxidation of gold in sulphuric acid was reported. This is very low in comparison to that obtained here where a 60 % change in sulphuric acid is obtained.

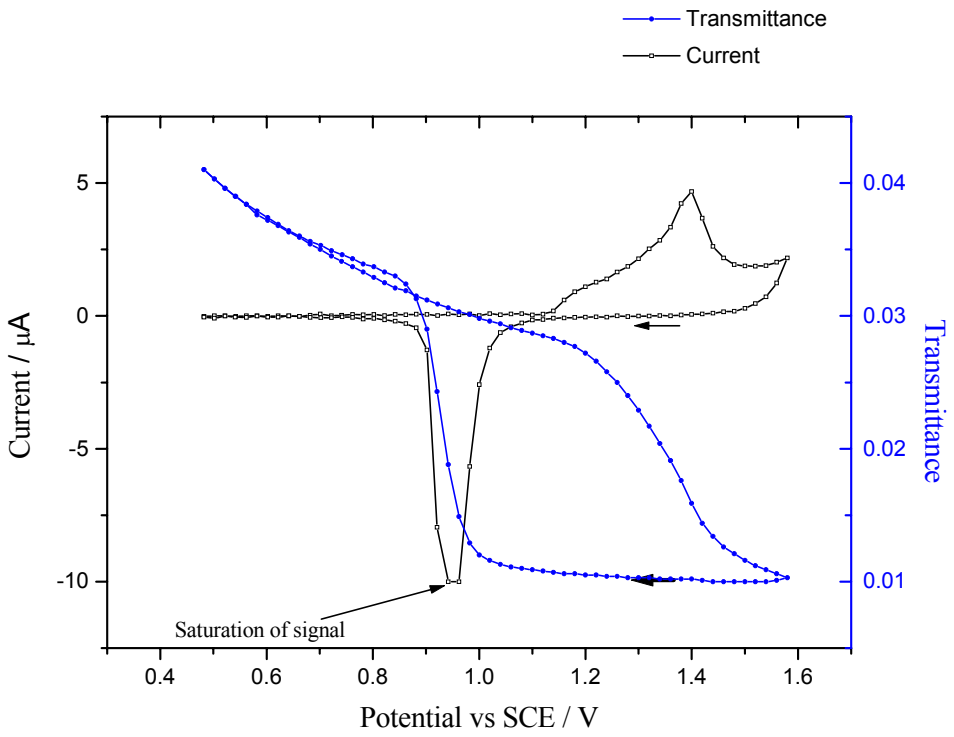

Fig. 5.2 Plot of optical response as a function of applied potential together with the corresponding cyclic voltammetry of the gold film (3 mm length) in 0.2 M sulphuric acid. The refractive index of the solution was 1.355, scan rate: 20 mV/s, potential limit: 0.5 V-1.6 V. Geometric area of the gold film is 0.055 cm^2 while the true area obtained by integration of stripping peak was 0.10 cm^2.

It should be noted that there is not a linear relationship between the ellipsometric parameter psi and the attenuation of the transmittance. The optical response for the oxidation of the gold film in this project using sulphuric acid was the same for solutions prepared at different times. Observed difference occurred in the direction of change of transmittance, that is increase or decrease in transmittance, which depends on the initial operating point of the device. This difference could have been due to the presence of particles or molecules over the surface of the gold film, which shift the operating position of the device further to the right. Looking back at the optical plot for the device's response to the variation of refractive index (chapter 4, fig 4.7), this surface plasmon resonance plot has a U-shape. If the initial refractive index of the test solution falls on the left hand arm of the U-shaped plot, as in the case of sulphuric acid 1.355, over a clean gold film, a reaction that causes an increase in the refractive index, would give rise to a fall in the transmittance. This is assuming that the firm

formed is transparent. The formation of the oxide film led to a decrease in the transmittance which when compared to the surface plasmon resonance plot of chapter 4, suggests that the oxide layer formed has a higher refractive index than the "film" previously present on the gold surface. The thickness and refractive index of the oxidised layer have been estimated by ellipsometry to be τ_{Ox} = 0.54 nm (see table 1) and n_{Ox} = 3.3 – j1.3, respectively, with an accuracy of about 10% on all values [5.2]. While the refractive index of the gold film at a wavelength of 633nm may be taken to be n_{Au} = 0.20 – j3.45 [5.8].

Table 1: Thickness of electrochemical formation of gold oxide.

Technique	**Thickness of gold oxide**	**Reference**
Ellipsometry	5.4 ± 0.6 Å	J. Horkans *et al* [5.2]
Ellipsometry	4 Å	Y-T. Kim *et al* [5.4]
Crystallography and Coulometry	3.7 Å	F.Chao *et al* [5.18]

The optical response to the oxidation of the gold film, in the anodic direction can be divided into 3 regions:

1. The pre – oxidation region [from 0.5 V to 1.15 V].
2. The oxidation region [from 1.15 V to 1.5 V].
3. The oxygen evolution region [beyond 1.5 V].

The pre–oxidation region (0.5 V to 1.15 V): Here a change in the transmittance is observed, this change is significantly greater than the limits of detection [± 0.00048]. Electrochemically a small current is detected. At these potentials the only process occurring is the charging or discharging of the metal-electrolyte interface, this is the so called double layer region in which the electrode-electrolyte interface behaves as a capacitor. Changing the potential modifies the charge distribution at the gold surface and this, in turn, alters the distribution of ions in the solution close to the electrode surface. This double layer region is typically no more than a few nanometres thick for a concentrated electrolyte solution. Thus as the potential of the electrode is made

positive, cations are repelled from the region of solution adjacent to the electrode surface and anions are attracted into this region so that its composition differs from the bulk solution composition and its composition varies as the electrode potential varies. Charging of the double layer is also accompanied by some rearrangement in the orientation of water dipoles at the interface. This potential-driven redistribution of ions involves the chemisorption of the anions HSO_4^- or SO_4^{2-} at the gold surface [5.1 see cited references, 5.16], giving rise to the observed current and to surface index changes which are clearly detected by the IOSPR sensor. Abelés *et al*. [5.18] were able to separate the contribution of the electronic effects of the metal from that of the electrolyte ionic effects, to the optical and electrochemical response observed at this region. This was achieved by interrogating the amplitude and phase change of the reflected component of the electric field vector of the p-polarised wave of an excited surface plasmon wave at the double layer region using ellipsometry (see appendix 3 for more detail). The contribution to the changes in refractive index (observed as a fall in transmittance) of free charges in the gold film has been shown to be significant when compared with the effect of adsorption of analyte ions [5.19]. The results obtained above suggest that the optical interrogatory technique applied here is more sensitive to the pre-oxidation region than the electrochemical analytical technique.

The oxidation region 1.15 V to 1.5 V: The second region of interest is the oxidation region between 1.15 V and 1.5 V. As the potential is increased, the current increases due to the formation of a gold oxide surface layer which is discussed in detail in chapter 2 of this thesis. In summary, OH groups are adsorbed among the anions adsorbed in the pre-oxidation phase; these anions are then desorbed in a place-exchange reaction leaving the OH groups on the surface of the gold film. A "replacement turnover" process then occurs, where the oxygen and gold atoms at the surface exchange places (see fig 5.3). Further OH^- ions adsorb onto the gold to produce two monolayers of oxygen atoms separated by a monolayer of gold atoms on the surface of the metal. The optical transmittance drops significantly in this region, showing that the oxidation of the gold surface can be clearly detected. Integrating the area under the oxidation peak and dividing by the scan rate gives the charge involved for the oxidation of the gold film. Here a value of 42.08μC is obtained, thus inferring that the true area of the electrode is 0.10 cm^2 (geometric area is 0.05 cm^2). Although

this value is equal to that obtained, carrying out a similar analysis on the oxide stripping peak to determine the true area of the working electrode (see fig 5.2), the area under the oxidation peak usually comprises of charge due to the double layer region and that due to oxygen evolution thus care should be taken when using area under the oxidation peak to determine the area of the electrode.

The gold oxide formed is stable as long as the potential is applied [5.20]. Schneeweiss *et al.* [5.21] suggested that the main step in the oxidation of the gold film occurs at the turnover process this was basically due to the fact that roughing of the surface was observed to start here using STM. The measured refractive index of sulphuric acid used for this analysis was 1.355, thus a decrease in transmittance as observed indicates rise in the refractive index of the sensing arm. The cyclic voltammetry for the oxide formation suggests that the gold film has predominately plane structure (111), as the shape of the CV obtained here compares well with that suggested by H. Angerstein-Kozlowska *et al.* for the (111) [see fig 8 of 5.22], [5.23]. The presence of other gold faces can not be ruled out as no step was carried out to selectively produce a gold film face of (111), following the deposition of the gold. D. Dickertmann *et al.* [5.23] using cyclic voltammetry showed that the position of the peak potential for the formation of the oxide film was dependent on the gold face and that the polycrystalline surface shows a monotonic curve.

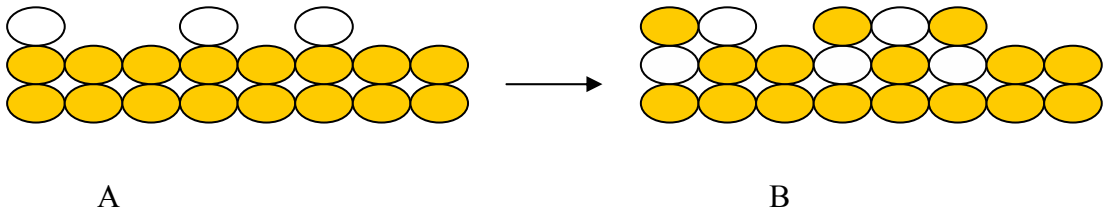

Fig 5.3 This illustrates the process of replacement turnover, where (A) shows the chemisorption of the OH species (white circle) unto the gold atoms (transparent gold coloured circle) and (B) the place exchange of the O species for the gold atoms. In addition, (B) shows further chemisorption of OH species onto anion free Au atoms.

Oxygen evolution region beyond 1.5 V:

In the third potential region, oxygen is produced by electrochemical reduction of water at the gold surface, resulting in a significant additional current. This is not reflected in the transmittance *T*, as the oxygen produced rapidly diffuses away from the electrode beyond the evanescent field of the surface plasmon wave

On reversing the direction of scan the transmittance increased slightly until 1.1 V after which the oxide layer was removed, the latter is reflected by a rapid increase in the transmittance. Although the current change before the removal of the oxide layer was fairly constant one might suggest that transfer of anions onto the gold surface is still going on, as an increase in the transmittance at this region is observed. Integrating the current over time for the reduction peak which, unlike the oxidation peak, is not distorted by oxygen evolution, the charge transferred to the electrode in oxidising the surface is 41.4 μC (fig 5.2, this was the 4^{th} cycle). The charge required to oxidise a gold surface has previously been estimated to be 3.8 $\mu C/mm^2$ [5.24], corresponding to a gold electrode area of 10.3 mm^2. While the optical measurements take place on only one gold pad, the electrochemical response is measured over all the gold pads connected in parallel, which have a geometric area of 5.5 mm^2. The charge obtained by integrating over the reduction peak for the first cycle is 21.3 μC, corresponding to an area of 5.3mm^2, in good agreement with the geometric area thus suggesting a roughening factor of 1. The apparent increase in area for subsequent electrochemical cycles is due to roughening of the surface following the replacement turnover process [5.25]. (See appendix - A1, for a description of the determination of the electrode area via integration of stripping peak). In fig 5.4, a large drop in the area below the oxidation peak after the first cycle is obtained, this has been attributed in the literature to the electrochemical cleaning of the gold surface via roughing of the surface as a result of the irreversible (that the integrity of the gold surface changes permanently) replacement turnover process [5.26]. One can assume the drop in the area under the oxidation peak was due to the presence of contaminant that was oxidised in the 1^{st} cycle as the difference of the area under the 1^{st} and 2^{nd} cycle stripping peaks was relatively small (0.4301 μAV for first cycle and 0.4663 μAV for the second cycle). This irreversibility of the replacement turnover process can be explained as follows. At potentials negative of that required for replacement turnover (RTO), anion

adsorption and partial decomposition of water, causes no surface roughing of the gold on reversing scan direction. As the potential is increased on the anodic scan, a further increase in the anion coverage and coadsorption of OH from water is obtained. Further, increase in the potential gives rise to the replacement turnover process, which occurs due to the repulsive interactions between the OH groups. The turnover process is accompanied by the desorption of the anion and its replacement by OH groups from water decomposition.

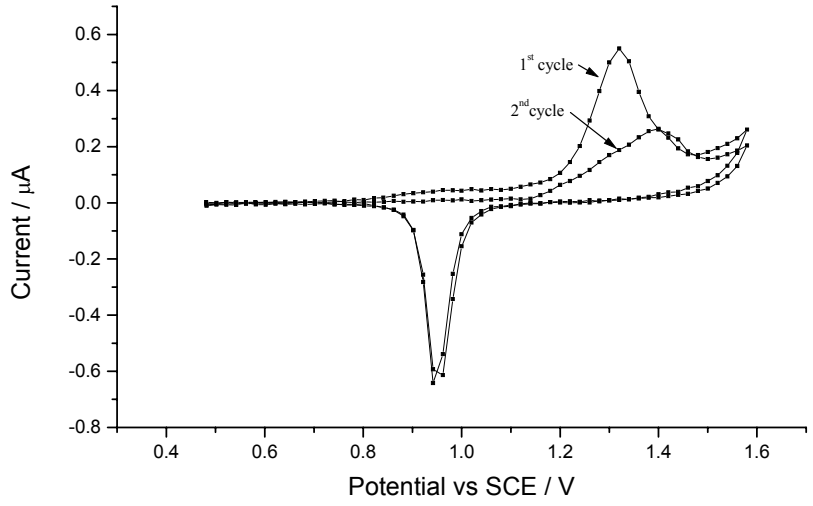

Fig. 5.4. A plot showing the 1st and 2nd cycle of 0.2 M sulphuric acid using a thin film gold electrode of length 3 mm, thickness 30 nm and scan rate of 20 mV/s.

The stripping of the oxide layer, by reversing the direction of scan, will lead to the roughening of the surface as the turnover process between gold atom and oxygen bond to the gold surface is irreversible [5.26]. The removal of the contaminate from the gold surface during the 1st cycle affects the optical response on the cathodic sweep, which does not re-trace the path of the anodic sweep, but ends up at transmittance, higher than the initial pre-oxidation transmittance at each potential fig (5.5). Electrochemically, the first scan is important as it gives quantitative data on the device such as the area of the gold film. The next three cycles showed the cathodic-sweep optical response re-tracing the path of the anodic-sweep optical response, see fig (5.6). The drift observed is a combination of temperature fluctuation, mechanical drift and slight changes in the structural face of the gold film with repeated CV (see chapter 7 for the effect temperature and mechanical drift). The main cause of the drift can be suggested to be due to the changes occurring on the gold film surface in

response to the electrochemical cleaning of the gold, as the mechanical (this can also be sudden) and temperature effect are pronounced over long time periods. Electrochemically for the next three cycles shows very slight changes in the area under the oxidation and reduction reaction in comparison to that observed for the first cycle.

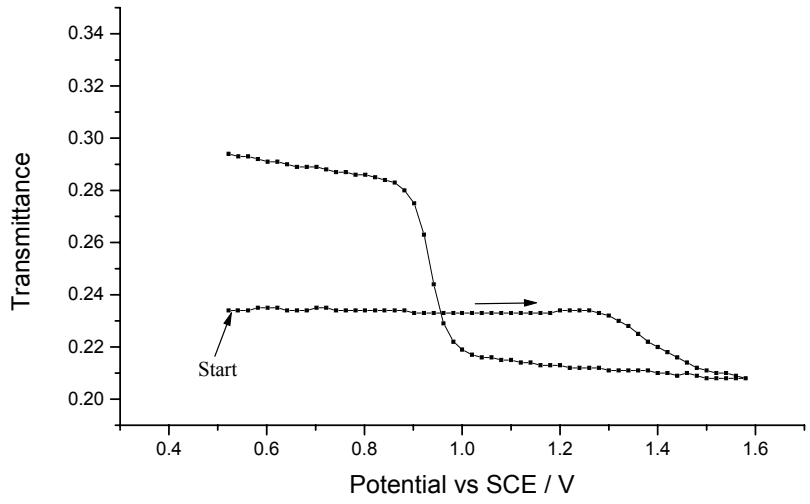

Fig. 5.5. Plot showing the optical response to the 1st cyclic voltammetry for 0.2 M sulphuric acid on a gold film with a scan rate of 20 mV / s.

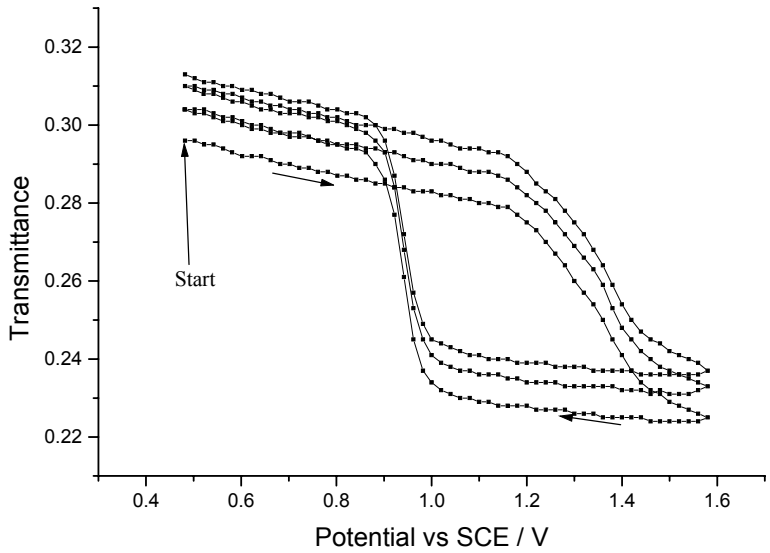

Fig. 5.6. Shows the optical response for the 2nd - 4th cyclic voltammogram for the oxidation of a gold film in 0.2 M sulphuric acid with a scan rate of 20 mV / s.

Confirmation that the optical observation was due to oxide formation is shown in figs (5.7) and (5.8). The transmittance is expected to be related to the extent of oxide film growth and, therefore, to the integral of the current over time, which corresponds to the charge transferred to the electrode. The derivative of the transmittance, *dT/dt*, against potential is plotted in Fig. 5.7 together with the current. Here very similar changes are observed both optically and electrochemically thus suggesting that both responses originate from a similar origin that is the oxide formation, confirming that the IOSPR device measures the oxidation and reduction of the gold film. At the pre oxidation region of the optical response on fig 5.7, the separation observed between the anodic and cathodic scan is due to the anion adsorption and desorption. Fig 5.8 is a plot of both transmittance and charge against potential where, the rapid change in the transmittance as the oxide is formed is mirrored by the plot showing the consumption of charge. Similar effects are observed during oxide removal where the optical response is mirrored by the charge. This is a good indication that what is been observed optically is the electrochemical oxide formation and removal.

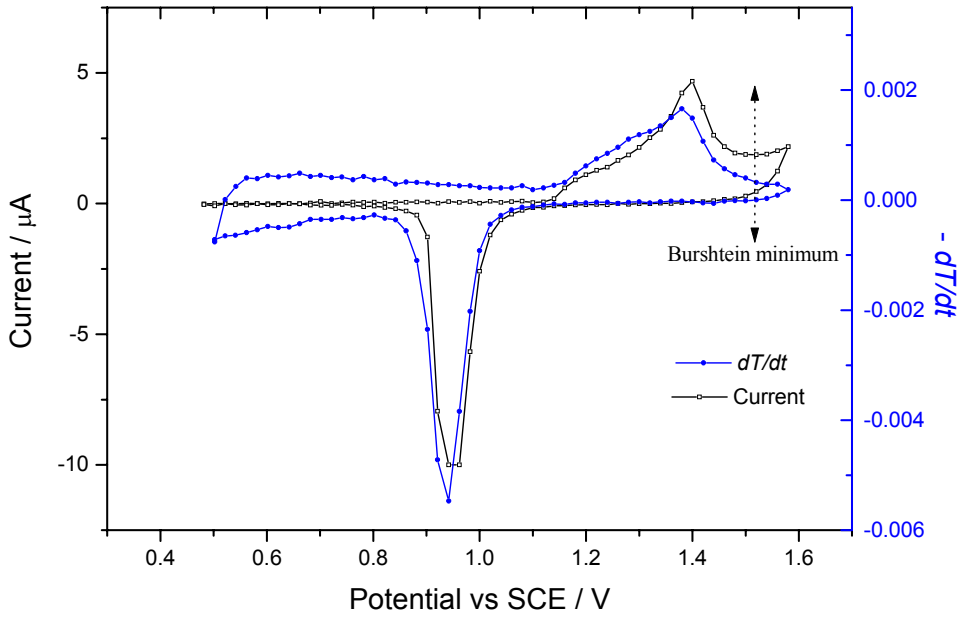

FIG 5.7. Plot of rate of change of transmittance and current against potential for cyclic voltammetry for 0.2 M sulphuric acid on a gold film of 3 mm length, 30 nm thickness with a scan rate of 20 mV / s. Burshtein minimum is the potential just before oxygen evolution on the current potential plot.

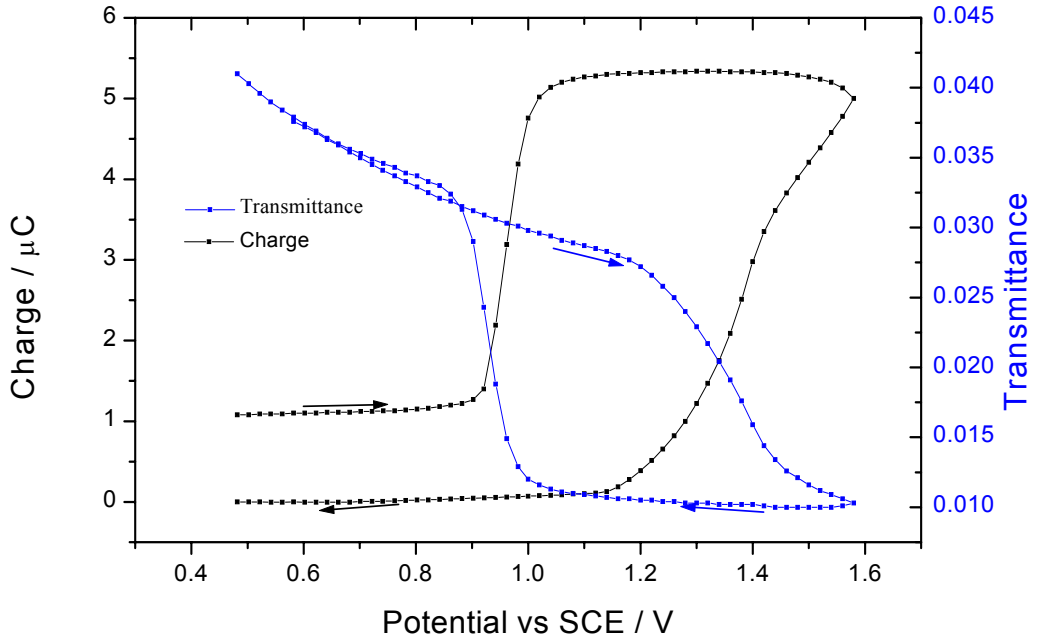

FIG. 5.8 Plot of transmittance and charge against potential for 0.2 M sulphuric acid on gold film of 3 mm length, 30 nm thickness with a scan rate of 20 mV / s.

In the plot of charge against potential, at potential range of 0.5 V to 0.9 V some charge was lost during the oxidation process, this is due to the charge used up in the evolution of oxygen, which is not regained.

Effect of the gold film length on sensitivity

Further analysis was carried out to determine the optimum length of gold that can be utilised in further analysis in terms of the sensitivity of response of the IOSPR device to oxidation of the gold film see figure 5.9. Since the experimental set up is limited by stability, the sensitivity of the device is determined by measuring dT/T. Where dT is the difference in the transmittance at the potential of 1.14 V in the anodic scan (T) and the transmittance at the potential of 1.14 V in the cathodic scan. As the length of the gold film is increased, an increase in the sensitivity of the device in response to the oxidation of the gold film is observed. This can be attributed to the increase in interaction length of the sensing area. The process of exciting the surface plasmon causes a drop in the transmittance due to the lossy nature of the surface plasmon, which causes damping of the waveguide mode following coupling of the guided mode and surface plasmon. The increase in the gold film length will thus lead to a drop in

the transmittance, as the amount of light coupled out of the waveguide increases with the increases in gold film length, this explains the peak in sensitivity observed at 3 mm. The drop in transmittance, as the length of the gold film is increased beyond 3 mm is due to the presence of substrate light, whose effect becomes pronounced as the gold film length is increased. The observed percentage change in response to the oxide formation, for the most sensitive gold film length (3 mm) was approximately 60%, see fig 5.9.

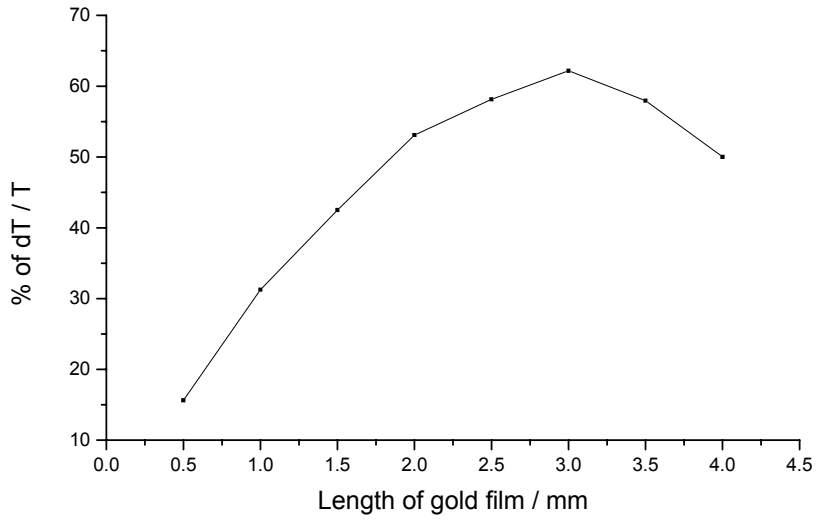

FIG. 5.9. Determination of the most sensitive length of gold film on the device based on mechanical stability and the presence of substrate light been the limiting factor during the analysis of gold film oxidation in sulphuric acid.

Optical and electrochemical response to step increase in potential limit.

Cyclic voltammetry was carried out from 0.5 V with the initial anodic potential limit set at 1.40 V. Following this, the percentage change was determined by taking the difference of the transmittance at a potential of 1.2 V on both anodic and cathodic scans and dividing the result by the transmittance at 1.2 V on the anodic scan. The potential limit was then increased by 0.05 V and the percentage change at 1.40 V was recorded again. This process was repeated until the potential limit of 1.60 V was

attained (see fig 5.10 and fig 5.11). In figure 5.10 as the potential limit of the anodic scan is increased from 1.40 V, the change in transmittance also increases this is also the case with the observed current peak of the stripping peak (fig 5.11).

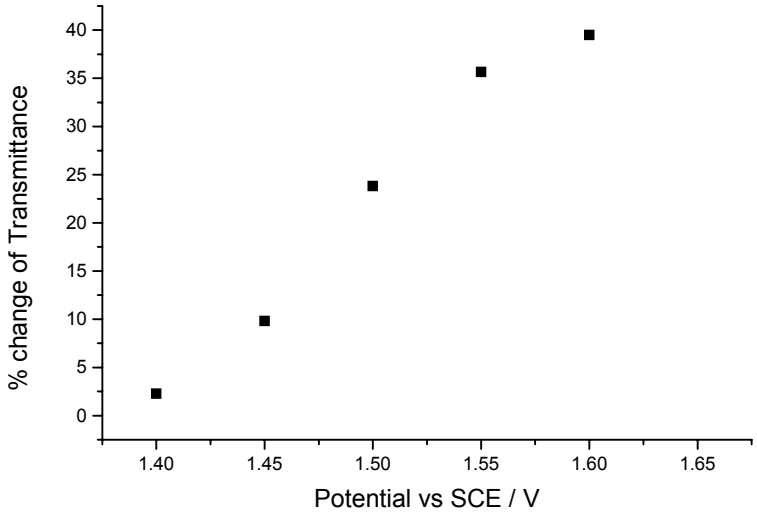

Fig 5.10. Plot showing % change in transmittance against potential limit, for the oxidation of a gold film in sulphuric acid (0.2 M). Scan rate = 20 mV / s. Length of the gold film used 3mm, the thickness 50 ± 5nm.

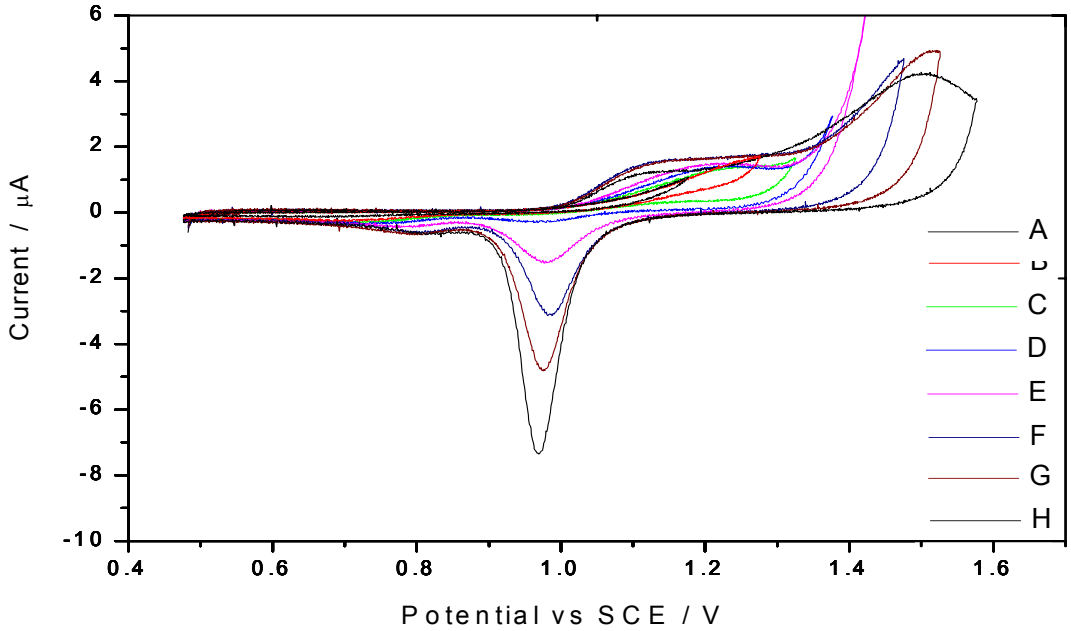

Fig 5.11 Plot showing the I vs E profile for varatiation of the anodic limit. N.B. there is a shift of 0.02V in the anodic direction for the data points. Scan limits: A) 1.2 V; B) 1.3 V; C) 1.35 V; D) 1.4 V; E) 1.45 V; F) 1.5 V; G) 1.55 V; H) 1.6 V.

Scan rate = 20 mV / s. Length of the gold film used 3mm, the thickness 50 ± 5nm.

Integrating the area under the stripping peak for the CV at 1.55 V, an area of 0.056 cm^2 which is close to the geometric area value of 0.055 cm^2 was obtained. At potential limits beyond 1.55 V, the calculated true area values obtained are significantly greater than that of the geometric area e.g. for 1.6 V the calculated true area was 0.074 cm^2. Overall, an almost linear response in the change in transmittance and increase in stripping peak current as the potential limit is increased is obtained. Beyond 1.55 V the transmittance appears to deviate from a linear plot, this might be due to the completion of a monolayer oxide on the electrode surface, but this can not be conclusive as the potential limit needs to be extended beyond 1.6 V in order to verify this assumption. Electrochemically, increasing the potential limit by steps of 0.05 V, that is going from 1.45 V to 1.50 V then to 1.55 V, an increase of 1.6 μA for every increase in 0.05 V was obtained, but beyond 1.55 V an increase of 2.55 μA in the stripping peak current was observed.

5.3 Perchloric acid.

This section report on the results obtained for the electrochemical oxidation of the gold film in perchloric acid. Perchlorate acid anions are weakly adsorped onto the gold surface in comparison to sulfate anions. Here the optical response to differing anion adsorption strength during gold oxidation is determined.

5.3.1 Results and discussion

The plot of the optical response to the oxidation of a gold film in 0.1 M perchloric acid is shown in fig 5.12. The cyclic voltammetry obtained for perchloric acid is very similar to that of the sulphuric acid except for the observed shift in the position of the oxidation and reduction peak potential of the gold film and the potential for the onset of oxygen evolution. This is attributed to the difference in the adsorption strength of these anions, where perchloric anion are comparatively weaker (see fig 5.13 and 5.14). The oxidation potential of Au (111) is generally shifted positively in H_2SO_4 compared to that of $HClO_4$ because of the strongly adsorbed HSO_4^- and SO_4^{2-} [5.22 & 5.27].

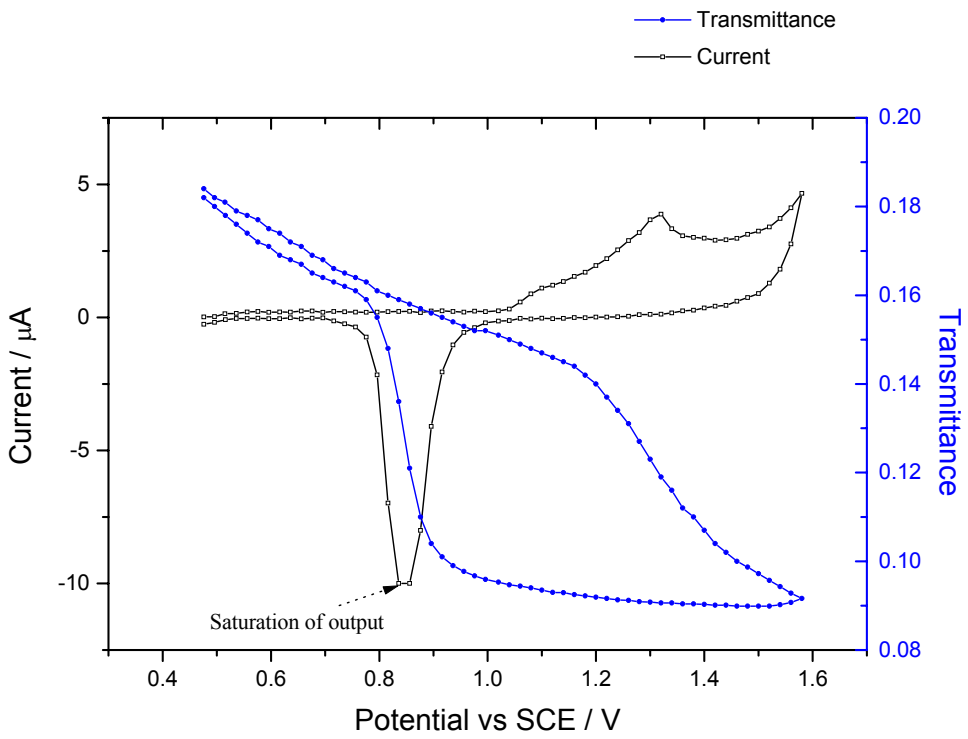

Fig.5.12. Plot of the optical and cyclic voltammetry for the oxidation of the gold film (3 mm length) in 0.1 M perchloric acid, at a scan rate of 20 mV / s.

Angerstein-Kozlowska *et al.* [5.28] reported on the oxidation of gold in perchloric acid on three different gold faces that is (100), (110) and (111). The cyclic voltammogram obtained in this thesis for the oxidation of the gold film in perchloric acid corresponds to that reported by Angerstein-Kozlowska *et al.* for the gold face (111). This observation suggests that the deposited gold film used in this thesis has a predominate gold face (111). The cyclic voltammetry of the gold film in $HClO_4$ acid on the anodic scan can be divided into three regions. These are the pre-oxidation region (0.5 V-1.0 V), the oxidation region (1.0 V-1.42 V) and oxygen evolution region (1.42 V-1.6 V). The gold face and the scan rate for the oxidation of the gold film, govern the shape and position of the cyclic voltammogram obtained. The pre-oxidation region, as in sulphuric acid, involves the adsorption of anions, in this case ClO_4^- anions. As with the sulphuric acid, the optical change, (for perchloric acid the optical change is 10 %), in the pre-oxidation region is due to electron rearrangement of the gold metal and the adsorption of ClO_4^- anions on the gold metal surface. In the oxidation region, the expected change in the transmittance in response to the formation of the oxide film occurred at the potential of 1.20 V, here a 35 % change in

response to the oxidation of the gold film surface is obtained. Integrating the area under the oxidation peak and dividing by the scan rate (20 mV/s), a value of 42.97μC is obtained. This is similar to that obtained using sulphuric acid that is 42.08 μC as the charge involved in the oxidation of the gold film.

The peak current potential for the oxidation of the gold film is cathodic to that observed for sulphuric acid. This is due to the weak association between the ClO_4^- anions and the gold surface, thus the ClO_4^- anions are easily replaced by OH groups at lower potentials. The characteristic steep slope of the transmittance, for the combined effect of the anion replacement by OH, the replacement turnover process (that is MOHMOH → MOHOHM, where M is the metal) and finally the formation of the gold oxide was observed after 1.2 V. The removal of the oxide layer is observed optically by a rapid increase in the output ratio as observed in sulphuric acid.

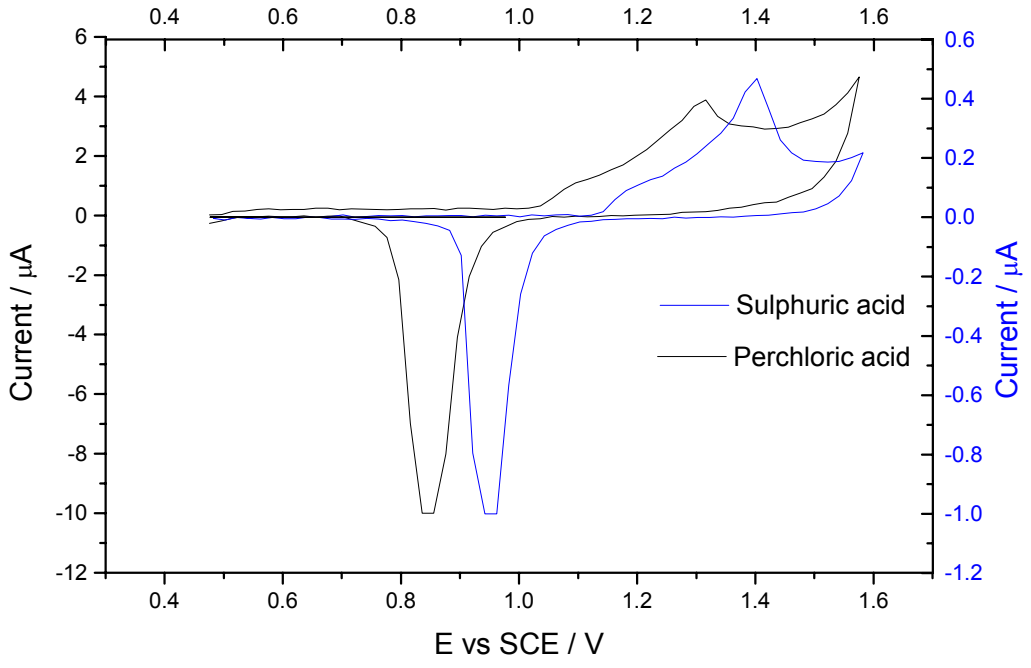

Fig 5.13 Comparing CV of sulphuric acid (0.2 M) and perchloric acid (0.1 M) for the oxidation of the gold film in both acids at a scan rate of 20 mV / s.

Fig 5.13 compares the cyclic voltammogram for the oxidation of the gold film in sulphuric and perchloric acid. The CV for both acids are similar with the difference occurring in the position of the peak potential for the oxidation and reduction of the gold film. In the cathodic scan, a difference of 0.1 V between the reduction peak potential in the CV of the sulphuric and perchloric acid is obtained. A similar result was obtained for the oxidation peak for both solutions. The charge consumed for the oxidation of the gold in perchloric acid is 47.5μC, which is similar that obtained using sulphuric acid, that is 41.4 μC, using the stripping peak. As with the electrochemical response the optical response (see fig 5.14) to the oxidation of the gold film in both perchloric and sulphuric acid were similar in terms of the overall shape.

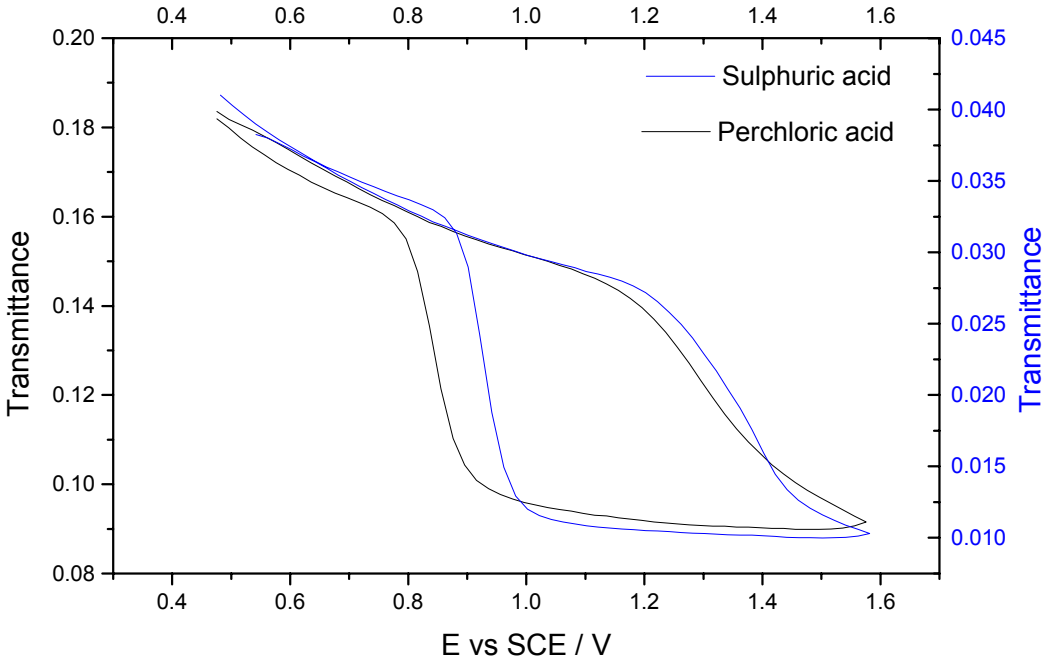

Fig 5.14 Comparing the optical response to the oxidation of sulphuric (0.2 M) and perchloric acid (0.1 M) for the oxidation of the gold film in both acids at a scan rate of 20 mV / s.

Differences in the optical responses occurred in the magnitude percentage change in response to the oxidation of the gold film, adsorption of anions and the width of the oxidation window. The percentage change in the optical response, for the oxidation of the gold film in perchloric acid was 35 %, while for the sulphuric acid was 60 %. This is due to the differences in the refractive indices of both solutions, 1.334 for perchloric acid and 1.357 for sulphuric acid, which inturn affects the operating point of the device and its sensitivity to a stimulus.

5.4 Conclusion

Using the integrated optical surface plasmon resonance device, the growth of oxide and its removal from a gold film was monitored, in real time. Confirmation that the optical response was due to the formation of an oxide layer was provided by the similarity between the plot of the derivative of the transmittance, dT/dt against potential and that of the current against potential. The CV obtained suggests that the gold film deposited was predominately (111) [5.28] although one would expect a polycrystalline surface. Roughening of the gold film occurred after the first cycle, giving rise to a roughing factor (1.3-2) that varied depending on the number of cycles carried out and the anodic scan potential limit. The optical plots obtained for the oxidation of the gold film in both sulphuric and perchloric acids correspond to those reported using ellipsometry and or reflectance spectroscopy, but the magnitude of the optical response to the oxide formation was much higher using the IOSPR device (60 % in sulphuric acid). The state of the gold film significantly affects the optical response, as its observed that electrochemical cleaning of the electrode gave rise to 94 % change in transmittance. The experimental result obtained for the oxidation of the gold film sulphuric acid suggest that the gold film of 3mm length of 30 ± 5 nm thickness was the most sensitive length for the analysis of oxidation carried out using this particular IOSPR device.

The optical technique used here provides a means of following the growth of oxide, quantitative data can be obtained following the calibration of the device against this process.

5.5 Reference:

5.1 R.S.Sirohi and M.A. Genshaw, J Electrochem. Soc. 116 (1969) 910.

5.2 J. Horkans, B.D. Cahan and E. Yeager, surface science 46 (1974) 1.

5.3 A. Hamnett, J. Chem. Soc. Faraday Trans, 89 no11 (1993) 1593.

5.4 Y.T. Kim, R.W. Collins, Surface Science 233 (1990) 341.

5.5 M.A. Schneeweiss, D.M. Kolb, Solid State Ionics 94 (1997) 171.

5.6 H.A Laitinen and M.S. Chao, J. Electrochem. Soc. 108 (1961) 726.

5.7 J.W. Schultze and K.J. Vetter, Ber. Bunsengers. Phys. Chem. 75 (1971) 470.

5.8 Y.Iwasaki, T.Horiuchi, M.Morita and O.Niwa, Electroanalysis, 9 (1997) 1239.

5.9 A. Hamelin, J.Electroanal. chem. 138, (1982) 395.

5.10 J. Clavilier and C. Nguyen Van Huong, J. Electroanal. Chem.80 (1977) 101.

5.11 H. Angerstein–Kozlowska, B.E. Conway, B. Barnett and J. Mozota, J. Electroanal chem. 100 (1979) 417.

5.12 D. Marcuse., Theory of Dielectric Optical Waveguides, Academic press, London (1991) 2nd edition.

5.13 C.M. Ferro, A.J. Calandra and A. J. Arvia, Electroanalytical Chemistry and Interfacial Electrochemistry, 59 (1975) 239.

5.14 C.M. Ferro, A.J. Calandra and A. J. Arvia, Electroanalytical Chemistry and Interfacial Electrochemistry, 55 (1974) 2911.

5.15 H. Angerstein – Kozlowska and B. E. Conway, Electrochimica Acta, 31 (1986) 1057.

5.16 T. Takamura, K. Takamura, W. Nippe and E. Yeager, J. Electrochem. Soc. 117 (1970) 626.

5.17 F. Chao, M. Costa, A. Tadjeddine, F. Abeles, T. Lopez-Rios and M.-L. Theye, J. Electroanal. Chem. 83 (1977) 65.

5.18 F. Abelés and T. Lopez-Rios, Solid State Communications. 16 (1975) 843.

5.19 C.R.Lavers and J.S. Wilkinson, Sensors and Actuators B 22 (1994) 75 see sited reference.

5.20 R. Greef, R. Peat, L.M. Peter, D. Pletcher, J. Robinson, Instrumental methods in electrochemistry *Southampton electrochemistry group* 179.

5.21 M.A. Schneeweiss and D.M. Kolb, Solid State Ionics 94 (1997) 171.

5.22 H. Angerstein-Kozlowska, B.E. Conway, A. Hamelin and L. Stoicoviciu, J. Electroanal. Chem, 228 (1987) 429.

5.23 D. Dickertmann, J.W. Schultze and K.J. Vetter, Electroanalytical Chemistry and Interfacial Electrochemistry, 55 (1974) 429.

5.24 B.E. Conway, Prog. Surf. Sci, 49 (1995) 331.

5.25 B.E. Conway, H. Angerstein-Kozlowska & W.B.A. Sharp, Anal. Chem. 45 (1973) 1331.

5.26 M. A. Schneeweiss, D.M. Kolb, D. Liu and D. Mandier, Can. J. Chem 75 (1997) 1703.

5.27 H. Honbo, S. Sugawara and K. Itaya, Anal. Chem. 62 (1990) 2424].

5.28 H. Angerstein-Kozlowska, B.E. Conway, A. Hamelin and L. Stoicoviciu, Electrochimica Acta. 31 (1986) 1051.

Chapter 6

Optical – Electrochemical interrogation of underpotential deposition of Cu onto gold surface

6.1 Introduction

Chapter 5 described the application of the integrated optical surface plasmon device in the study of oxide layer formation on gold and its removal from the gold film, then compared the performance of the IOSPR device with other reported optical studies. Another process that modifies the gold surface and its characteristics is the electrochemical deposition of a monolayer of a foreign metal onto the gold surface of the IOSPR device. This is achieved by the process of underpotential deposition (UPD), where the application of a potential, cathodic of the resting potential but anodic of the Nernst potential (potential required for electroplating) leads to the deposition of a monolayer of the foreign metal onto the gold surface of the IOSPR device. Under these conditions the deposited foreign metal is bond to the working electrode more strongly than to themselves [6.1]. The deposition of a monolayer of metal onto gold surface allows modification of the gold surface catalytic attributes, while in some cases it introduces catalytic properties. The catalytic reactions of interest involving modification of gold film surfaces are reactions such as hydrogen evolution, oxygen reduction and oxidation of small organic molecules. The study of copper UPD on gold surface is aided by the fact that Au/Cu show strong interaction and the similarity in atomic radius will give rise to an epitaxial growth of the copper atoms over the gold atoms. There is a strong trend in the application of surface techniques such as scanning tunneling microscopy (STM), atomic force microscopy (AFM) and low energy electron diffraction (LEED) [6.2,6.3], in the study of UPD of metals and very little application of optical techniques. One could suggest this to be due to previously, reported poor performance of optical techniques such as ellipsometry [6.4] and electroreflectance [6.5] when employed in UPD studies as these techniques yield low sensitivity. Recently, Chinowsky *et al.* (6.6) reported using the surface plasmon resonance technique combined with anodic stripping voltammetry to monitor the change in reflected intensity as the wavelengths is varied during the bulk deposition of Cu and Pb onto gold. This chapter describes the combination of an IOSPR sensor with cyclic voltammetry to study the

electrochemical underpotential deposition of a monolayer of copper on a gold electrode surface.

6.2 Experimental procedure

A silica cell was clamped to the waveguide surface and filled with 2 cm^3 of 1.0 x 10^{-3} M Cu^{2+} in 0.1 M perchloric acid (n = 1.334). A three-electrode cyclic voltammetry circuit was established by introducing a platinum wire counter electrode and a saturated calomel (SCE) reference electrode into the cell, with the gold film pads acting as the working electrodes. Permanent contact was made to the gold electrodes outside the cell at the edge of the substrate using a crocodile clip. All three electrodes were connected to a conventional potentiostat, allowing the potential of the working electrode, with respect to the reference electrode, to be controlled and the current, I, through the working electrode to be measured. Optical measurements were performed using the apparatus shown in figure 6.1.

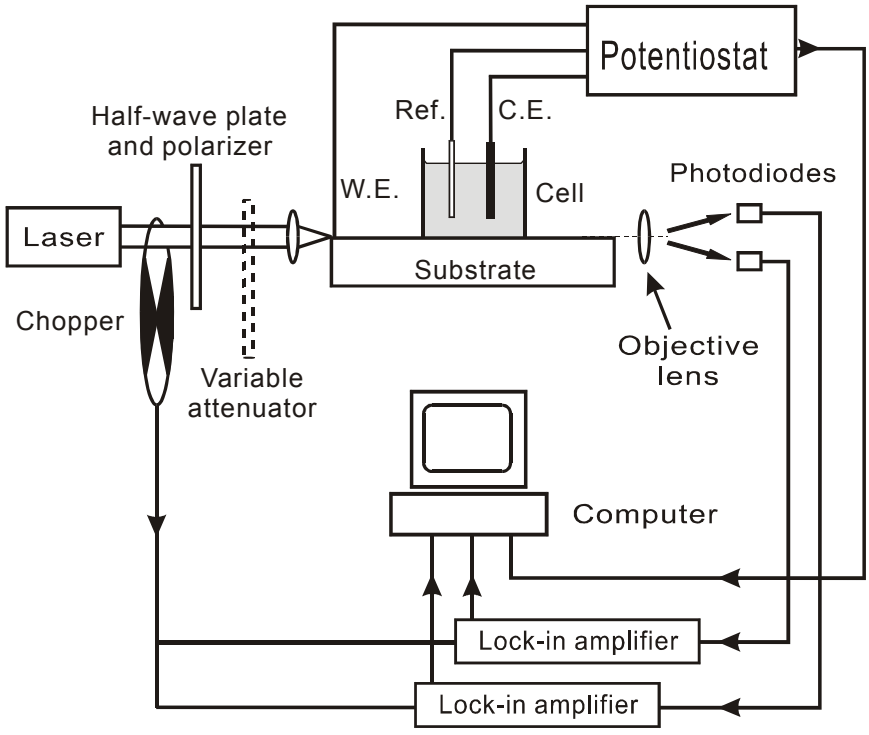

Fig 6.1 Experimental setup

Light from a HeNe laser at 633 nm was chopped and passed through a half-wave plate and polariser, to select the TM polarisation supported by the SPW and through a variable attenuator to adjust input power. The light was end-fire coupled into the device under test and the waveguide outputs were focussed onto two silicon photodetectors. The transmittance of the gold-coated waveguide, T, was recorded after removal of the effects of ambient light using lock-in amplifiers. Potential was applied between the working electrode and the reference electrode during analysis and between each cycle the film was electrochemically cleaned.

6.2 Results

Figure 6.2 shows the current and optical transmission against potential for a 37 nm ± 5 nm gold film coated IOSPR sensor in the absence of copper ions in perchloric acid. For this experiment the potential scan rate was 20 mV/s resulting in larger currents for the oxidation and reduction, in comparison to that previously discussed during the UPD process. In the absence of copper ions, there is no current peak corresponding to UPD at 0.24 V and the optical transmission continues to increase with decreasing potential due to anion desorption. The significant current flowing at potentials between 0.0 V and 0.1 V is due to hydrogen ion discharge ($2H^+$ (aq) + $2e^- \rightarrow H_2$ (g)) and as observed for oxygen evolution there was no corresponding change in transmittance. Since both Figure 6.2 and 6.7 show the steady-state situation after several cycles, it is clear that the underpotential deposition process does not strongly affect the oxidation and reduction of the gold film as the optical and electrochemical response are generally similar in the presence and absence of Cu^{2+}.

Fig 6.3 shows the optical transmission, (T) and the electrochemical current, (I) as a function of the applied potential, E, after seven cycles, in response to the application of a triangular potential waveform between the gold film and the reference electrode, from 0.1 V to 1.6 V (scan rate 5 mV/s) in a cell containing 0.1 M perchloric acid and 1 mM copper (Cu^{2+}). The potential range of 0.5 V to 1.6 V in the anodic scan covers the potentials required for the anodic oxidation of the gold surface and oxygen evolution, which are observed electrochemically as a rise in current and optically as a drop in transmittance [6.8].

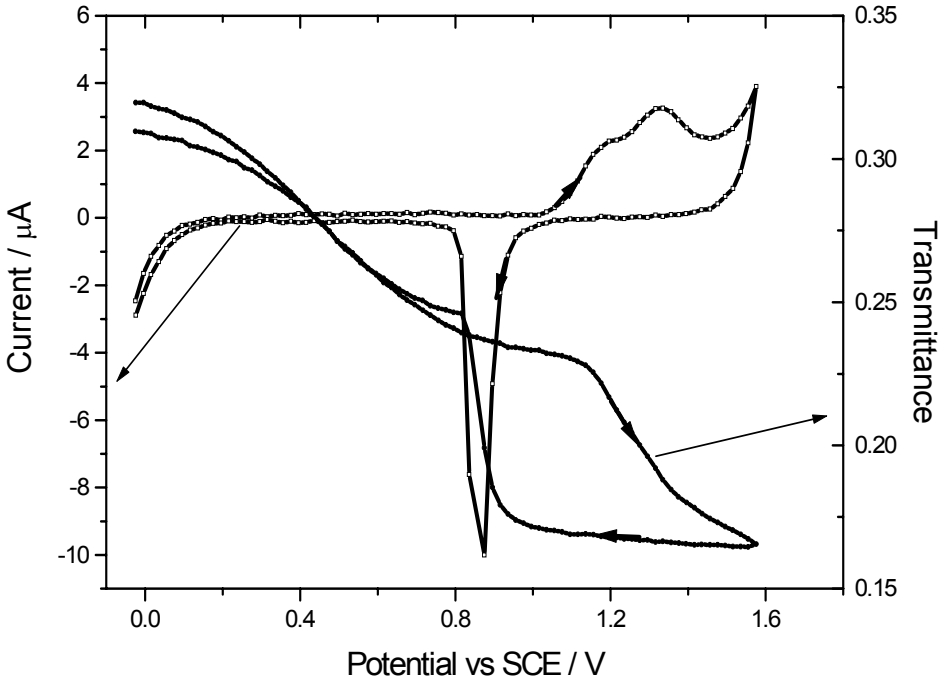

Fig (6.2) Optical and electrochemical response to oxidation of a gold film in 0.1 M $HClO_4$, scan rate 20 mV / s.

The cathodic scan in the potential range of 0.5 V to 1.6 V shows the corresponding reduction peak current and increase in the optical transmission, which are due to the removal of the oxide layer previously formed during the anodic scan, this process has been addressed in detail in chapter 5. The reduction is completed at about 0.7 V with the optical transmittance returning to its pre-oxidation value. Cycling between the potential range of 0.5 V to 1.6 V electrochemically cleans the gold surface before UPD.

As the potential decreases from 0.7 V to 0.4 V, the transmittance increases due mainly to the electronic effects on the optical properties of Au surface and alteration of the ionic distribution of the double layer at the metal – electrolyte interface. This ionic redistribution involves the chemisorption of ClO_4^- anion at the gold surface and results in a small displacement current. At a potential of 0.24 V a peak in the current is observed, which is due to the deposition of a monolayer of Cu onto the gold film surface. The deposition of this monolayer, of approximate thickness 0.3 nm [6.9]

gives rise to a 10 % drop in the optical transmittance. This compares favourably with that reported for other optical techniques such as ellipsometry were a change of 0.1 % in Ψ [6.4] and a 1 % change for reflectance were reported [6.5]. The refractive index of the gold film at a wavelength of 633 nm may be taken to be $n_{Au} = 0.20 – j3.45$ [6.7] while that of a 0.8 nm thick film of copper on gold has been estimated to be 0.70 – j2.25 at 546.1nm [6.4], in reasonable agreement with accepted values for thicker films [6.10]. The refractive index of copper at 546.1 nm may be interpolated to yield an estimate of $n_{Cu} = 0.27 – j3.40$ for the index of the copper film at 633 nm, which is close to that of a gold film. Visscher and Cox [6.4] suggested this to be the reason for the poor performance of their ellipsometric analysis for this particular study.

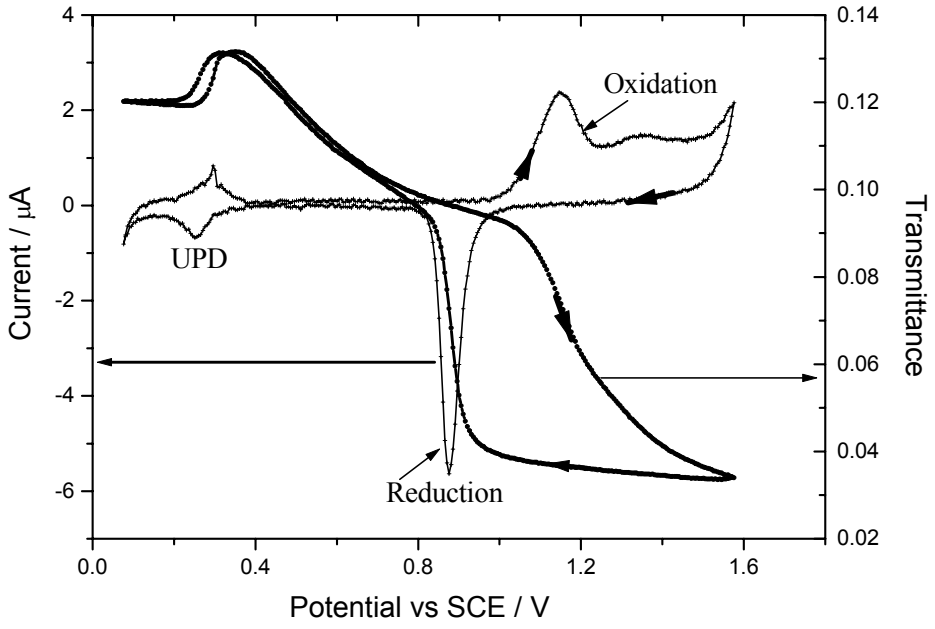

Fig 6.3 Optical and electrochemical response to UPD of copper and the oxidation of a gold film in 0.1 M $HClO_4$ containing 1 x 10^{-3} M of Cu, sweep rate 5 mV / s.

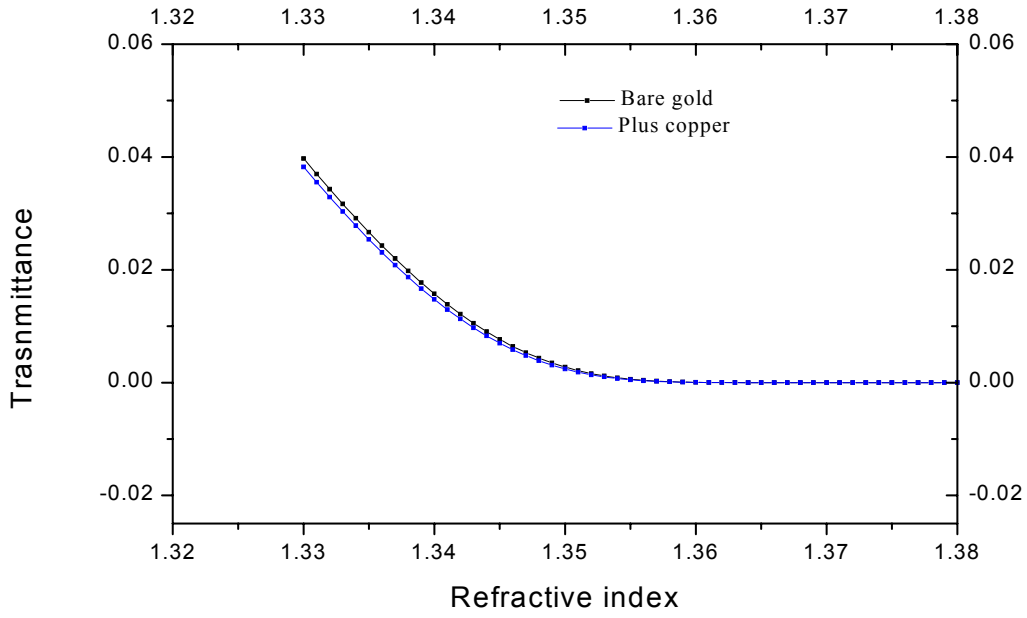

Fig 6.4 Theoretical plot showing the effect of copper deposition on the gold film

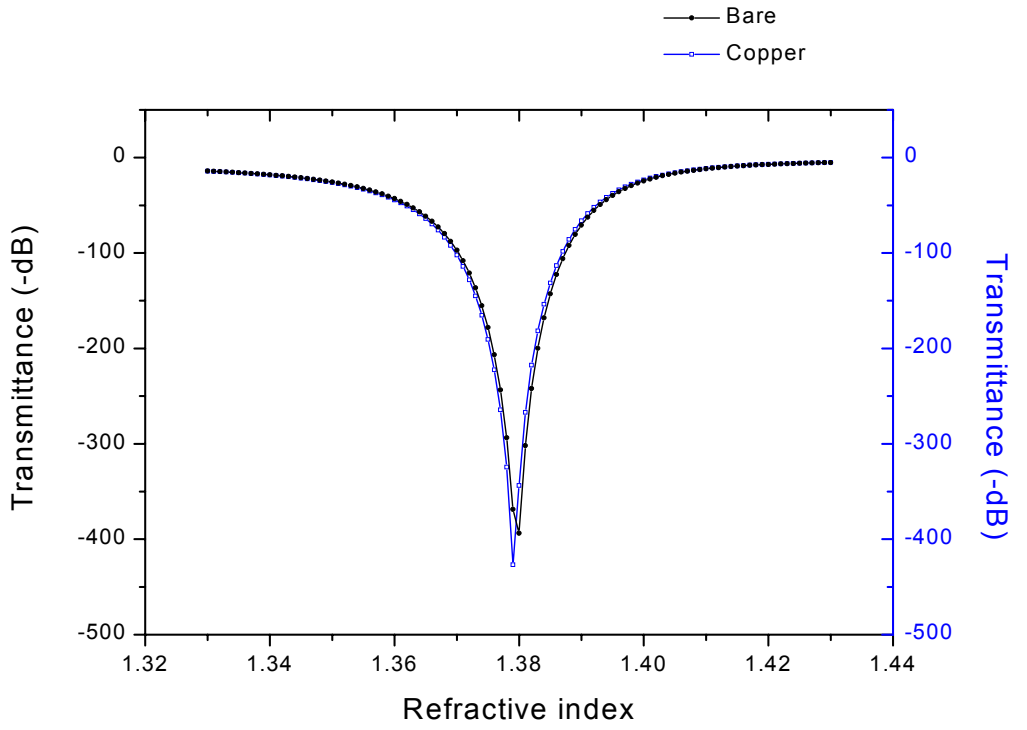

Fig 6.5 Log of the theoretical plot showing the effect of copper deposition on the gold film

The simple homogeneous slab waveguide model described in chapter 3 yields a theoretical drop of approximately 5 % in transmission when a 0.3 nm copper film with the index of 0.27 – j3.40 is deposited on a 35 nm gold film coated IOSPR sensor. Considering the approximations made in the model (see chapter 3) and the experimental uncertainties, this is in good agreement with experimental results. Integration of the peak current over time during deposition gives a charge of 0.41mC/cm^2, which is close to the theoretical value of 0.44 mC/cm^2 for a monolayer of Cu^{2+} ions transferring two electrons per ion to an ideal Au (111) surface [6.3]. This is expected, as any deviation of the gold face from (111) would lead to a reduction in the measured charge for the deposition process, as the face of the gold electrode affects the deposition process. The number of atoms per cm^2 on the gold face reduces following deviations from Au (111) surface. After the deposition of copper on the gold film, further increase in the applied potential results in a rise in transmittance although not as steep as that observed before adsorption of Cu. This change in slope could be associated to the adsorption of the anion onto a different surface (Cu). The direction of the potential scan is reversed at 0.1 V and a peak in current is observed at 0.29 V, corresponding to stripping of the Cu monolayer and the transmittance increases correspondingly. The hysteresis observed optically confirms that the adsorption and desorption of the copper monolayer occur at different potentials.

Effect of structural face on UPD process.

The cyclic voltammogram obtained for the UPD of Cu on a gold film without extending the potential to that required for the oxidation of the gold film is shown in figure 6.6.

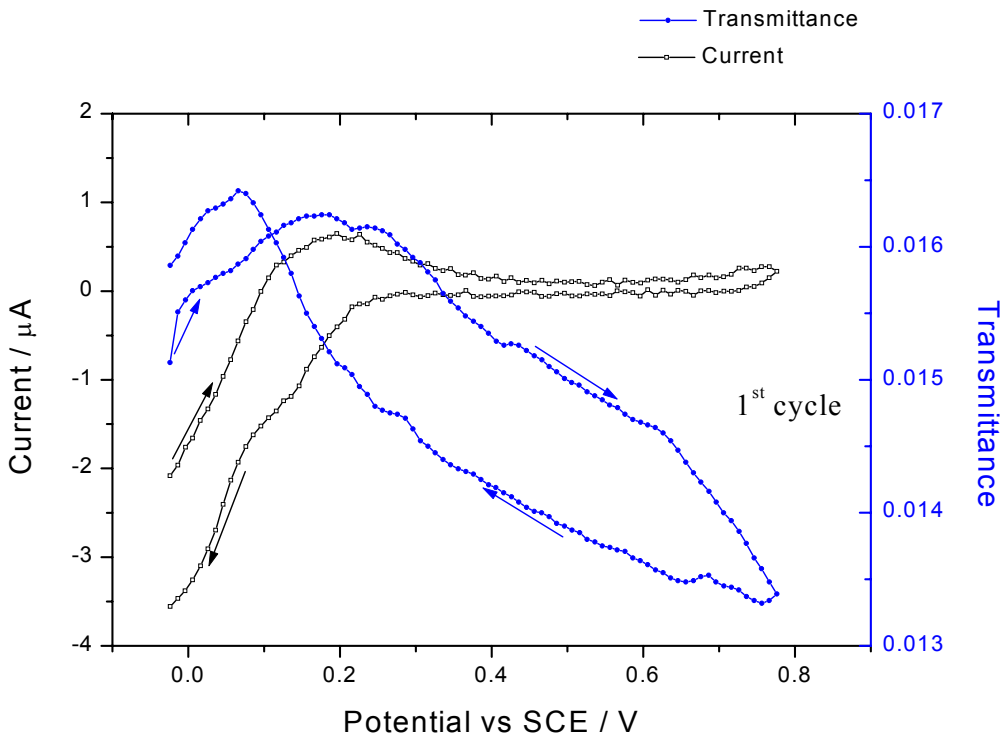

Fig 6.6 Optical and electrochemical response to UPD of Cu on an un-oxidised gold surface in 0.2 M H_2SO_4 containing 5 x 10^{-3} M of Cu, scan rate 10 mV / s.

The conductive electrolyte used here was 0.2 M sulphuric acid. Figure 6.6, when compared to figure 6.3 where oxidation of the gold firm preceded the underpotential deposition of copper on the gold film, shows that the magnitude of both electrochemical and optical response to the deposition of a monolayer of copper is reduced for figure 6.6 where no oxidation of the gold film had been carried out. This observation suggests the presence of a foreign adsorbate, blocking the transfer electrons between the bulk electrolyte and the gold film. Oxidation of the gold results in the removal of this adsorbate (see section 5.2.2 and fig 5.4). The removal of the foreign adsorbate shows up both electrochemically and optically, with the optical response having the more significant change see fig 6.7. Here a rise in transmittance of 94 % at 0.1 V between the anodic and cathodic scan was observed, with the typical optical response to UPD adsorption and desorption. While electrochemically the typical rise in current in response to the UPD process that is the peak current, was broad for the first cycle.

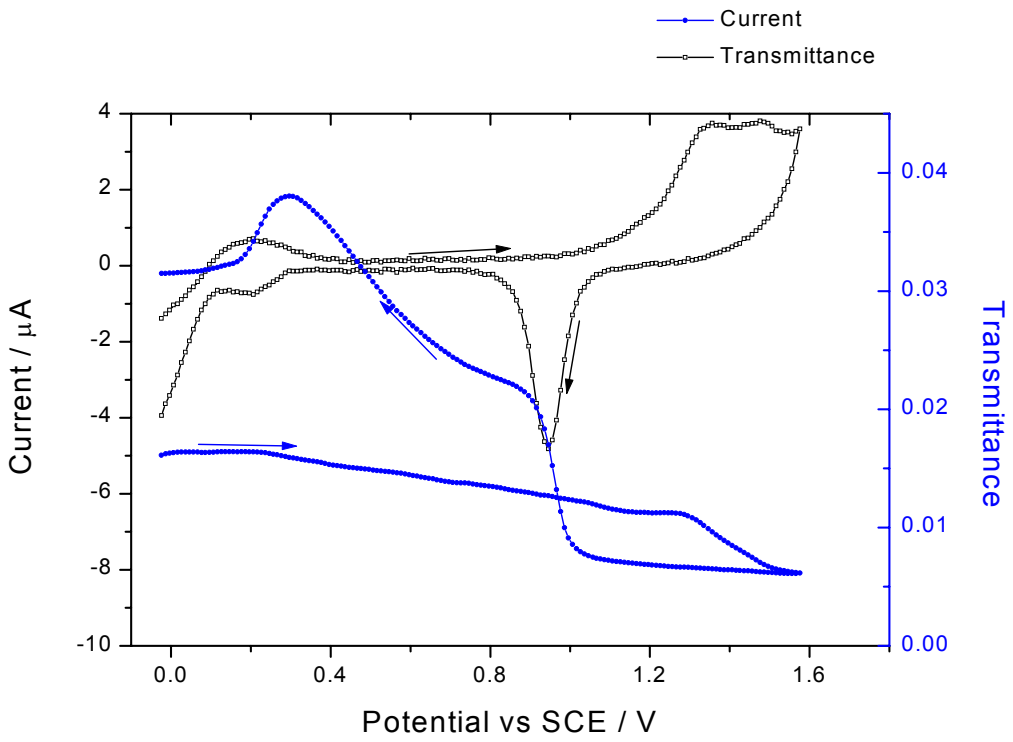

Fig 6.7 Optical and electrochemical responses to UPD of Cu on the gold film following the first cyclic scan into oxidation region. Conductive electrolyte was 5 x 10^{-3} M of Cu in 0.2 M H_2SO_4 with a scan rate of 10 mV / s.

Upon carrying out repeated cycles that extend into the oxidation-reduction region the deposition and stripping peaks become sharper, this is illustrated in figs 6.8 and 6.9. These results suggest that the condition of the gold film face has a strong influence on both optical and electrochemical results obtained here, as one would expect for a surface sensitive technique.

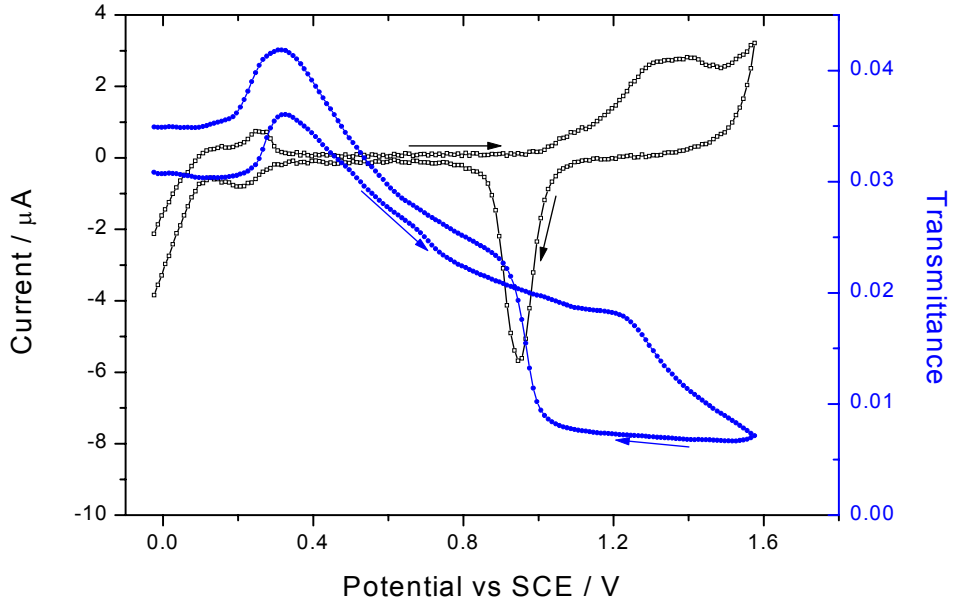

Fig 6.8 Optical and electrochemical response to UPD of Cu on the gold film following the second cycle into oxidation region. Conductive electrolyte was 5 x 10^{-3} M of Cu in 0.2 M H_2SO_4, scan rate 10 mV / s.

Optical and electrochemical comparison of weakly and strongly adsorbing anions on underpotential deposition of copper on gold.

As with the study of oxidation and reduction of gold film in chapter 5, comparison between ClO_4^- and HSO_4^- anions was carried out. Comparing figure 6.3 and figure 6.9, the overall plots are very similar with the difference occurring at the potential of the peak currents in response to the deposition and stripping of Cu^{2+} off the gold film. With sulphuric acid the adsorption peak occurred at 0.23 V while that of perchloric acid occurred at a more positive potential of 0.25 V (see fig 6.9), this compares well with that observed during the oxidation and reduction of the gold film. Recalling the latter, the peak currents for oxidation of the gold film in perchloric acid occurred at a lower potential, as ClO_4^- are weakly adsorbed thus easily "replaced". This suggests that the process of the UPD of Cu involves a competitive step between the anions present and the metal deposited. Desorption of Cu^{2+} in sulphuric acid occurred at a potential of 0.27 V while that in perchloric acid occurred at 0.29 V. The peak separation for the deposition and stripping peak of copper in sulphuric acid was 0.05

V while that for perchloric acid was 0.04 V, reasons for this are not conclusive as the scan rates are different.

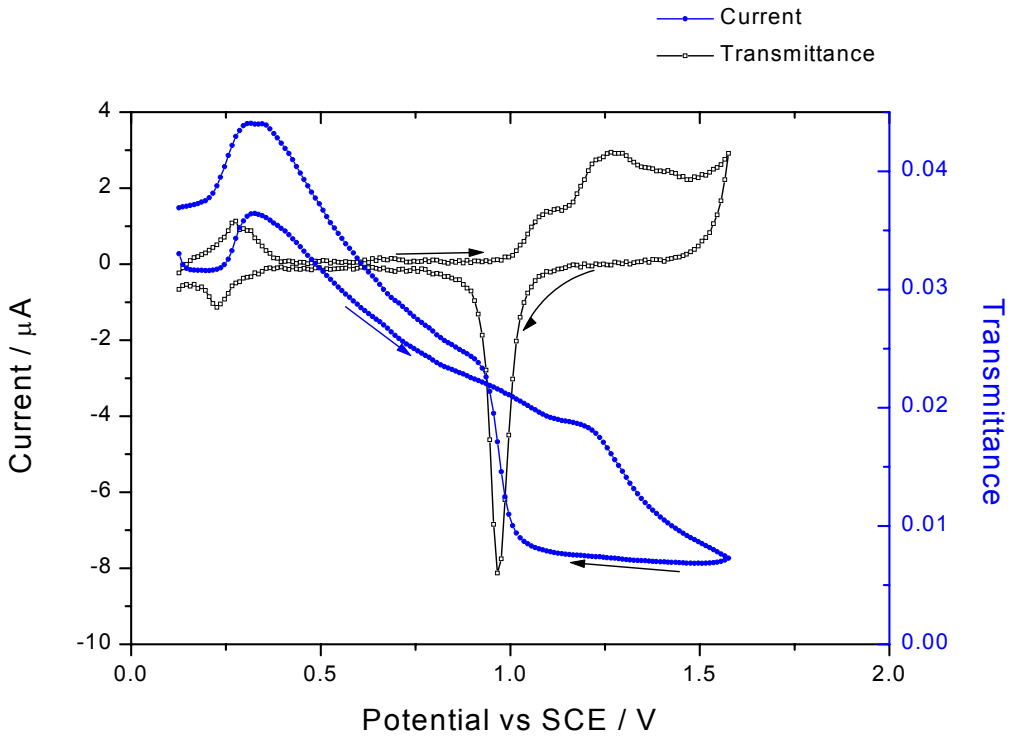

Fig 6.9 Optical and electrochemical response to UPD of Cu on the gold film following fourth cycle into oxidation region. Conductive electrolyte was 5 x 10^{-3} M of Cu in 0.2 M H_2SO_4, scan rate 10 mV / s.

Effect of repeated scans

Following repeated scans involving UPD of Cu and the oxidation–reduction of the gold film the shape of the CV changed slightly. The peak at 1.17 V which is due to the adsorption of OH group and the replacement of ClO_4^- anions increases while that due to replacement turnover (1.35 V) reduces with every scan (see fig 6.10).

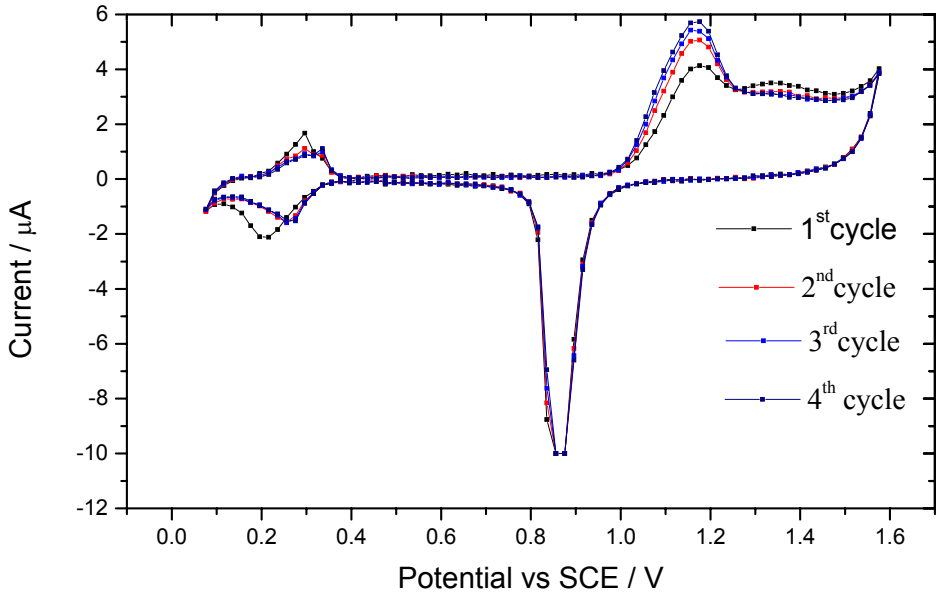

Fig 6.10 Four cycles of optical and electrochemical response to the underpotential deposition of Cu and oxidation of a gold film. 1 x 10^{-3} M of Cu in 0.1 M $HClO_4$, scan rate 20 mV / s.

Effect of variation in scan rate

The alteration of the scan rate effects both the optical and electrochemical responses. Fig 6.11 shows the electrochemical response to underpotential deposition of Cu and oxidation of a gold film in response to varying the scan rate from 20 mV/s to 5 mV/s. As expected the peak current is directly proportional to the sweep rate, here for the deposition of Copper on a gold film, peak current at; 5 mV/s = -0.6 μA, 10 mV/s = -0.9 μA and 20 mV/s = -1.5 μA. Increasing scan rate led to increases in the separation of copper deposition and stripping peak optically (see fig 6.12). The rise in transmittance observed after each cycle is a direct consequence of drift in the system due to contribution from fluctuation in temperature and mechanical drift. The optical oxidation – reduction window (see fig 6.12) reduces with scan rate, while electrochemically (fig 6.11) the peak current usually associated with the replacement turnover reduces as the scan rate is reduced, this is significant at scan rate of 5 mV/s. This cannot be attributed wholly to the slow scan rate of 5 mV/s as keeping the scan at 20 mV/s and running several repeated scans, similar effects as that observed with the slow scan rate of 5 mV/s was obtained.

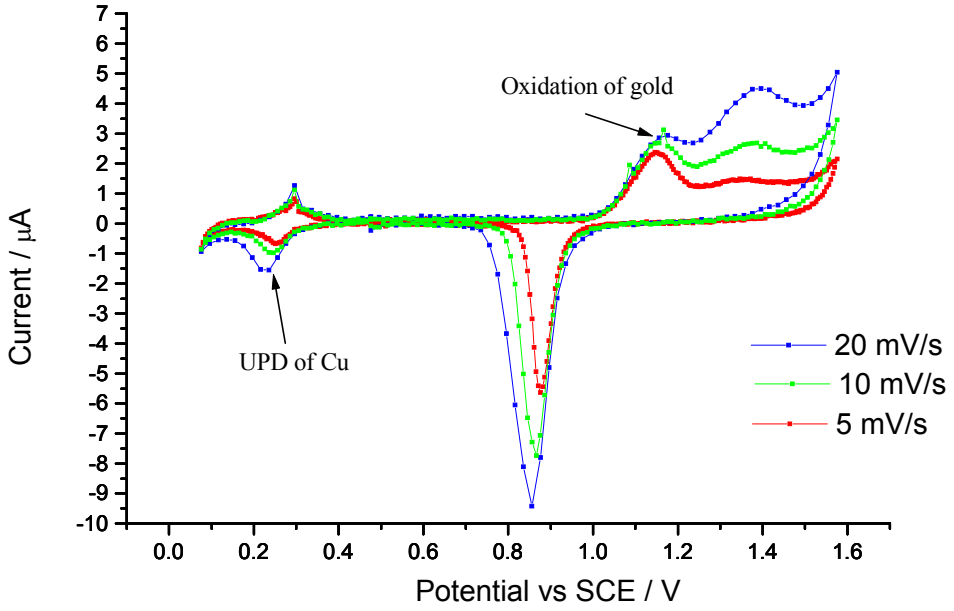

Fig 6.11 Electrochemical response to underpotential deposition of Cu and oxidation of a gold film. Showing the effect of varying the scan rate from 20 mV / s to 5 mV / s. Conductive electrolyte was 1 x 10^{-3} M of Cu in 0.1 M $HClO_4$.

The current peak due to desorption of the anions and its replacement by OH groups (1.17 V) increases while that due to replacement turnover (1.35 V) reduces suggesting that monolayer of oxide has been completely formed at a lower potential or that the gold face has changed. No change to the Cu stripping peak potential position in response to the increase in scan rate was observed, while the Cu deposition peak moves to the negative direction in response to the increase in scan rate. Increase in scan rate leads to a decrease in the mass of Cu deposited. Figure 6.13 is a plot of mass deposited in response to the increase of the scan rate (see appendix A2 for process involved in determining the mass of metal deposited). This response is expected as the UPD process is affected by mass transport, which in this case is diffusion. The change in mass in response to variation of scan rate observed in this work agrees with studies carried out by Mauro C. Santos *et al*. [6.11], where holding the potential for over 120 seconds a similar response to that obtained here was reported. Omar *et al*. [6.12] studied the effect of varying copper concentration on the peak potential and found that decreasing the concentration of Cu^{2+} lead to the whole UPD peaks shifting towards the lower potential.

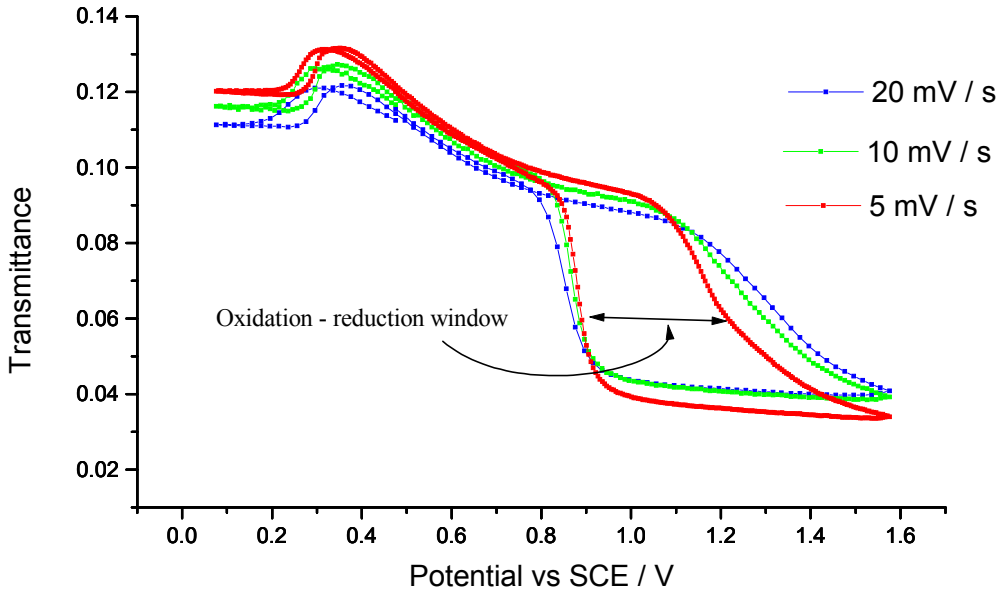

Fig 6.12 Optical response to the variation of the scan rate from 20 mV / s to 5 mV / s for the UPD of Cu on gold and oxidation of the gold film. Conductive electrolyte was 1 x 10^{-3} M of Cu in 0.1 M $HClO_4$.

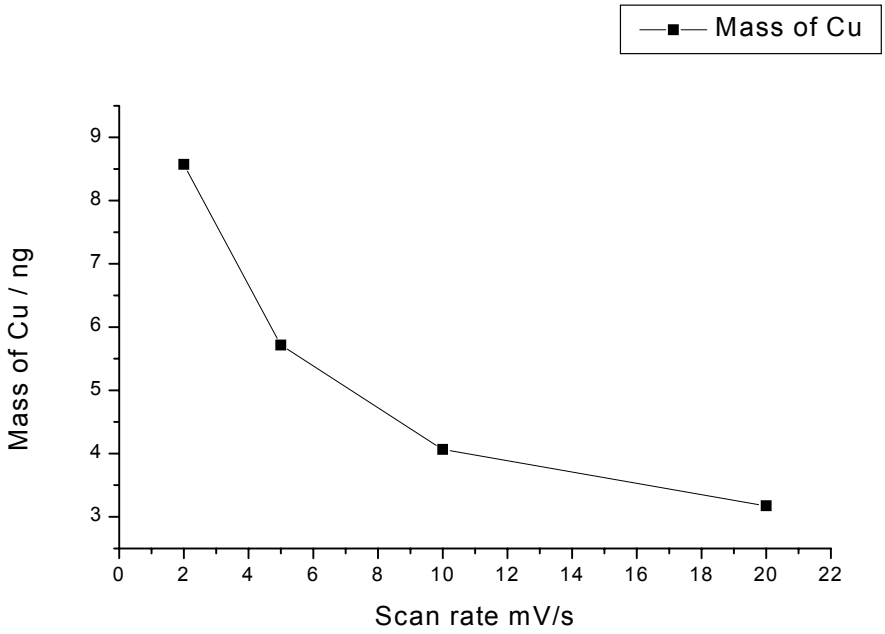

Fig 6.13 Plot showing the mass of Cu deposited on the gold film against scan rate. Conductive electrolyte was 1 x 10^{-3} M of Cu in 0.1 M $HClO_4$.

6.3 Conclusion

The process of underpotential deposition of copper on a gold film has been monitored for the first time using the surface plasmon technique. Other optical techniques have been used previously in the study of the underpotential deposition of copper on gold, such as ellipsometry (0.1 % in ψ) and reflectance (1 %) but in all cases the magnitude of the optical response using the IOSPR device (10 %) here was much greater. The closeness of the value obtained from integrating the area under the peak current for the deposition of Cu (0.41 mC / cm^2), to the theoretical value of 0.44 mC / cm^2, expected for the deposition of a monolayer of copper on gold film, confirmed the deposition of a monolayer of copper on the gold film (at scan rate of 5 mV/s). The optical and electrochemical response to both oxidation and the underpotential deposition of copper were affected by the presence of foreign adsorbate on the gold film signifying the importance of the surface state during analysis. Other factors that affect the response of the device during the study of UPD of copper on gold was the type of anion present and the scan rate. Shown here is the point that the processes involved in the electrochemical oxidation and reduction of a gold surface and the underpotential deposition of Cu^{2+} on gold can be continuously monitored in-situ with high sensitivity using a compact integrated optical surface plasmon resonance sensor. The waveguide approach is ideally suited for multisensor integration and the results compare favourably with those obtained using ellipsometry and reflectance measurements. Sensor arrays for interrogation of thin surface films are expected to find wide application in chemical sensing applications and combined monitoring of electrochemical and optical parameters represents a powerful combination.

6.4 Reference.

6.1 J.G. Xu and X.W. Wang, Surface Science. 408 (1998) 317.

6.2 J. Hotlos, O.M. Magnussen, R.J. Behm. Surface Science. 335 (1995) 129.

6.3 T. Nishizawa, T. Nakada, Y. Kinoshita, S. Miyashita, G. Sazaki, H. Komatsu, Surface Science. 367 (1996) L73.

6.4 W. Visscher and A.P Cox, Electrochimica Acta 37 (1992) 2245.

6.5 K. Takamura, F. Watanabe and T. Takamura, Electrochimica Acta 26 (1981) 979.

6.6 T.M. Chinowsky, S.B. Saban, S.S. Yee, Sensors and Actuators B 35-36 (1996) 37.

6.7 R.D. Harris, B.J. Luff, J.S. Wilkinson, A. Brecht, G. Gauglitz, R.A. Abuknesha, Biosensors and Bioelectronics 14 (1999) 377.

6.8 Y.Iwasaki, T. Horiuchi, M.Morita & O. Niwa, Electroanalysis 9 (1997) 1239.

6.9 D.M.Kolb, D. Leutloff and M. Przasnski, Surface Science, 47 (1975) 622.

6.10 P.B.Johnson and R.W. Christy, Physical Review B, 6 (1972) 4370.

6.11 Mauro C. Santos, Lucia H. Mascaro and Sergio A. S. Machado Electrochimica Acta. 43 (1998) 2263.

6.12 H.I. Omar, H.J. Pauling, K. Juttner, J. Electrochem. Soc. 140 (1993) 2187.

Chapter 7

Optical – Electrochemical interrogation of lipid layers

7.1 Introduction

A bare gold electrode lacks molecular selectivity and specificity, which reduces its potential application in numerous areas such as analytical sensor development and electroorganic synthesis [7.1]. To over come this problem the electrode surface is functionalised using biomembranes such as phospholipid layers, which allows the electrode to be used in chemical sensing, biosensing, biomimetics and biocompatibility electrocatalysis [7.2].

Interest in phospholipid layers (biomembranes) for biological application is two-fold; firstly, they provide simple models of biological membranes, which can be studied using a variety of spectroscopic and microscopic techniques. Secondly, the incorporation of functionally active peptide, or protein, ion-channels into this single supported bilayer has potential for biosensor applications. One of the main tasks of biomembrane functions is molecular recognition, which entails selectivity and specificity. These attributes can be introduced to the gold surface of the IOSPR device by the adsorption of the lipid layer onto the gold film. The application of biomembranes supported on solids, have grown rapidly in both scientific and practical applications due to the stability and bond strength of these solid supported lipid layers [7.3]. The bond strength and stability are improved by indirect immobilisation of the lipid to the gold surface via a thiol layer, due to the chemical interaction between the thiol and the metallic support. The bonding of the thiolate group to the gold surface is very strong (homolytic-bond strength ≈ 40 kcal mol-l) [7.4]. A value of -5.5 kcal mol-l (exothermic) was calculated for the net energy for adsorption of alkanethiolates on gold by Schlenoff *et al.* using electrochemical data [7.5]. The number of reported surface active organosulphur compounds that form monolayers on gold has increased in recent years. These include, among others thiophenols, mercaptopyridines, mercaptoanilines, thiophenes, cysteines, xanthates, thiocarbaminates, thiocarbamates, mercaptoimidazoles, thioureas and alkaneselenols [7.6]. The phospholipids layer formed over the thiol layer retains its hydrophobic-hydrophilic character, which is governed by the functional group present at the tail end of the phospholipid layers. The formation of the multilayer structure of thiol and phospholipid on a gold film can

be carried out by self-assembly or Langmuir-Blodget techniques, or a combination of both.

The present understanding of the molecular structure of SAMs made of alkanethiols on Au is largely derived from methods such as reflectance, infrared spectroscopy, transmission electron diffraction and X-ray diffraction. The generally agreed structure of the alkanethiols over a gold film is that of (√3X√3) R30° overlayer and that the molecule is tilted 33° from the surface normal. This tilt is a result of the chains re-establishing van der Waals contact in an assembly where the sulphur-sulphur distance is approximately 5 Å larger than the alkyl chains in a close packed layer. The bonding interaction exhibited by the molecule and the device is a balance of the sulphur–gold chemisorption, sulphur–sulphur interactions and interaction between the chains.

This chapter examines the application of the IOSPR device in monitoring the effect of adsorbing a thiol layer and the subsequent electrochemical desorption of the thiol layer from the gold film. It also addresses the application of the IOSPR device in the adsorption of phospholipid layer onto a monolayer of thiol and looks into the effect of mechanical and temperature changes to the optical response of the device. Surface plasmon resonance potentially allows for the process of phospholipid layer formation to be followed in real time, while cyclic voltammetry is used to investigate the capacitive behaviour and coverage of the films.

7.2 Electrochemical studies on gold wire electrodes:

7.2.1 Procedures

Chemicals

TRIS buffer (0.1 M, pH 8.0) was prepared from stock solutions of tris(hydroxymethyl)aminomethane (0.2 M, Aldrich, Ultrapure grade), hydrochloric acid (0.2 M, BDH, AnalaR grade, 37 %) and deionised water with the pH adjusted to 8.00, using a pH meter (Corning 145). Buffer-electrolyte solutions were prepared by the addition of sodium chloride to the buffer solution (0.1 M, BDH and AnalaR grade). The redox couple solution, hexaamine ruthenium (III) chloride solution, $Ru(NH_3)_6Cl_3$, (1 mM, Aldrich) was made using the buffer and electrolyte solution

described above, all buffered solutions were made immediately before use. The alkanethiols *tert*-dodecanethiol was from Aldrich, stored in a sealed container in a fume cupboard and used as received. Dioleoyl phosphatidylcholine from sigma (10 mg cm^{-3} in methanol,) was used as received. All phospholipids were stored at -15 ºC, ethanol was from BDH (AnalaR grade)

Preparation of gold wire

Five Eppendorf pipette tips were stuck unto a flat cover-lid using epoxy. A strand of gold wire of 1 cm length (0.2 mm diameter) was attached to a silver wire by pushing the gold wire between the silver wire and the insulating material. This was carried out to provide support for the gold wire and point of electrical contact. This wire was placed in the Eppendorf pipette such that the gold strand was directly at the middle of the pipette. Next, slow set epoxy (Epofix Kit Steurs) were added into the pipette and left over night to harden at 40 °C. The electrodes were removed from the pipette and polished using 25μm, 1μm, 0.3μm, and finally 0.05μm aluminium oxide powder (Buehler), giving rise to an electrode which exhibited a mirror surface. The electrodes were electrochemically cleaned, ready for surface functionalisation using thiol layers.

Self-assembly of an alkanethiol monolayer on gold

Deposition of alkanethiol monolayer onto the electrochemically cleaned gold surface was carried out using a standard self-assembly procedure. Prior to self-assembly, the gold wire electrode was placed in a solution of sulphuric acid and a potential was then applied between a reference and working electrode resulting in the oxidation and reduction of the gold film. Following this cleaning procedure, the electrode was rinsed in ethanol and immersed in a freshly prepared solution of alkanethiol in ethanol (1 mM). The electrode was left undisturbed for at least 12 h, allowing a monolayer of the thiol film to be formed on the gold surface [7.7]. The modified electrode (substrate) was then removed and rinsed thoroughly in fresh ethanol, soaked in pure ethanol for at least 30 min, re-rinsed in ethanol and dried in a stream of nitrogen gas for a further 5 min. Finally, a gold wire electrode with a monolayer of thiol adsorbed over it was placed in a solution of buffer electrolyte containing a hexaamine

ruthenium (III) chloride. The preliminary study of the electrochemical desorption of the thiol layer over the gold electrode is discussed below.

7.2.2 Results

Probing the desorption of a thiol layer

Determination of the potential at which the thiol can be electrochemically desorbed is important, as it reveals the useful working potential range of the IOSPR device using thiol layer, before the thiol is lost. This potential limit can also be applied to intentionally remove the thiol layer for cleaning purpose such as when replacement of the older thiol layer by a new one is required. This removes the need to fabricate a new device after every use. In addition this attribute can allow for electrochemically switching on and off sensing pads in multi-sensing device during the functionalization of the surfaces. The aim of this experiment was to determine the potential at which a nucleation loop would be obtained that is the potential at which the surface of the gold wire electrode changes due to the loss of the thiol layer.

Using the gold wire electrode placed in a solution of buffer electrolyte containing hexaamine ruthenium (III) chloride (redox probe), an anodic scan was applied first from -0.6 V to 0.4 V and then in the reverse direction. This gave rise to the typical electrochemical response to the oxidation / reduction of a redox probe (see fig 7.1). The anodic potential limit was then increased in steps of 0.05 V (fig 7.2) and at potentials exceeding 1 V a nucleation loop was obtained (see fig 7.3).

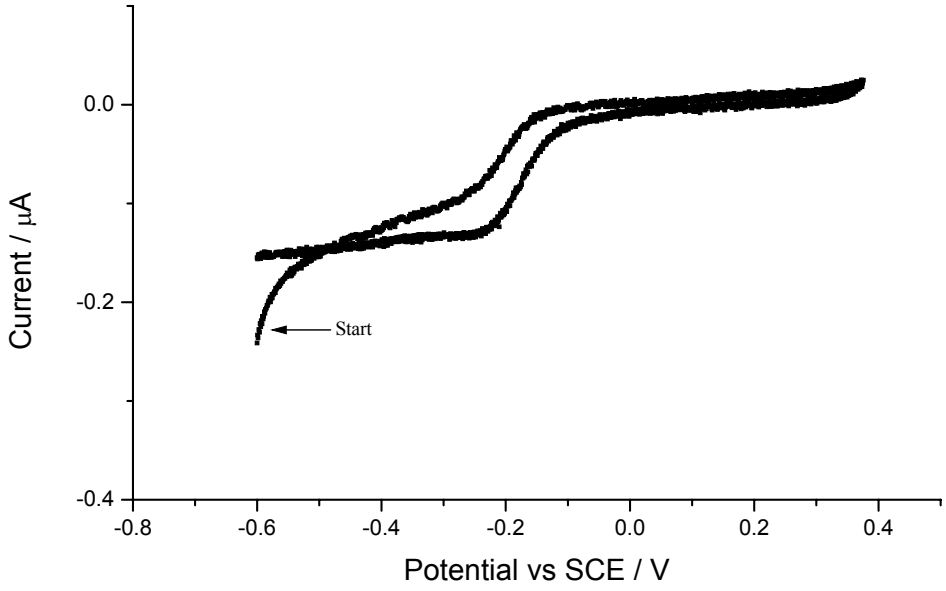

Fig 7.1 Cyclic voltammogram (100 mV/s) of hexaamine ruthenium (III) chloride (1mM) in 0.1 M buffer electrolyte) on a gold wire.

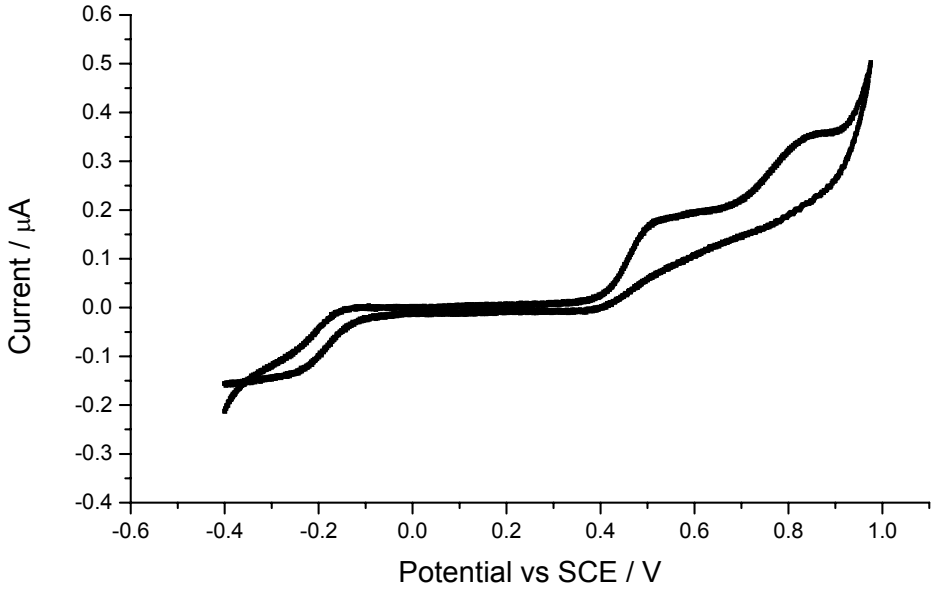

Fig 7.2 Cyclic voltammogram (100 mV/s) of hexaamine ruthenium (III) chloride (1mM in 0.1 M buffer electrolyte) on a gold wire. Plot shows the typical oxidation-reduction plot for a redox probe and peak currents due adsorption of chloride ion (0.5 V) and the oxidation of the gold film (0.85 V).

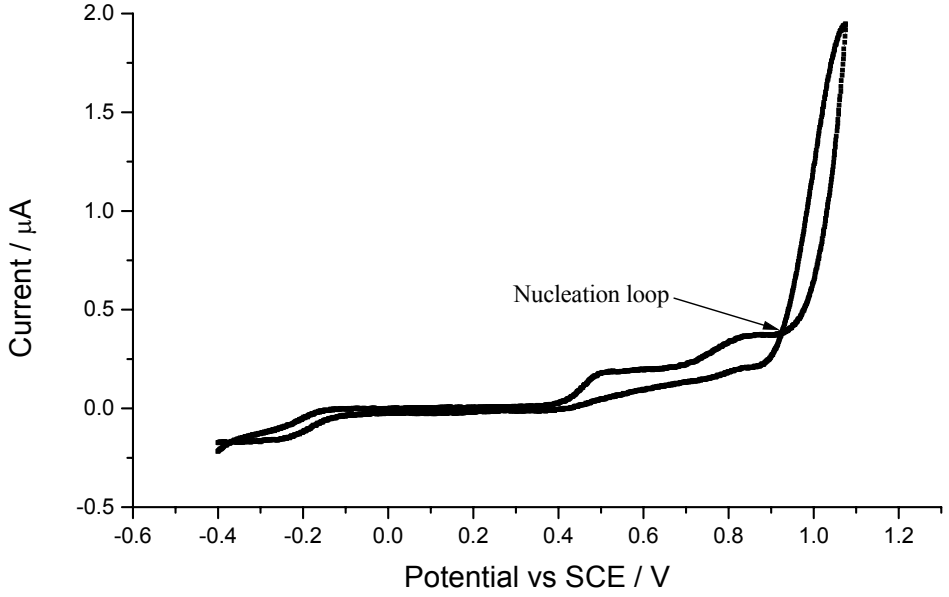

Fig 7.3 Cyclic voltammogram (100 mV/s) of hexaamine ruthenium (III) chloride (1mM) in 0.1 M buffer electrolyte) on a gold wire showing the formation of a nucleation loop.

7.3 Electrochemical and optical studies of thiol layers on IOSPR device.

Having determined the potential at which the thiol layer was lost following the application of potential between the working and reference electrode in the anodic scan using the gold wire electrode, the process was repeated using the IOSPR device. Firstly, the gold film was oxidised in the buffer solution which, in addition to giving the electrochemical and optical response in the presence of the buffer-electrolyte, allows a quantitative analysis to be carried out by comparing the area under the oxide stripping peak in the presence of thiol and its absence. This shows the percentage of thiol layer removed from the gold film following each oxidation-reduction cycle. The structural integrity of the thiol layer was probed using hexamine ruthenium chloride solution.

7.3.1 Procedures

The gold film on the IOSPR device was oxidised in a solution of buffer-electrolyte, then functionalised using a thiol layer. The chemicals and procedure applied here are similar to that carried out on the gold wire electrode (section 7.2.1). Following the adsorption of the thiol layer over the gold film of the IOSPR device, the substrate was

rinsed in buffer-electrolyte solution and then set up as shown in fig 6.1 ready for measurements.

7.3.2 Results

Optical and electrochemical response to bare electrode on buffer-electrolyte.

Fig 7.4 is the optical and electrochemical response to the oxidation and reduction of a bare gold film in 0.1 M buffer electrolyte. Two current peaks were obtained, at 0.471 V and 0.767 V with the corresponding drop in the transmittance. The fall in transmittance between 0.1 V and 0.6 V is due to the adsorption of anions with the current peak at 0.471 V due to chloride ion adsorption. The second peak at the anodic scan, at 0.767 V is due to the formation of an oxide layer, this is complemented optically with the steep fall in the transmittance between 0.6 V and 0.9 V. Here a 45 % drop in transmittance was obtained, comparing the difference of the transmittance value at the onset of oxidation, that is 0.061 V and during the cathodic scan at that same potential of 0.061 V.

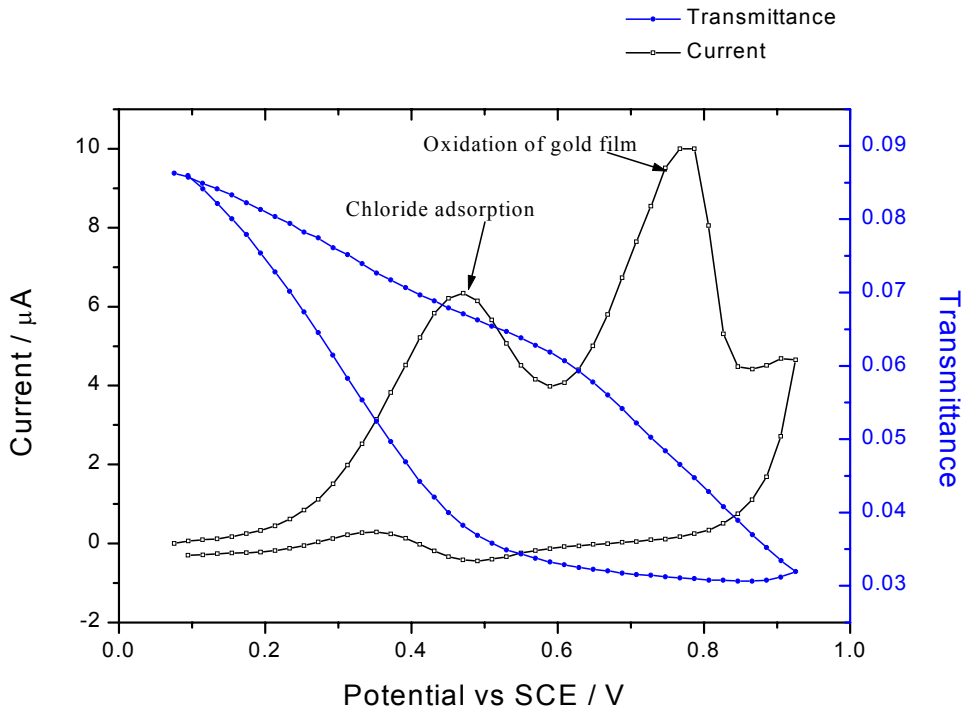

Fig 7.4 Optical and electrochemical response to the oxidation of a bare gold film (45 ± 5 nm) in buffer electrolyte, with a scan rate of 20 mV / s.

The direction of the potential scan was reversed at 0.9 V and a peak current was observed in the cathodic scan at 0.497 V, this peak current is due to the reduction of the oxide layer previously formed. In response to the removal of the oxide film formed during the anodic scan, a sharp rise in the transmittance back to its original point was observed. The positions of the peak currents did not change with repeated cycles (fig 7.5) but the magnitude of the current associated with the oxidation peak was significantly reduced. A drop from 10 μA to 6.2 μA, which could be associated with the cleaning of the electrode by the oxidation – reduction process, was observed using sulphuric acid.

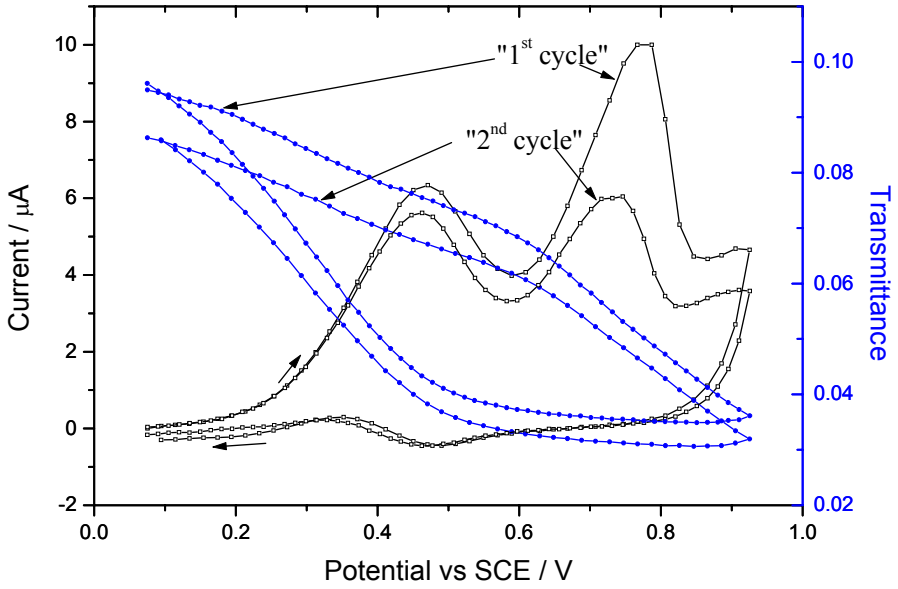

Fig 7.5 Optical and electrochemical response to the oxidation of the gold film (45 nm) in buffer electrolyte (0.1 M), with a scan rate of 20 mV / s comparing the first and second cycle of the oxidation process of the gold film.

Probing the deposition of a thiol layer

Monitoring of the deposition of the thiol layer in real time was not carried out as this would require housing the optical set up in a fume – cupboard due to the strong odour generated by the thiol compound. Previously reported studies of alkanethiol adsorption onto Au (1ll) surfaces have shown that at relatively dilute solutions (10^{-3} M), two distinct adsorption kinetics can be observed. First a very *fast step*, which takes a few minutes, by the end of which the contact angles are close to their limiting

values and the thickness are about 80-90% of its maximum. Followed by a *slow step*, which lasts several hours, at the end of which the thickness and contact angles reach their final values. The fast step was found to strongly depend on thiol concentration and using 1 mM solution the first step was complete after ~1 min, while it required over 100 min at 1 μM concentration. The slow step can be described as a surface crystallization process, where alkyl chains get out of the disordered state and into unit cells, thus forming a two-dimensional crystal [7.8-7.9].

Probing the structural integrity of the thiol layer

Following the introduction of the thiol layer, cyclic voltammetry of the functionalised gold film was carried out in a solution of buffer electrolyte containing a redox probe, hexaamine ruthenium (III) chloride solution. A potential was applied between the working and reference electrode to oxidise and reduce the redox probe. The cyclic voltammogram obtained (fig 7.6) gave an indication of the structural integrity of the thiol layer formed over the gold film. Here the interest is to determine the presence of structural defects in the thiol layer. The thiol layer adsorbed onto the gold surface had the number of defective sites deliberately increased by using the highly substituted alkanethiol, *tert* dodecanethiol. The presence of the defective layer can be detected by the relatively high current obtained in response to the oxidation and reduction of the redox probe, which will be absent in a defectless layer (fig 7.6). A defective layer was used here as, future experimental application of the IOSPR device in the biological analysis of phospholipase A will require the thiol layer to be defective. This will allow for the hydrolytic action of the enzyme phospholipase A on the lipid layer deposited over the thiol layer to be followed by monitoring the increase in current in response to the loss of the lipid layer, which not be possible if the thiol layer is defectless.

Fig 7.6 is the optical and electrochemical response to the oxidation and reduction of the redox probe carried out over a gold film modified by the *tert* dodecanethiol ($C_{12}H_{25}SH$). As expected the presence of the thiol layer does not block the electrochemical response to oxidative and reductive reaction. Optically, a reduction in the transmittance as the potential is scanned in the anodic direction was observed, this corresponds to the adsorption of anions onto the gold film and electronic effects

on the optical properties of Au surface. In addition to this, there is a change in the rate of change of the transmittance at 0.283 V, in both the anodic and the cathodic scans, but reason for this is not presently known. The peak separation of the oxidation and reduction peak is 0.12 V (.244 V-.124 V), which is significantly greater than that obtained on a bare electrode [7.10].

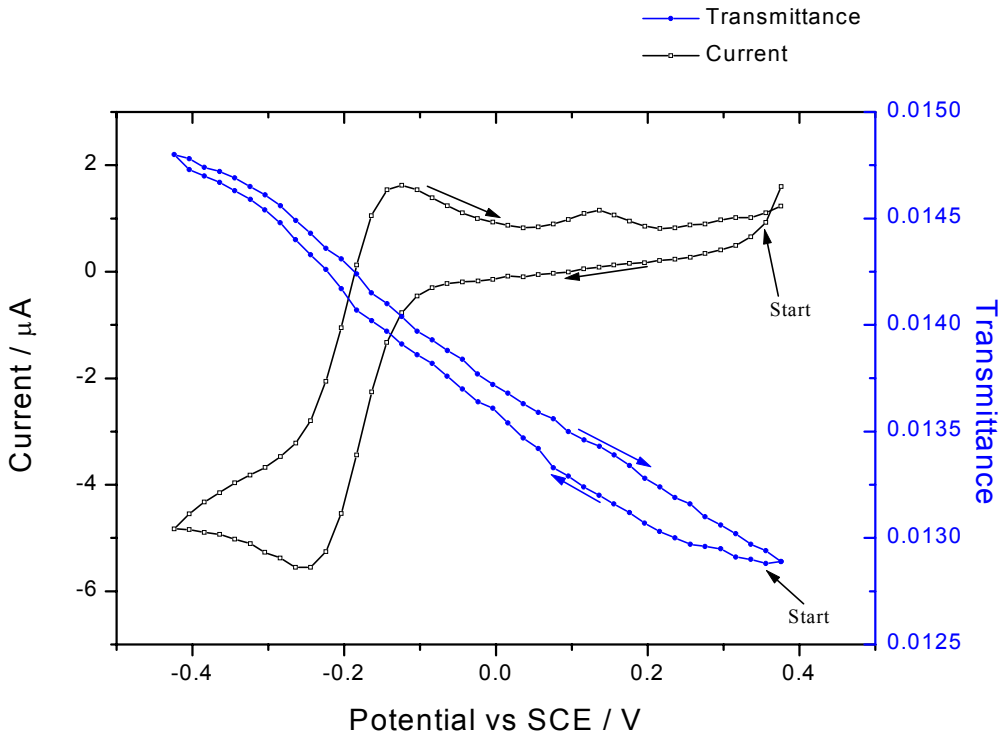

Fig 7.6 Optical and electrochemical response to the oxidation of 1 mM Hexaamine ruthienum (III) chloride in 0.1 M buffer-electrolyte (0.1 M tris buffer + 0.1 M NaCl) on a gold film. Scan rate of reaction was 20 mV/s.

The self assembled membranes on electrodes can be viewed as a pure capacitor in most studies of alkanethiol monolayers at electrode surfaces. Determination of the state of the adsorped layer in terms of whether it is mono or multi-layered can be obtained from the interfacial capacitance of the electrode. This capacitance can be estimated from a CV of its charging current

$$C_{total} = \Delta I / 2v$$

Where C_{total} is the total interfacial capacitance in F/cm^2

ΔI is the difference in current between the forward and reverse scans in A/cm^2 and v is the potential scan rate in v/s. Running the potential between -0.2 and 0.8 V a capacitance value of 5.81 μF/cm^2 was obtained, which suggests that a monolayer of thiol had been formed.

7.3.3 Probing desorption of thiol layer using the IOSPR device

The desorption reaction was first carried out using a gold film, placed in a beaker containing just buffer electrolyte, here at potential exceeding 0.95 V the nucleation loop was formed. Nucleation loop reveals changes in the electrode surface, which result in changes in the kinetics of reaction. This is illustrated in plot-b of fig 7.7, where following the formation of the nucleation loop in plot-a of fig 7.7, the peak current due to the oxidation of the gold film becomes visible. The low current (oxidation peak) in comparison to that of the bare gold film suggests that the gold film surface is still coated with the thiol layer.

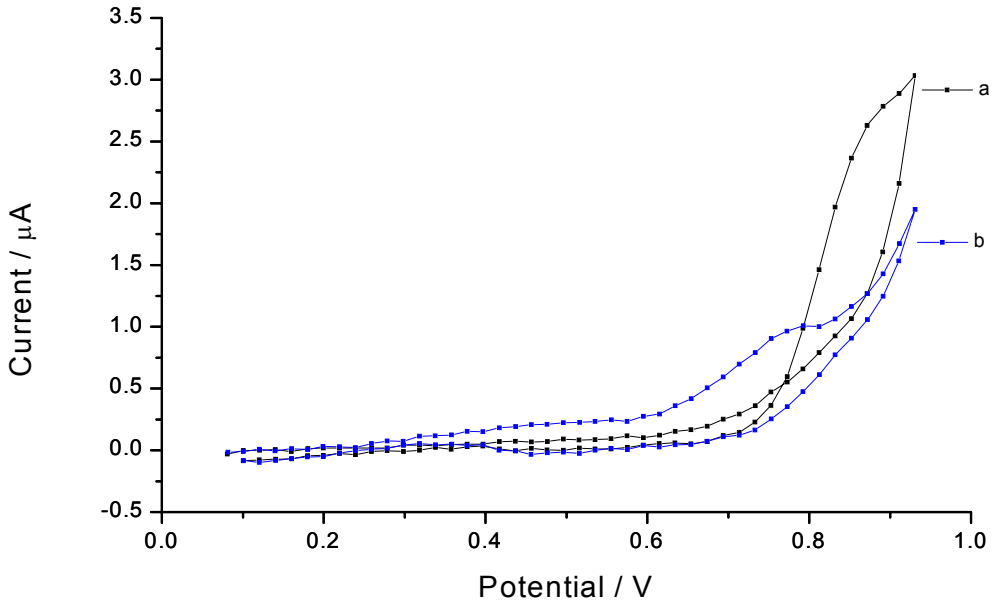

Fig 7.7 Cyclic voltammogram (20 mV / s) of buffer electrolyte (0.1 M) showing the formation of an oxide layer (a) following the removal of the thiol layer (b) indicated by the formation of the nucleation loop in (a). The current flipped on itself at a potential of 0.767 V.

Desorption of the thiol layer from the gold film was repeated again, but this time the analysis of the gold film was carried out using both optical and electrochemical interrogation techniques. Using the thiol-functionalised gold film exposed to buffer electrolyte, an anodic scan was applied from 0.1 V to 0.9 V (see fig 7.8). Between 0.1 V and 0.8 V no current was obtained, as the thiol layer blocked any transfer of electrons between the gold film and the electrolyte. A further increase in potential to 0.9 V resulted in a rise in the current, on reversing the direction of the scan, a drop in the current was observed. The significant feature of the electrochemical response here is the fact that the current plot flips on itself, indicating the formation of a nucleation loop on the cathodic scan. In addition to the formation of the nucleation loop, scanning further in the cathodic direction, an increase in the current, which peaks at 0.4 V was obtained.

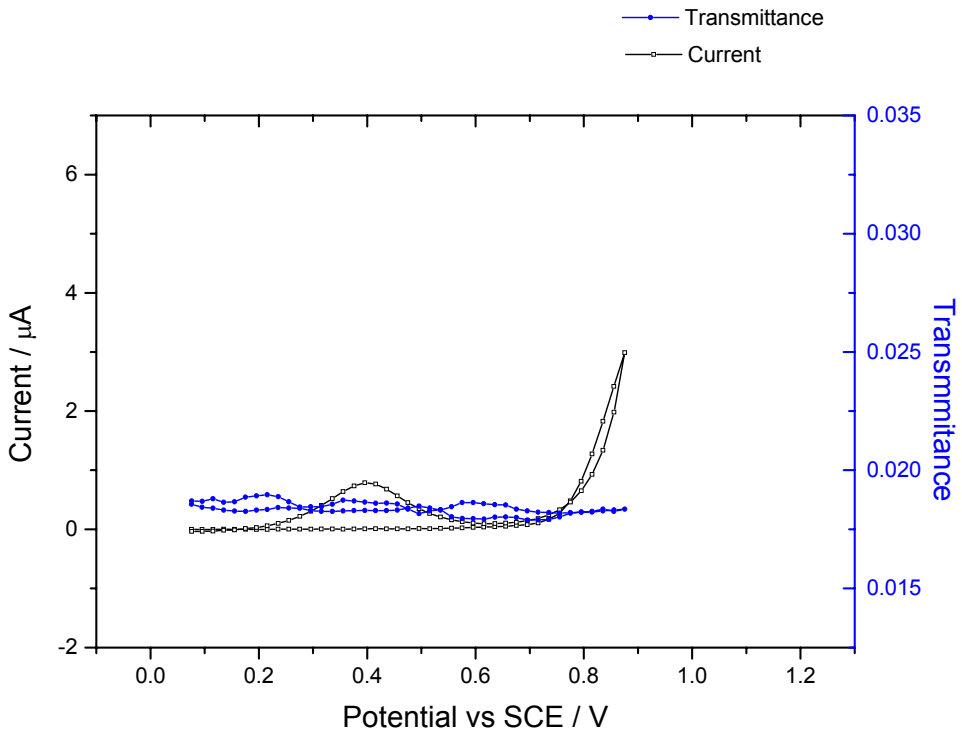

Fig 7.8 optical and electrochemical response to cyclic voltammetry (20 mV / s) of buffer electrolyte (0.1 M) on a gold film.

This peak current is a result of the adsorption of chloride ions, which had been previously blocked, by the presence of the thiol layer during the anodic scan. The formation of the nucleation loop and the peak current in the cathodic scan both

suggests the loss of the thiol layer, but as will be shown this was in no way a complete loss of the thiol layer. This is obvious from the relative small change in the optical and electrochemical response to loss of the thiol layer when compared to that of the bare gold film (fig 7.4). Optically a change of approximately 3 % in the transmittance was obtained in response to the adsorption of anion when scanning between 0.1 V and 0.9 V.

The cycle was then repeated again and an increase in the percentage change in the transmittance in response to the adsorption of anion and oxidation of the gold film (see fig 7.9) was observed. The cathodic scan shows an increase of 12 % in the transmittance at 0.1 V when compared to the transmittance at 0.1 V on the anodic scan (fig 7.9). Increase in the potential limits gave rise to two distinct peak currents in the anodic scan (fig 7.10). At the potential limit of 1.1 V the cyclic voltammetry was repeated 5 times and as observed in fig 7.11 the transmittance and electrochemical current in response to the adsorption and oxidation of the gold film increased with every cycle.

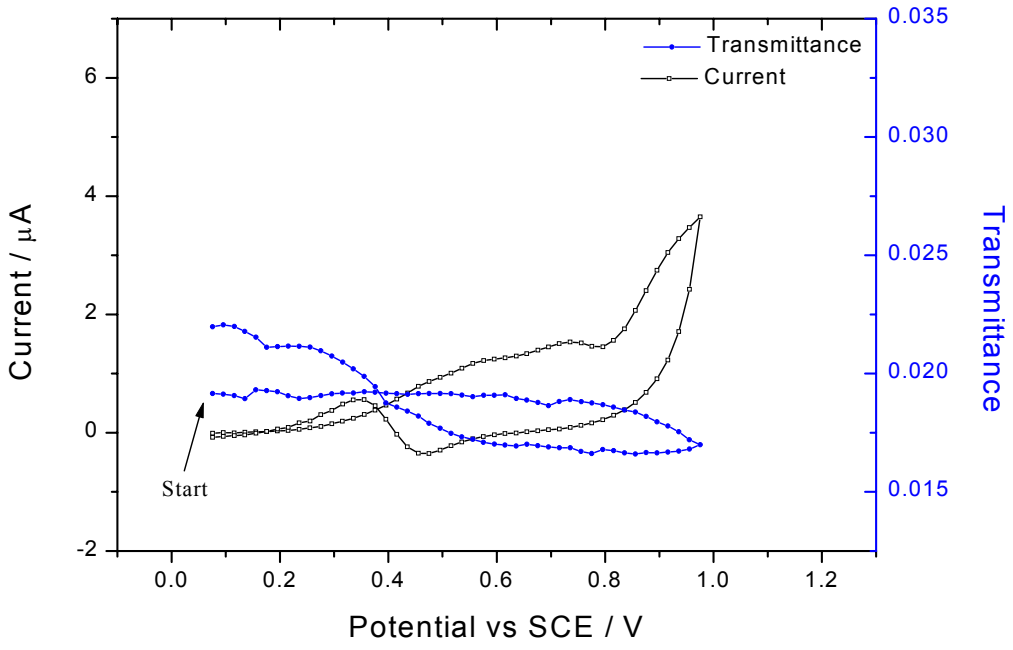

Fig 7.9 Optical and electrochemical response to the desorption of thiol layer from a gold film, in addition to the oxidation and adsorption of anions during the cyclic voltammetry (20 mV / s).

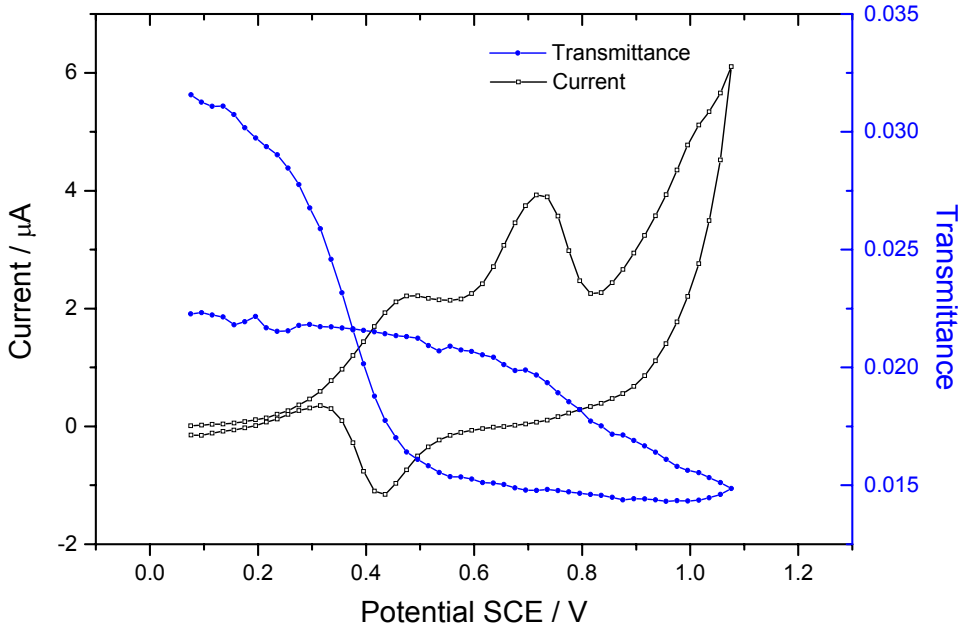

Fig 7.10 Optical and electrochemical response to the desorption of thiol layer from a gold film, in addition to the oxidation and adsorption of anions during the cyclic voltammetry (20 mV / s).

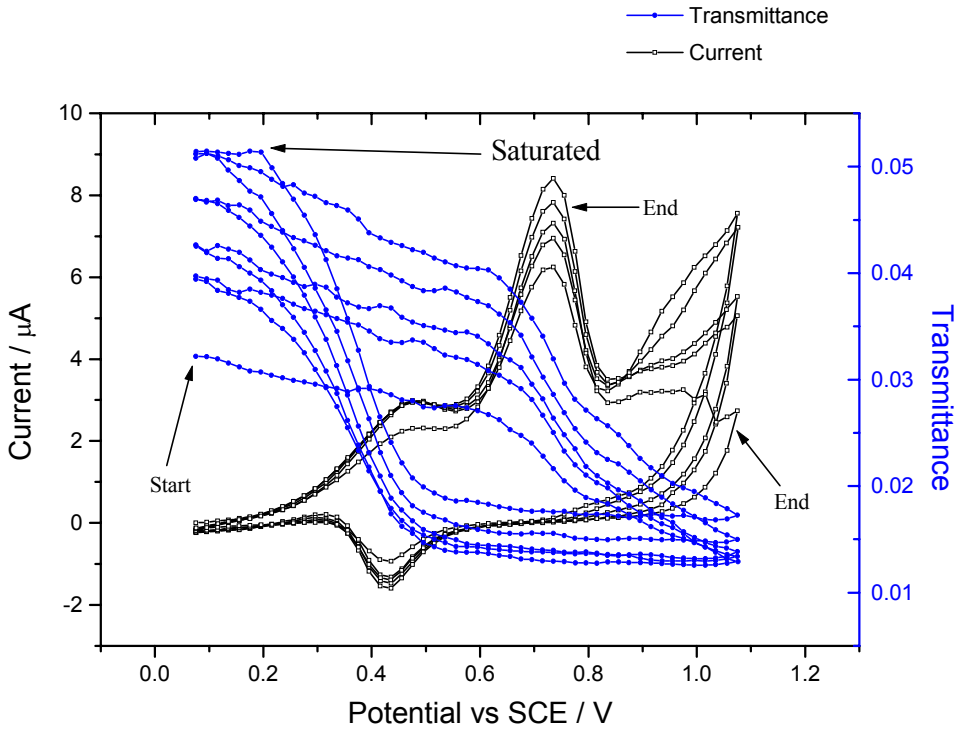

Fig 7.11 Optical and electrochemical response to the desorption of thiol layer from a gold film, in addition to the oxidation and adsorption of anions during the cyclic voltammetry (20 mV / s).

7.4 Optical studies of phospholipid films on IOSPR devices

An optical interrogation of the deposition of phospholipid layer onto the thiol layer, previously deposited on the gold film surface was carried out in real time using the IOSPR device. This analysis will require collection of data over prolonged periods, which will be significantly affected by drift in the transmittance. The thermal and mechanical contribution to this drift was studied first.

7.4.1 Procedures

A thiol layer was deposited over the gold film of the IOSPR device using similar procedures similar to that carried out using the gold wire electrode (section 7.2.1). Following the adsorption of the thiol layer over the gold film of the IOSPR device, the substrate was rinsed in buffer-electrolyte solution and then mounted in the experimental apparatus shown in fig 6.1 ready for phospholipid deposition and measurement.

Preparation of the phospholipid solution.

5 μg cm^{-3} of dioleoyl phosphatidylcholine (DOPC) solution was prepared by rapidly injecting the phospholipid solution (50-100 μl) into 20 cm^3 of buffer and electrolyte solution (pH 8.0) contained in a sampling tube connected to the flow injection analyser via a loading loop. The phospholipid solution was briefly vortexed to homogenise it and then loaded into a sample loop on the FIA before being injected in to the flow cell.

Loading procedure for the phospholipid solution into the flow cell for analysis.

A wall-jet flow cell, having a central input port and two output ports located at the edges of the cylindrical cell, was clamped onto the waveguide under test and the flow cell was connected to the flow injection analyser using high density Teflon tubing. The inlet/outlet needles of the flow cell had an internal diameter of 400μm, while the active volume of the wall-jet cell had a diameter of 12.5 mm and a depth of 75μm, resulting in a volume of 9.2 μl. A steady state condition was created by passing buffer-electrolyte over the sensor surface for a period of 20 minutes, during which, the transmittance was recorded to establish a baseline. The homogenised phospholipid solution was then loaded into a sample loop on the FIA then injected into the flow

cell. On contact with the modified gold film, the phospholipid layer was formed by vesicle fusion to a hydrophobic alkanethiol self-assembled monolayer. Data was acquired by the computer at a rate of one data point every second, with the time constants of the lock-in amplifiers set to 1 second.

7.4.2 Results

Drift of transmittance

A major problem encountered while applying the IOSPR device for the study of processes that required long periods of data acquisition was the drift in transmittance over time. Mechanical drift and temperature fluctuations were the main contributory factors to the observed drift in transmittance. Generally over a 12 hour period with the flow cell subjected to a constant flow of buffer electrolyte a 4 % change in transmittance due to drift is obtained.

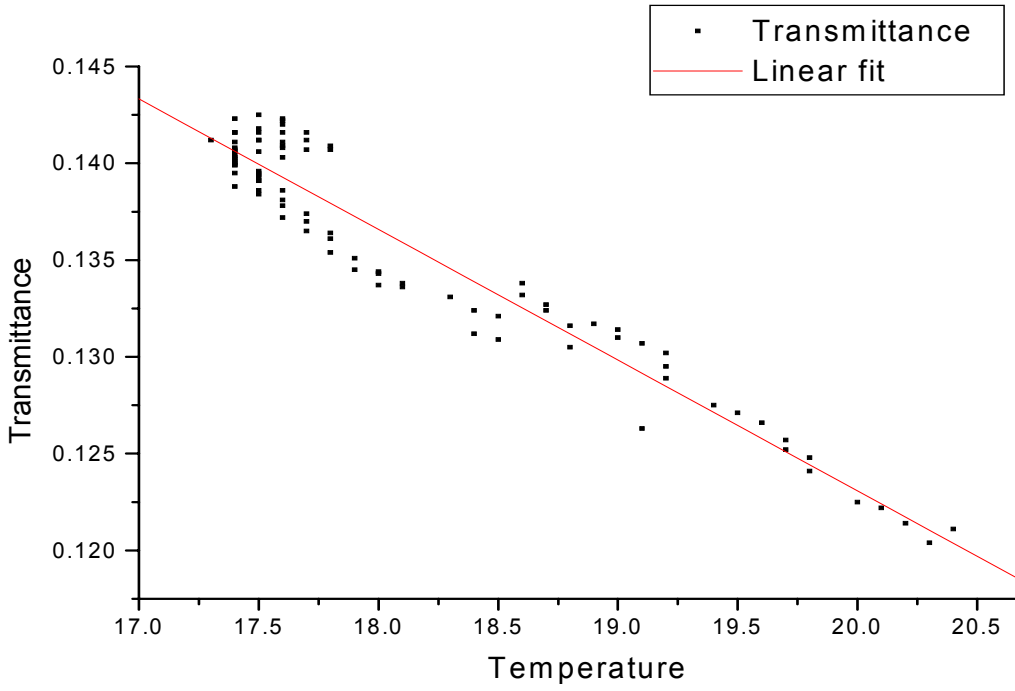

Fig 7.12 Plot showing the effect of temperature on transmittance of the IOSPR device.

The effect of temperature on the observed transmittance is shown in fig 7.12 here a reduction in temperature gave rise to an increase in transmittance. This plot of transmittance against temperature change gave a linear plot showing that for every

1°C shift in temperature, a change of 0.006 in transmittance is obtained, for this particular analysis.

Optical probing of the adsorption of phospholipid

Fig 7.13 shows the optical response to the deposition of dioleoyl phosphatidylcholine (DOPC) over the thiol layer and its removal using octyl glucoside (n-octyl-B-D-glucopyranoside). This plot is divided into 6 regions. Region 1 is the optical response to the presence of buffer electrolyte of refractive index 1.337 flowing over the flow cell. The drift in transmittance observed over this region was due to a combination of mechanical and temperature variation, discussed above. Region 2 sees the introduction of the calibration solution of refractive index 1.3446 and, as expected a drop in transmittance was observed. The IOSPR response to the introduction of the calibration solution shows that an index increase of 0.0076 gave a 50 % change in transmittance. Following the introduction of the calibration solution at region 2 of fig 7.13, the cell was flushed with buffer electrolyte of refractive index 1.337. Region 3 shows that the transmittance returns back to values similar to that of region 1 (see fig 7.14).

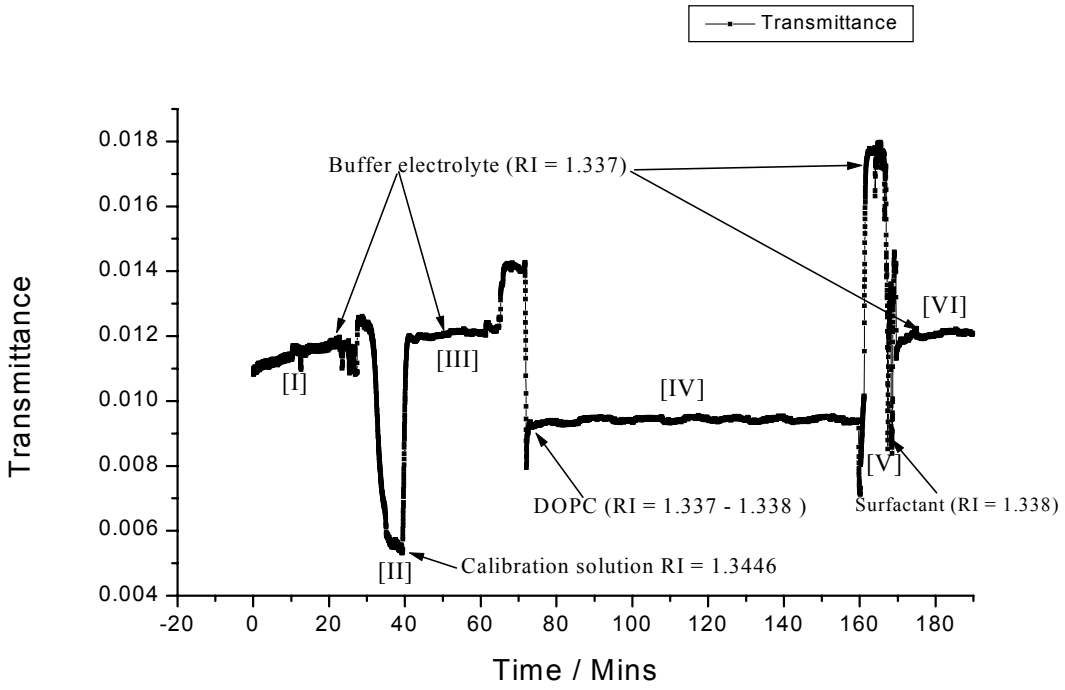

Fig 7.13 optical response to the automated deposition and removal of phospholipid layer using a flow injection analyser.

Region 4 is that due to the adsorption of the phospholipid layer over the thiol layer. Here a sharp drop in the transmittance is obtained following the introduction of DOPC. This was followed by a rise in the transmittance, which plateaued after one minute. The transmittance obtained here was higher than that in region 2, following the addition of the calibration solution of refractive index 1.345.

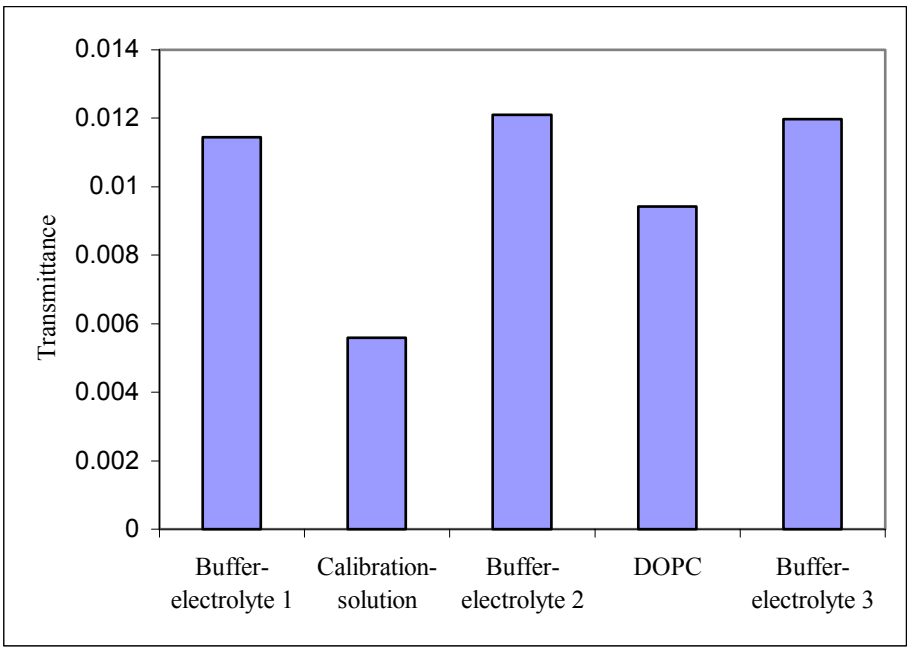

Fig 7.14 Average transmittance in regions 1-4 and 6. The transmittance value at buffer electrolyte 1 is the background, this is flowed by that of the calibration solution and that due to flushing of the calibration solution out of the flow cell. Transmittance at buffer electrolyte 3 is that obtained following the removal of the thiol layer using octyl glucoside.

The transmittance for the deposited phospholipid layer was much higher than that of the calibration solution suggesting that the transmittance had gone though the bottom of the resonance curve and ended at the right hand side of the surface plasmon curve due to the formation of multi layers of phospholipid over the gold film. The transmittance value obtained with only thiol on the gold film was 0.012, which is a factor of 10 lower than that of the device with bare gold in the presence of perchloric acid. Thus, suggesting that the operating point is at a much lower point of the resonance curve. The transmittance value for the calibration solution of refractive index 1.345 for this analysis is 0.006, which is very close to the noise limiting region of the device that is 0.002. Fig 7.15 is a theoretical model plot that shows what effect the introduction of a monolayer phospholipid to the thiol layer has on the initial transmittance of the device with thiol on the gold film. The introduction of a

phospholipid layer gave a change of approximately 95 % while that of the thiol gave a value of 43 %. If it assumed that the transmittance passed through the bottom of the SPR curve, this makes it difficult to carry out any quantitative analysis of the data obtained for the introduction of the phospholipid layer onto the thiol layer.

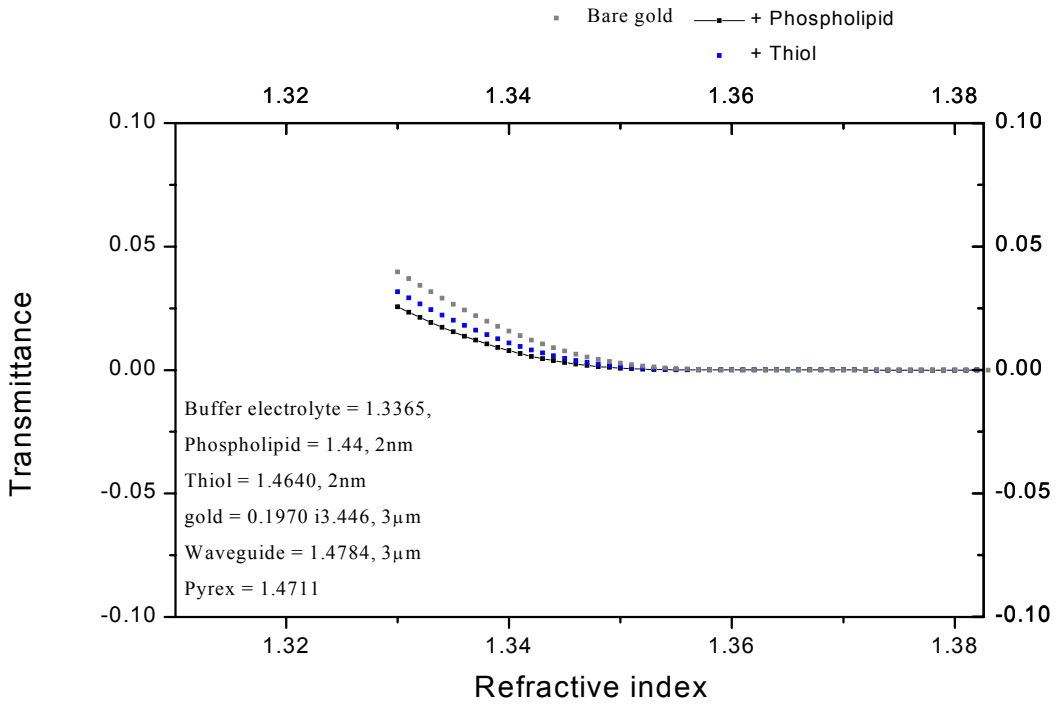

Fig 7.15 Theoretical plot showing the effect of building up the multilayer system of the device using thiol and phospholipid layer.

Following the introduction of dioleoyl phosphatidylcholine into the flow cell, the pump was switched off (3 min after DOPC inject) for 90 minutes to allow complete adsorption. The transmittance remained constant over the 90 minute period. The temperature of the room was logged every 10 minutes and the maximum temperature fluctuation observed during this period was 0.2°C. At the end of the 90 minute period, the cell was flushed with the buffer electrolyte solution (region 5), then with octyl glucoside (region 5) and finally with buffer electrolyte (region 6). The surfactant, octyl glucoside, was introduced to remove the phospholipid layer this returned the transmittance back to similar values as that of region 1 and 2 following the introduction of the buffer electrolyte (see fig 7.14). The increase in transmittance

following the introduction of each solution is maintained over a 7 minute period in all cases, reasons for this observation is presently not known.

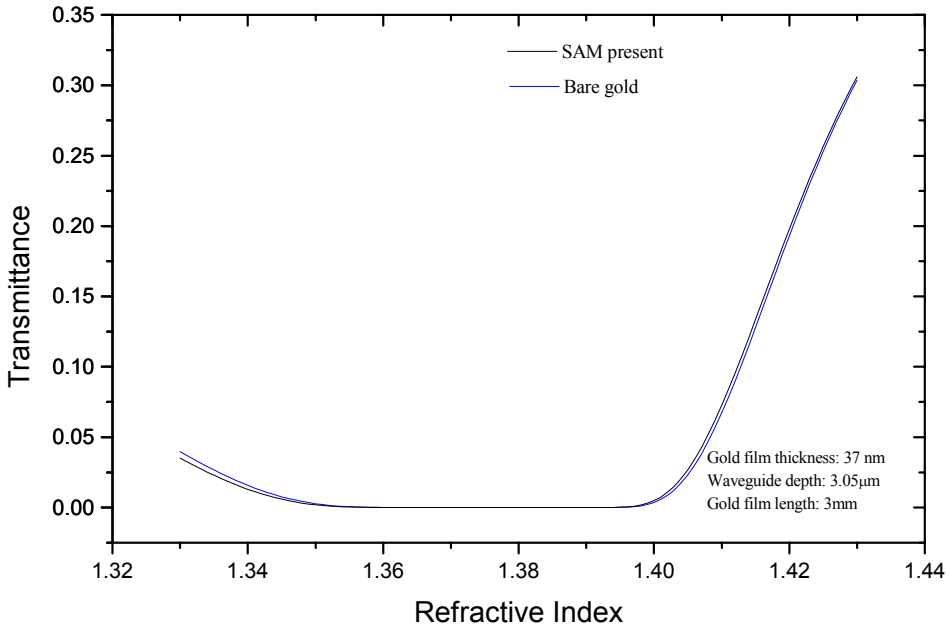

Fig 7.16 Theoretical plot showing the surface plasmon resonance of the gold film in the presence and absence of a thiol layer. The difference in the transmittance value at the refractive index of 1.336 for bare gold and functionalised gold was 20 %.

7.5 Conclusion

An integrated optical surface plasmon resonance device has been applied here in probing the adsorption, desorption of the thiol layer and monitoring real time adsorption of a monolayer of phospholipid onto a monolayer of thiol. Real time adsorption of the thiol layer was not carried out using the device due to the requirement to house the apparatus in a fume cupboard. A drop in the transmittance of approximately 80 % in response to the addition of the thiol layer from bare gold was obtained, this is greater than that predicted by the model, approximately 43 % (see fig 7.16). The desorption of thiol layer was achieved at potentials exceeding 0.95 V, at this potential and above. Here an increase in transmittance in response to the removal of the thiol layer and reactions such as the oxidation of the gold film became visible. Study of phospholipid assembly over a thiol layer was also carried out, using the IOSPR device. The optical result obtained suggests that the adsorption of the

phospholipid layer was complete in 1 minute as the rise in transmittance plateaued after 1 minute. The result obtained suggests that future application of the device in biological analysis involving the thiol and phospholipid layer would require modification of the device to move the operating point of the device from the positions close to the bottom of the surface plasmon resonance curve. This is due to the observation that the introduction of the phospholipid layer onto the thiol layer moved the transmittance to values indicating that the operating point of the device was now at the right hand side of the surface plasmon resonance curve. The device works well as a qualitative sensor for its present application. Drift in the transmittance occurred during the adsorption of phospholipid layer, which require data collection over long periods. The drift in transmittance was due to mechanical movements of the optical manipulators and changes in temperature. The mechanical effect was reduced by tighten up the optical manipulators. The contribution of temperature can be controlled if the temperature of the set up can be kept constant, this is not restricted to the transducer as, the laser is also affected by temperature. The application of a temperature stabilised laser can reduce this effect.

7.6 Reference

7.1 P. Krysinski, M.R. Moncelli, F. Tadini-Buonmsegni, Electrochimica Acta 45 (2000) 1885.

7.2 Gregory E. Poirier Chem. Rev. 97 (1997) 1117.

7.3 D.A. Brevnov and H.O. Finklea, Langmuir 16 (2000) 5973.

7.4 L.H. Dubois, R.G. Nuzzo, Ann. Phys. Chem. 43 (1992) 437.

7.5 J.B Schlenoff, M. Li, H. Ly, J. Am. Chem. Soc. 117 (1995) 12528.

7.6 Abraham Ulman, Chem. Rev. 96 (1996) 1533.

7.7 H.O. Finklea, J. Electroanal. Chem. 19 (1996) 109.

7.8 K.A. Peterlinz and R. Georgiadis, Langmuir 12 (1996) 4731.

7.9 Y-S. Shon and T.R. Lee, J. Phys. Chem. B 104 (2000) 8182.

7.10 P. Krysinski and M. Brzostowska-Smolska, J. Electroanal. Chem. 424 (1997) 61.

Chapter 8
Conclusion

The main aim of this project was to design and test the analytical potential of an integrated optical surface plasmon device, which combined an optical interrogatory technique, surface plasmon resonance and an electrochemical interrogatory technique, cyclic voltammetry in the analysis of the interfacial region at the sensing region of the device. This design was initiated by fabricating a device that exhibited analytical characteristic features of both optical and electrochemical techniques in an aqueous environment.

Firstly the introduction of the electrochemical techniques placed a requirement for an improvement of the adhesion of the gold film, on the Pyrex glass. This was achieved by the treating the surface of the Pyrex glass with (3-mercaptopropyl) trimethoxysilane and modifying the treatment process previously suggested by other authors. This resulted in a device that was used for a 3 month period without loss of activity due to gold loss. Following the improvement of the adhesion of the gold film onto Pyrex, characterisation of the device optically was undertaken. This involved monitoring the device response to changes in the refractive indices at a given film length and the effect of varying the interaction length of the gold film in the presence of water and air. The results obtained here compared well with those reported in the literature and that derived from the theoretical model.

Using the integrated optical surface plasmon resonance device, the changes in the charge distribution at the gold surface as the potential between the working electrode and the reference electrode was increased, the formation of an oxide film with thickness of 0.54 nm and optical constant of 3.3 - j1.3 and the stripping of the oxide was monitored, optically and electrochemical simultaneous and in real time. Both techniques complemented each other and gave added information, specific to each technique. Attributes such as the true working electrode area, the roughening factor and charge consumed in carrying out surface reactions such as oxidation of a gold surface was determined electrochemically by integrating the peak area associated with that particular reaction. Other factors such as the determination of the crystal face of the metal was obtained via a simple cyclic voltammetric analysis. The optical

component of the device gave real time qualitative and quantitative (if ran along side a numerical model or calibrated against the intended analyte) information of the reaction occurring over the sensing surface.

Comparisons drawn between the optical technique applied in this project and that reported using ellipsometry and reflectance spectroscopy show that the surface plasmon technique is a more sensitive technique when working with very thin films of the order applied in this thesis. Here a 60 % change in response to the formation of an oxide film over a gold surface in sulphuric acid was obtained, while reported studies with the other optical techniques did not show better than a 1 % change. The form of the plots obtained in response to the formation of an oxide film was similar in all optical techniques.

The integrated optical surface plasmon resonance device was used for the first time in monitoring the underpotential deposition of copper on a gold film and as observed in the oxidation study this device performed better than other reported optical analysis such as such as ellipsometry (0.1 % in ψ) and reflectance (1 %) where the IOSPR device gave a 10 % change. This change, can be associated mainly to the increase in film thickness over the sensing gold surface as the refractive index of the copper monolayer 0.27 - j3.4 is very close to that of the gold film 0.20 - j3.45. This point allows one to introduce characteristics of the device, which one might view as disadvantages but really are positive points that allow the broad application of this device. The device, optically responses to the refractive index of the layer introduced over the gold film, the changes in the bulk refractive index and the thickness of the introduced film. This puts the question of selectivity, but this lack of selectivity allows the device as in the case of the study of the underpotential deposition of copper onto gold film where both metals have similar refractive index to be used in the analysis as based on its sensitivity to film thickness. The issue of selectivity is addressed by functionalisation of the gold film surface as discussed below.
Electrochemically, in the study of the underpotential deposition of copper onto gold the IOSPR device response compared well with previous reported studies. The charge obtained for the deposition of copper onto the gold film by integrating the area under the peak current for the deposition of Cu (0.41 mC / cm^2) was close to the

theoretical value of 0.44 mC / cm^2, expected for the deposition of a monolayer of copper on gold film

Following from the study of electrochemically modified charge distribution of the interfacial region of the gold film and the introduction of a monolayer of copper onto the gold film, the IOSPR device was then functionalised using thiol layers and phospholipid layers. This thesis concentrated on monitoring the devices response to the addition of the biological layer and its removal, determining how the positioning of the operating point of IOSPR device is affected following the introduction of the thiol layer, potential of electrochemically removing the thiol layer and the addition and removal of the phospholipid layer previously adsorbed over the thiol layer.

The adsorption of a thiol layer onto the gold film gave an 80 % change in the transmittance, this although significantly greater than that predicted by the model, illustrates the sensitivity of the device to the introduction of a film having a refractive index of 1.46 and thickness of approximately 2 nm. The combination of the optical and electrochemical technique showed that the electrochemical desorption of the thiol layer required several cycles for complete desorption to occur with the optical response allowing a real time observation of the process. The potential of the device acting as a sensor for biological enzymes such as phospholipase A was shown by monitoring the addition of the phospholipid layer over the gold film and its removal using a surfactant, the surfactant mimics the hydrolytic action of the enzyme. The real time monitoring capability of the device allowed visual observation of the adsorption of the phospholipid layer, here a significant percentage change in response to the adsorption process was obtained and this adsorption process was over in 1 min.

There are several factors that need to be noted for the application of the device in sensing. The state of the sensing surface is important as this affects the sensitivity of the device and shifts the operating point of the device which could move the device into a less sensitive operating point or in some cases cause the response to go through the resonance minimum, there by preventing qualitative or quantitative analysis from been carried out. When the IOSPR device is used for analyses that occur over short periods (1hr), the drift in the transmittance is not a problem. This drift in transmittance becomes a problem with analysis requiring monitoring over long length

of time. Here the main contributing factors observed were mechanical and temperature effect. Temperature affects the transducer and the laser. With the laser this can be solved by introducing a temperature stabilised laser, while that of the transducer requires the temperature at the sensing area to be controlled. There are ways of controlling the temperature at this site in the lab but this might not be appropriate if the device is intended to be portable. Improvement in the referencing attribute of the device could solve this problem and can be easily achieved by introducing multichannel sensing architecture to the overall lay out of the device. The waveguide approach is ideally suited for multisensor integration. Finally the phenomenon of SPR is completely non-specific. It cannot distinguish between different chemical changes. While this may appear to be a limitation, it is really a powerful advantage. As shown in this thesis the IOSPR device is one that allows the individual to take up the device and functionalise it to suit the operators needs, in what ever area of operations, such as environmental, medical, defence, research, etc.

Appendix

Appendix 1

Determination of the area of a gold electrode via analysis of stripping peak of an oxidation-reduction plot.

For faradaic surface reaction such as that involved in this oxidation-reduction reaction, the coverage fraction θ, is related to the charge passed q(V) for adsorption or desorption of the atoms by [1]:

$$\theta(V) = q(V)/q_1$$

Where q_1, is the charge for the formation of a monolayer ($\theta = 1$)

$$q_1 = NF/N_A \text{ cm}^{-2} ,$$

Where N is the number of substrate atoms per cm^2, N_A, is Avogadro's and F = 96,500 C $mole^{-1}$ The number of atoms per cm^2 for polycrystalline Au is usually taken from the average of the main low index faces of gold film. Burshtien, [2] calculated from the charge required to form a monolayer of AuO that for polycrystalline Au we have 1.25×10^{15} atoms/cm^2.

$$q \equiv q_1 \cong 1.25 \times 10^{15} \times 96{,}500/6 \times 10^{23} \text{ C cm}^2 = 200 \ \mu\text{C cm}^{-2}.$$

As the reaction involves two electron transfer the total charge is $\underline{400\mu\text{C cm}^{-2}}$.

In determining the surface area of the electrode electrochemically, the method employed, assumes that a monolayer of oxygen is chemisorbed onto the gold film in a 1:1 relation with the surface gold atoms. Here the charge under a volumetric peak for the oxidation or reduction of a gold film is assumed to correspond to the adsorption (oxidation peak) or desorption (reduction peak) of one oxygen atom onto (or from) one gold substrate atom (1:1 relationship). Integrating the i(V) plot over the voltage range (that is V_2-V_1) covering that involved in the reaction gives the charge passed during the reaction.

$$q = \int_{v_1}^{v_2} i(V).dt = \int_{v_1}^{v_2} i(V)/s.dv$$

Where s is the sweep rate (s = dV/dt).

The charge obtained from the plot is then related to the theoretical value (400 $\mu C/cm^2$) expected for the coverage of 1 cm^2 of a polycrystalline gold film in order to determine the area of the gold film been interrogated.

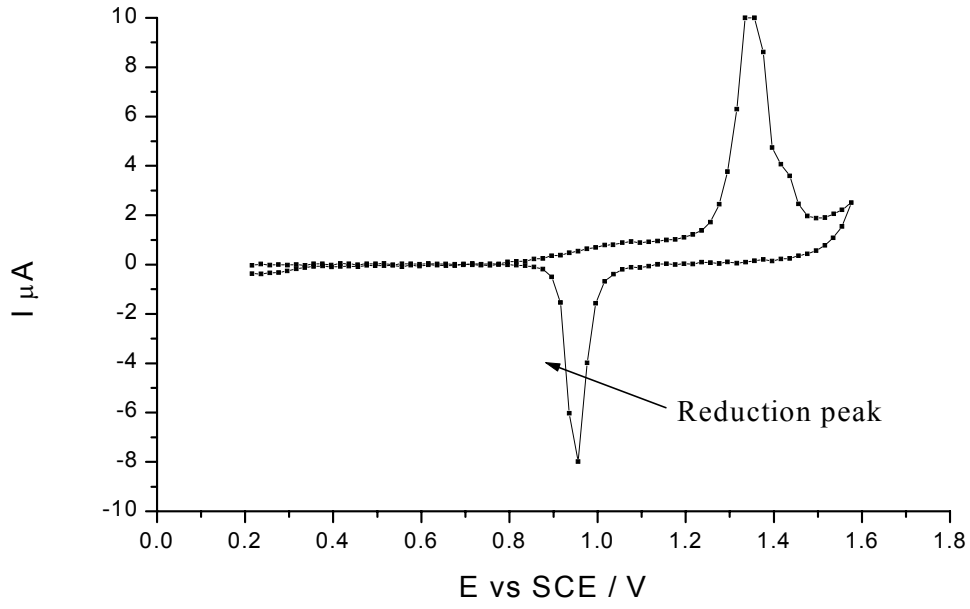

Fig 1

The area of the reduction peak is derived by integrating this part of the plot, which is given in ampere volts (AV). The x-axis varies with time and it is linked to the chosen scan rate, dividing the area by the scan rate (V/s) the electric charge is obtained.

A coulomb is equal to the charge transferred by a current of one ampere in one second Below is an example of the calculation carried out.

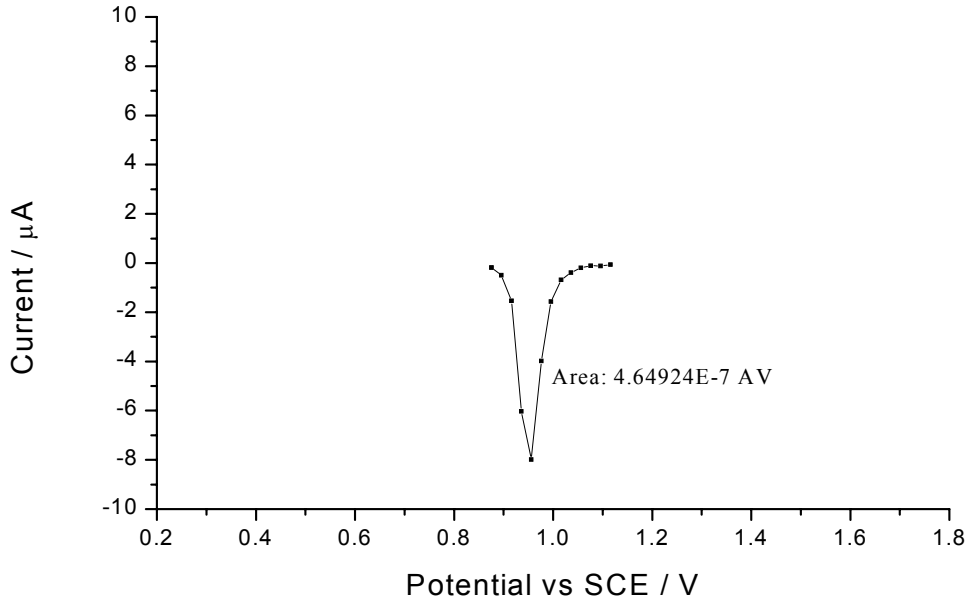

For polycrystalline gold 400μC = 1cm^2 therefore 23.25 μC = 0.0581cm^2.

The expected area =0.0551 cm^2 .

The preferred peak, for such analysis is the stripping peak as charge passed during charging of the double layer (oxidation peak) and the faradaic charge for the O_2 evolution (reduction peak) are not included in the sums, which is the case if the oxidation peak is used.

Reference:

1. S. Trasatti and O.A. Petrii., J. Electrochem, 327 (1992) 353.
2. R.K. Burshtein, Electrokhimiya, 3 (1967) 349.

Appendix A2

Determination of the amount of metal deposited during UPD.

For adatoms deposited with the passage of two electrons per atom e.g. Cu on Au and having approximately 1.25 x 10^{15} atoms per cm^2 on a polycrystalline gold surface [1], the charge, q, (2q as the reaction involves two electrons) required is

$$2q \equiv q_1 \cong 1.25 \times 10^{15} \times 96{,}500/6 \times 10^{23} \text{ C cm}^2 = 400 \ \mu\text{C cm}^{-2}.$$

NB. $q_1 = NF/N_A \text{ cm}^{-2}$, where N is the number of substrate atoms per cm^2 , N_A, is Avogadro's and F = 96,500 C $mole^{-1}$ q_1, is the charge for the formation of a monolayer. This can be determined by electrochemical measurements, e.g. cyclic voltammetry, involving integrating the current with respect to time,

$$q = \int i(t).dt$$

over the potential range, ΔE, covered at a sweep rate s V/s that is over a time interval. Using the same method as previously described the electrical charge associated with the deposition of the metal is obtained, which in this example is Cu. Now applying one of faraday's laws describing electrolysis, the charge required to deposit or liberate a mass *m* is given by

$$Q = F\ n\ M = F\ n\ (m/\text{molar mass})$$

Where *F* is faraday constant, *n* is the charge of the ions and *M* is the no of moles, *M = m/molar mass,*

.

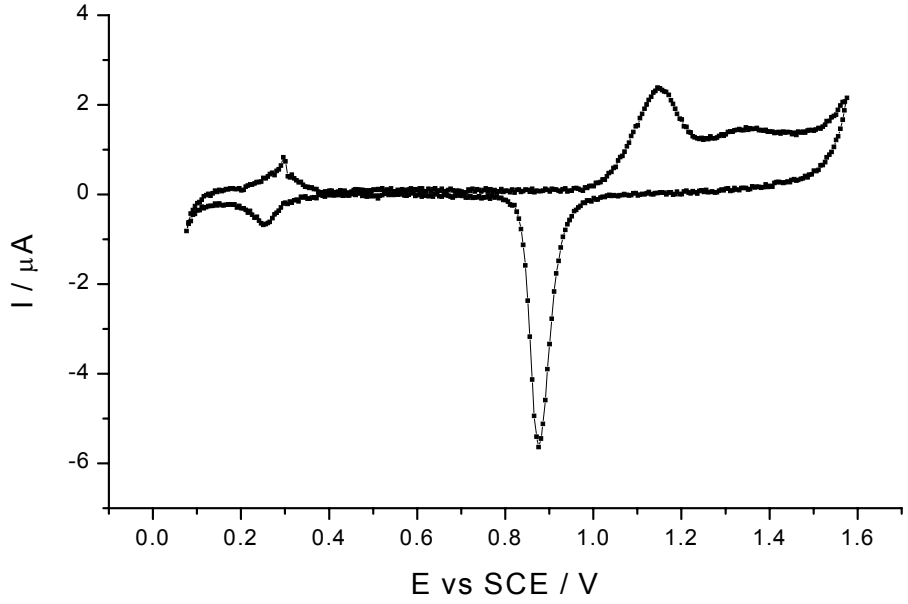

Integrate the area of the peak associated with the deposition of the monolayer of Cu.

- Divide this by the scan rate to obtain the electric charge
- Substitute value into the equation given below.

$$Q = F\,n\,M$$

To obtain the no of moles of Cu deposited.

Reference:

1 R.K. Burshtein, Electrokhimiya, 3 (1967) 349.

Appendix 3

Separation of ionic double layer effect and metal electronic effect.

This sections briefly looks at the process of separating the ionic double layer effect and the metal electronic effect as suggested by Abeles *et al.* [1]. As shown in chapter 3, the excitation of surface plasmon occurs when the component of the wave vector of the incident light parallel to the interface of the gold and dielectric, is equal to the surface plasmon wave vector. Modifications at the interface of the gold will affect the wave vector. If the wave vector, K, is viewed as a complex no; $K = K_1 + iK_2$ then any modifications will give $\Delta\mathbf{K} = \Delta K_1 + i\Delta K_2$.

For example, when a potential is applied between the working electrode and the reference electrode such that the ionic distribution at the working electrode-electrolyte interface changes, this causes a change in the wave vector. Here the $\Delta\mathbf{K}$ is the sum of the ionic double layer effect and metal electronic effect, that's is $\Delta\mathbf{K} = \Delta\mathbf{K}_{metal} + \Delta\mathbf{K}_{electrolyte}$. The imaginary part of each $\Delta\mathbf{K}$ is proportional to the imaginary part of the dielectric function of the corresponding thin layer. Since the dielectric function of the electrolyte is real $\Delta K_2 = \Delta\mathbf{K}_{metal}$, Abeles *et al.* [1] were able to separate contributions due to the electronic effects and ionic effects in the electrolyte. Here the analysis was carried out by monitoring the amplitude and phase change of the reflected component of the electric field vector of the p-polarised wave of excited surface plasmon wave at the double layer region using ellipsometry.

Reference:

1 F. Abeles and T. Lopez-Rios and A. Tadjeddine, Solid state communications 16 (1975) 843.

Appendix 4

Publications arising from this research.

1, Abanulo J.C., Harris R.D., Bartlett P.N., Wilkinson J.S. Underpotential Deposition of a Copper Monolayer on a Gold Film Sensed by Integrated Optical Surface Plasmon Resonance, Proc. Optical Fiber Sensors conference (OFS 2000) Venice.

2, Abanulo Jude, Harris R D, Bartlett P N, Wilkinson, J S. Waveguide surface plasmon resonance sensor for electrochemically-controlled surface reactions: Accepted - Applied Optics-June 2001.

3, J.C. Abanulo, R.D. Harris, J. Wilkinson and P.N. Bartlett. Waveguide surface plasmon resonance studies of studies surface reactions on gold electrodes: Accepted - Faraday discussion-June 2001.